THE SPATIAL AND TEMPORAL EVOLUTION OF THE ARGENTINE PRECORDILLERA AT 30° S: SHORTENING OVER A SHALLOW SLAB

A Dissertation

Presented to the Faculty of the Graduate School

of Cornell University

in Partial Fulfillment of the Requirements for the Degree of

Doctor of Philosophy

by

Phoebe Ames Judge

January 2012

THE SPATIAL AND TEMPORAL EVOLUTION OF THE ARGENTINE PRECORDILLERA AT 30ºS: SHORTENING OVER A SHALLOW SLAB

Phoebe Ames Judge, Ph. D

Cornell University 2012

The Argentine Precordillera is a foreland fold-and-thrust-belt in western Argentina that overlies the central Chilean flat slab region of the subducting Nazca plate. The Precordillera has accommodated shortening over the past ~20 million years; over this time, the Nazca slab evolved from a relatively steep subduction angle to horizontal subduction. Because the shortening in the Precordillera spans the shallowing of the slab, changes in the deformation patterns can provide insight into the relationship between the down-doing slab and the over-riding plate at zones of shallow subduction. In this thesis, I present field-based structural data, cross sections of the Precordillera, and estimates of shortening magnitude and rates for the region in an effort to characterize the impact of a shallowing slab on deformation at the surface.

To calculate shortening magnitudes for cross sections that have rigorous uncertainty estimates, I developed an algorithm that propagates known input uncertainties through an area balancing calculation and yields both Gaussian and maximum uncertainty estimates. The area balancing method is complementary to the

line-length balancing method and allows one to include known initial uncertainties, such as the uncertainty on stratigraphic thicknesses and the location of the decollement, neither of which are included in the "minimum shortening" estimates often cited in line-length balanced shortening calculations.

I constructed two cross sectional profiles through the Precordillera to determine shortening magnitude and rates since 20 Ma. Calculations for the profiles yield ~115 ± 44 (100) km of shortening in the Precordillera, where the uncertainty values are both Gaussian and maximum respectively. This shortening magnitude agrees with other published values of shortening for the Precordillera (72 – 136 km) determined via line-length balancing, and the variation in published values falls within the calculated uncertainty estimates. Variations in shortening rate throughout the Precordillera correlate temporally with changes in the geometry of the Nazca slab. Prior to the shallowing of the slab, the Precordillera accommodated 2 – 3% of the total plate convergence; after the slab began to shallow, shortening in the Precordillera accommodated 10 – 12% of the convergence rate.

BIOGRAPHICAL SKETCH

Born of the wilds of western Massachusetts in 1981, Phoebe Judge spent much of her early childhood outside or reading. At age 8, her family moved to the land of milk and honey and established a dairy farm in the southern Champlain valley of Vermont. Set loose on 300 acres of ridges and lake-bottom clay, she and her younger sister spent their free time constructing elaborate forts in the woods and pulling frogs out of ponds. Being home schooled, Phoebe traded in classroom lessons for hours wondering why certain pastures were flat, why the rocks outcropped where they did, and how to construct castles in the hayloft.

In high school, Phoebe avoided all mention of "physics" and studiously avoided learning anything at all in her biology classes. However, her chemistry class, called "Why Water is Weird," had a certain detail-inspired order that appealed to her and even provided a reason to finally try to do well in mathematics classes. A strong desire to eschew college was thwarted by attending the Breadloaf Young Writers Conference at Middlebury College, the first setting in which she had been surrounded by other young women who had a desire to engage with their education.

Phoebe attended Mount Holyoke College, back in western Massachusetts, and did yeoman's work trying to foster communication between the Physics and Geology departments. Finding little success in bridging the departments, she majored in both independently and wrote theses in both departments on topics as disparate as feedback

in lasers and magnetic fabrics in granites in Maine. Camping in Maine and California was more seductive that being tethered to the optics table, and she decided to see if a graduate program would pay her to continue her travels to collect geologic data in far-flung locations. This turn of events occurred only after two years of fervently eschewing pressure to attend graduate school for any reason; Phoebe is a reluctant scholar.

Returning to Vermont to complete a masters degree in geology from the University of Vermont, Phoebe worked with Keith Klepeis to determine the evolution of the strain field near the Alpine fault in Fiordland, New Zealand. After working in a field area that is accustomed to 10 m of rain annually, and remembering the mountains in California, she decided to apply to work with Richard Allmendinger at Cornell University in the rain-shadow of the Andes. Despite their aggressive introduction, Professor Allmendinger graciously accepted her application to work on upper crustal structural problems in the Precordillera.

Throughout this all, Phoebe has benefited from the bemused support of her parents and siblings, who suffered through many photos of rocks and valleys throughout the years. Her future is open and will certainly involve field work, fresh tomatoes, and an appreciation of the absurd.

"We must not then add wings,
but rather lead and ballast to the understanding,
to prevent its jumping or flying,
which has not yet been done;
but whenever this takes place
we may entertain greater hopes of the sciences."

- Sir Francis Bacon
from "Aphorisms on the Interpretation of Nature and the Empire of Man"[1]

I dedicate this work, whatever its worth,
to those who encouraged me to look more closely,
pay more attention to detail,
and observe before all else.

[1] Francis Bacon, Lord Chancellor of England A New Edition: with a Life of the Author, p. 364, by Basil Montago, Esq. (1848)

ACKNOWLEDGEMENTS

There are many people to whom I am greatly indebted for their support, guidance, help, and kindness during my time as a graduate student at Cornell, as well as many people who helped me even before my move to Ithaca. First and foremost among them, I thank Richard Allmendinger for serving as my primary advisor and mentor. I benefited greatly from all our discussions, scientific and political, and I truly appreciate your vision in the field as well as the lab. Your guidance throughout this project has helped me to think more linearly, carefully, and visually. You have been a patient and thorough mentor, helping me to craft my work even when I was driven to pursue a project according to my own method. Thank you for understanding when I needed to take my sabbatical and for helping me return to Cornell relatively seamlessly. Thank you for showing me the Precordillera; I will work to show you New Zealand!

Matthew Pritchard and Alan Zehnder served as my minor committee members and as professors and teachers during my time at Cornell. Matt and Alan, it is my great loss that my project did not require greater input from you. I enjoyed my time meeting with you and learning from you, and I appreciated your thoughtful questions during my exams. Thank you for your help, and I only hope that our paths cross in the future.

Other faculty in the department have also contributed enormously to my development and progress at Cornell. I owe a great deal of gratitude to Christopher Andronicos for his help, guidance, and listening over the years. Your kindness and

support, both academic and personal, has been elemental to my perseverance in my dissertation. Many thanks for your help when I felt stuck on a project and for when I felt lost at sea. Thanks for calling on me every day in New Mexico and for telling me when I was wrong. Having two structural geologists in the department has been a huge boon to me, and it is Cornell's enormous loss that you have a brighter future in Indiana.

Terry Jordan patiently answered an endless stream of rudimentary questions about basin dynamics, stratigraphy, and the Precordillera; to my knowledge, she never warned Rick of my ignorance. Thank you for your insight and patience, and for your incredible memory of outcrops and road-cuts. The more I understand about sedimentology and stratigraphy, the more amazed I am of your profound insight into these complex and dynamic models.

Jack Loveless, now at Smith College but recently of Harvard and Cornell Universities, exchanged many emails with me during my time at Cornell, providing more academic and personal support than I could have ever predicted after our first 6 months in the SLab together. Your humor and perspective has been incredibly helpful over the years, and I know that my time at Cornell would have been much more difficult without your help. There was never a reason for you to read as many drafts of proposals and letters as you did, and you have been both a true friend and true role model; thank you.

Gregory Hoke at Syracuse University and Manfred Strecker at the University of Potsdam were both incredibly fun and instructive in the field during our junket to the Precordillera to look at high elevation gravels in 2009. I greatly appreciate Manfred's kindness and support as I struggled to learn to read a landscape, as well as his cooking and humor. Greg was also an incredible help during my 2010 field season—I would never have thought to light a fire under the frozen diesel engine without him! Moreover, Greg has been a good friend and a professional supporter of mine over the past several years, and I am grateful for that.

Gregory Kirkpatrick and Chao Shi taught me almost everything I know about MatLab during our overlapping years at Cornell. Despite having had an entire class devoted to MatLab, I learned significantly more from them than any other source. They helped me to read and improve code as well as to think of clever short-cuts. More importantly, Greg and Chao were supportive and generous friends who were always encouraging and always true.

Many other people in the department at Cornell were helpful and supportive during my time here. Suzanne Mahlburg Kay was always a source of interesting and helpful questions during my Andes seminars and our other discussions. I am grateful for the breadth of her knowledge and ability to ponder interesting scientific questions. Jason Phipps Morgan also had a talent for asking interesting questions that I was not expecting during my Andes seminar. Jason also patiently helped me visualize spatial

problems that had initially been far outside my grasp. Steve Gallow is one of the most patient and kind people I know, and is surely the main reason this department is as functional as it is! Finally, the terrific administrative support staff has been incredibly helpful over the past several years. Amy Colvin, Savannah Sawyer, Judy Starr, and everyone who has helped in the front office: thank you for keeping the train on the rails and reaching the station when it should!

Many thanks to my field assistants over the years: Jordan Garroway, Rowan Gaffney, Bill Barnhart, and Rachel Valletta at Syracuse University. They provided me with many laughs during our time in the desert, if nothing else. Whether Rowan was busy inventing 'flip tectonics,' Bill was discovering our gear destroyed by pumas, or Rachel was taking pictures of the condors, I appreciated everyone's valor and willingness to walk for a whole day to take one measurement. I realize that none of you may do more field work in the future, but I am thankful that you were willing to be covered in red dust for weeks on end with me.

My fellow graduate students at Cornell provided me with insightful conversations and interesting Andes seminars, as well as much personal and emotional support during my time here. David Wolf and Danielle Glasgow were two of my earliest friends at Cornell and we had many entertaining outings as well as much sympathizing about graduate school and dogs. Amanda Baker has been a true and loyal friend during our time together in the SLab. Thank you so much for much-needed

sweet treats, words of kindness, scientific insights, and a dedication to one's self. Your humor and emotions have helped me in ways you cannot know. Bill Barnhart was more than just a field assistant: he has been an academic peer with whom I always knew I could have an interesting conversation. Thank you; I know that you will have an opinion about something, even if it is something about which you know almost nothing. Sander Hunter was always up for going dancing, and for talking science, when I needed it most. I so appreciate your kindness and integrity. Naomi Kirk-Lawlor took many beautiful evening strolls with me, and visited me in Vermont to go swimming in streams. Thank you so much for your quiet insights and for your excitement at my latest piece of good news. A girl truly cannot do it alone.

I owe a huge debt of gratitude to my previous academic advisors: Keith Klepeis at UVM, and Janice Hudgings and Michelle Markley at Mount Holyoke. Janice and Michelle especially encouraged me to continue with science when I thought I was at the end of the road. I am grateful to Janice for not giving me a choice about working in her lab: I was to apply for money and work tuning lasers for her whether or not I thought I was going to like it. No one else has ever been more supportive of my scientific career than she, and I am at a loss to describe my gratitude for her faith. I am also indebted to Peter Lynch, my high school science teacher, who taught me why water is weird, and encouraged me to enjoy physics and chemistry. I do not know how Peter managed to

find a love of science in the profoundly literature-biased 16-year old that I was but he did, for which I am grateful.

Much thanks to Rick and his success with the National Science Foundation for funding my time here through NSF grants #EAR-0510785 and #EAR-1019252.

Last but most definitely not least, I owe my family and friends a huge thanks for their support and love. My parents have provided the most open-hearted kind of love and support possible; thank you. Pandora made the trip to Ithaca several times to provide laughter and support when I needed it; thank you. Rachel has spent endless hours discussing everything with me and has recently added 'graduate school' to her repertoire; thank you. My dear friends Amanda Getsinger and Samantha Tilton made me laugh on days I did not think possible, and have always willingly provided love or a much-needed swift kick in the ass; thank you. Finally, a recent addition: great heaping thanks to Alyx Lyons for driving to Ithaca and providing me a respite in the form of a loving home by the lake. Thank you!

TABLE OF CONTENTS

LIST OF FIGURES

LIST OF TABLES

CHAPTER ONE:

Introduction

In Argentina, the central Chilean flat slab region is overlain by the Argentine Precordillera at ~30° S and is the type locality for flat slab subduction (Barazangi and Isacks, 1976). The Precordillera is a thick- and thin-skinned fold-and-thrust belt in the foreland of the Andes that has been deforming since ~20 Ma (Allmendinger et al., 1990; Jordan et al., 1993; Zapata and Allmendinger, 1996). The Precordillera displays all of the surface expressions associated with shallow subduction: a lack of a volcanic arc; thick-skinned basement uplifts in the foreland that are simultaneously active with a thin-skinned thrust belt; increased release of seismic energy; and increased shortening in the foreland (Allmendinger et al., 1990; Cross and Pilger, 1982; Gutscher et al., 2000; Jordan et al., 1983; Jordan et al., 1993; Kay and Abbruzzi, 1996; Kay et al., 1988; Pilger, 1981). The evolution of these features and the development of the flat slab subduction are temporally and spatially correlated, but the details of their development is not clear. For example, previous estimates of shortening magnitude and rates in the Precordillera do not include rigorous uncertainty values or shortening directions throughout the thrust belt (Allmendinger et al., 1990; Cristallini and Ramos, 2000; Jordan et al., 1993; Zapata and Allmendinger, 1996). By examining the details of the development of shortening in

the Precordillera, it may be possible to more clearly relate the shallowing of the Nazca slab and the evolution of the thrust belt.

Shortening in the Precordillera began at ~20 Ma and continues today; the western and central thin-skinned portions of the thrust belt likely evolved in a typical foreland-breaking sequence (Jordan et al., 1993; Siame et al., 2005; Zapata and Allmendinger, 1996). The thick-skinned uplifts in the east and the associated folding of the foreland basin sediments are the youngest features in the Precordillera (Zapata and Allmendinger, 1996). While the thin-skinned thrusts accommodate the majority of shortening in the Precordillera, the thick-skinned folding has only been active for the past 2.7 Ma and may accommodate significant shortening as activity continues.

A comparison of the shortening in the Precordillera and the geometry of the Nazca slab may point to common periods of development. Yáñez and others (2002) propose a model of the shallowing of the slab that overlaps temporally and spatially with the development of the thrusts in the Precordillera. Yáñez and others (2002), building off of the analysis by Gutscher and others (2000) that links aseismic ridges and shallow subduction, suggest that the shape of the subducting Juan Fernández ridge influenced the onset of flat slab subduction. Because the location of the ridge subduction was not stable until ~11 – 10 Ma, shallow subduction was not able to initiate until after the location of the ridge remain fixed below the Precordillera.

Because previous work does not relate the shortening evolution of the Precordillera to the history of the Nazca slab, there is a gap in our understanding of how these processes relate. By collecting field data to reassess both shortening activity and magnitude in the Precordillera, I am attempting to relate the history of both plates to construct a more complete picture of whether shallow subduction influences upper plate deformation history.

This thesis combines structural field data with quantitative analyses of these data to construct a more rigorous assessment of the shortening history of the Precordillera and its relationship to the evolving geometry of the Nazca slab. The field data is primarily fault slip data for the major and minor fault populations throughout the Precordillera, including the strike and dip of the faults, the sense and direction of motion on the fault planes, as well other data to characterize the motion on the fault. I have collected the orientation of strata in hanging and footwalls of a majority of the major thrusts in the region, as well as the orientation of fracture sets in the regions surrounding the faults. I have also documented the location and extent of unconsolidated gravels at high elevations throughout the western Precordillera. My quantitative analyses include calculating the fault plane solutions for fault populations in the Precordillera, as well as area balancing to determine shortening magnitude along several profiles of the thrust belt.

Chapter 2 outlines a new method to calculate shortening of cross sections based on area balancing instead of line-length balancing. This new method is a quantitative approach that relies on an algorithm for calculating the area of a polygon that encloses the deformed area and then restores the area to a wedge with known edge thicknesses but an unknown width. The benefit of using this area balancing method is that the algorithm also allows the user to input known uncertainties on the initial values and then propagate the uncertainties through the calculation to determine an uncertainty value for the shortening magnitude. The uncertainty calculation can determine both errors with a Gaussian distribution as well as a maximum error value. After developing the new method, I then analyze three cross sections along strike in the central Andes to compare the shortening determined via line-length balancing with the area balanced shortening magnitudes.

In Chapter 3, I apply the area balancing method to two profiles across the Argentine Precordillera to calculate shortening and uncertainty values for deformation since 20 Ma. The cross sections are based primarily on structural field data and existing seismic reflection data for the Precordillera. I also determine a shortening activity history for the major faults in the Precordillera and identify three distinct periods of activity. The first period of shortening was from 21.6 – 19.5 Ma as the thrusts in the western Precordillera formed and moved. After a period of quiescence, shortening resumed at ~11 Ma as the many faults in the central Precordillera formed and the faults

in the western Precordillera were reactivated. This phase lasted until ~3 Ma, when motion transferred to the east as the basement-rooted thrusts in the eastern Precordillera began forming the large anticlines in the western portion of the Bermejo basin. Shortening in the western and central Precordillera is ~115 ± 44 km, projecting the decollement well below the high topography of the Andes to the west.

Chapter 4 shows the consistency of shortening directions in the Precordillera even as the shortening activity and magnitudes change. The periods of activity correlate to changes in the geometry of the Nazca slab: low shortening rates from 20 – 11 Ma, sharply increased shortening rates immediately following the shallowing of the slab at ~9 – 8 Ma, and then a reduction in shortening rate at 3 Ma as the plate convergence rate continues to slow. In addition to the shortening rate increasing following the shallowing of the slab, the plate convergence rate slows as the slab shallows. These two phenomena are predicted in models that show an increase in the coupling between the down-going and over-riding plates as the slab shallows. In the models, as the interplate surface area increases, the locking between the plates becomes more efficient, the plate convergence rate is reduced, and strain is accommodated away from the plate boundary and in the foreland. The shortening rates for the Precordillera support such a model.

1.2 References

Allmendinger, R. W., Figueroa, D., Snyder, D., Beer, J., Mpodozos, C., Isacks, B. L., 1990. Foreland shortening and crustal balancing in the Andes at 30ºS latitude. *Tectonics* 9, 789-809.

Barazangi, M., Isacks, B. L., 1976. Spatial distribution of earthquakes and subduction of the Nazca Plate beneath South America. *Geology* 4, 686-692.

Cristallini, E. O., Ramos, V. A., 2002. Thick-skinned and thin-skinned thrusting in the La Ramada fold and thrust belt: crustal evolution of the High Andes of San Juan, Argentina (32ºSL). *Tectonophysics* 317, 205-235.

Cross, T. A., Pilger, R. H., 1982. Control of subduction geometry, location of magmatic arcs, and tectonics of arc and back-arc regions. *Geological Society of America Bulletin* 93, 545-562.

Gutscher, M.-A., Spakman, W., Bijwaard, H., Engdahl, E. R., 2000. Geodynamics of flat subduction: Seismicity and tomographic constraints from the Andean margin. *Tectonics* 19, 814-833.

Jordan, T. E., Allmendinger, R. W., Damanti, J. F., Drake, R. E., 1993. Chronology of motion in a complete thrust belt: The Precordiller, 30–31ºS, Andes mountains. *Journal of Geology* 101, 135-156.

Jordan, T. E., Isacks, B. L., Allmendinger, R. W., Brewer, J. A., Ramos, V. A., Ando, C. J., 1983. Andean tectonics related to geometry of subducted Nazca plate. *Geological Study of America Bulletin* 94, 341-361.

Kay, S. M., Abbruzzi, J. M., 1996. Magmatic evidence for Neogene lithospheric evolution of the central Andean "flat-slab" between 30ºS and 32ºS. *Tectonophysics* 259, 15-28.

Kay, S. M., Maksaev, V., Mpodozis, C., Moscoso, R., Nasi, C., Gordillo, C. E., 1988. Tertiary Andean magmatism in Argentina and Chile between 28–33ºS: Correlation of magmatic chemistry with a changing Benioff zone: *Journal of South American Earth Sciences* 1, 21-38.

Siame, L. L., Bellier, O., Sébrier, M., Araujo, M., 2005. Deformation partitioning in flat subduction setting: Case of the Andean foreland of western Argentina (28ºS–33ºS). *Tectonics* 24, TC5003, doi:10.1029/2005TC001787.

Yáñez, G., Cembrano, J., Pardo, M., Ranero, C., Selles, D., 2002. The Challenger–Juan Fernández–Maipo major tectonic transition of the Nazca–Andean subduction system at 33–34ºS: geodynamic evidence and implications. *Journal of South American Earth Sciences* 15, 23-38.

Zapata, T. R., Allmendinger, R. W., 1996. Thrust-front zone of the Precordillera, Argentina: A thick-skinned triangle zone. *AAPG Bulletin* 80, 359-381.

CHAPTER TWO:

Assessing uncertainties in balanced cross sections[1]

2.1 Abstract

Balanced structural cross sections are models that are fit to incomplete data. The models are under-constrained with respect to any particular two-dimensional line- length model, but enough data generally exists to yield a well constrained area balance solution. Furthermore, the area balance encompasses all possible line-length solutions. Therefore, where the primary objective of section balancing is the determination of horizontal shortening magnitude, area balancing provides an analytical solution. We use this analytical solution to develop a comprehensive, robust analysis of the uncertainty in shortening estimates resulting from cross section balancing. The analytical solution allows us to propagate errors formally on the input parameters—stratigraphic thicknesses, depth to decollement, eroded hanging wall cutoffs—through the equations and produce the resulting uncertainty on the magnitude of shortening. Balanced cross sections from the Subandean belt of the Central Andes are used to demonstrate the relative importance of stratigraphy and eroded hanging wall cutoffs in the contribution to the overall error.

---

[1] A version of this chapter was originally published as: Judge, P.A. and R.W. Allmendginer (2011): Assessing uncertainties in balanced cross sections, *Journal of Structural Geology, 33,* 478–467, doi: 10.1016/j.jsg.2011.01.006. Reprinted with permission of Elsevier.

2.2 Introduction

Balanced cross sections have been a fundamental tool of the structural geologist for more than 50 years, providing both a geometric model of the subsurface as well as an estimate of the shortening in a specific region of an orogen. Once derived, shortening magnitudes are often used as input "data" for large scale geologic models, such as geodynamic models or palinspastic restorations. For example, Kley and Monaldi (1998) use surface shortening estimates in the Central Andes to suggest that crustal thickness cannot be derived from shortening alone, and thus call on underplating or flow of lower crustal material to produce the excess thickening. While this type of analysis may help advance tectonic modeling, these models rely on shortening data that do not include a rigorous assessment of the uncertainty. Without a standardized way to assess the goodness of fit of a specific balanced cross section to the data on which it is based, no independent method exists to determine the validity of conclusions based on shortening estimates from line-length balanced sections.

Though often well known to the structural geologist who constructed the original line-length balanced section, users of the calculated shortening values may overlook the uncertainty inherent in any cross-sectional model as well as the fact that the cross sections are extrapolated from incomplete data. Viable cross sections may follow generalized rules for construction, assuring that the cross section does not violate

physical laws such as the continuity and compatibility equations. Such rules, however, do not guarantee that a calculated shortening value has negligible uncertainty.

We present a new method to calculate a rigorous estimate of uncertainty in shortening values from regional line-length balanced sections. This method includes all potential sources of error on input parameters except for the assumption of plane strain deformation. Based on area balancing, the method encompasses all possible kinematic fold-fault models, accommodates shortening due to plane strain deformation smaller than the scale of the cross section, and is computationally simple. By including a full assessment of the uncertainties in a cross section, it is possible to propagate formally the known, measurable uncertainties from the input data through the shortening calculation and determine an uncertainty estimate for the final shortening value.

To demonstrate the application of the concept, we test the method on several cross sections from the Subandean belt of the Central Andes. We compare between blind and emergent thrust belts, as well as sections drawn by the same and different authors. While we describe the results of the formal approach, the primary outcome from this test is to emphasize that the goodness of the calculated uncertainty values depends on the goodness of the initial uncertainties on the input data.

2.3 Existing methods of cross section construction

The physical justification for all section balancing methods arises from the continuity equation, which states that the change in density of a volume with respect to time plus the flux of mass into and out of the volume must be equal to zero (e.g., Malvern, 1969). In volume balancing, we assume that the change in density with time is also zero, yielding the incompressibility condition, requiring the divergence of the velocity field to be zero. For area balancing, one additional condition is required: plane strain, or the condition that there is flow of material only in the plane of the cross section. This final condition is justified where structures are long and continuous parallel to strike, as is true in many thin-skinned fold thrust belts. Specific fold-fault models, including trishear (Zehnder and Allmendinger, 2000), fault bend- and fault propagation folding (Hardy, 1995; Hardy, 1997), explicitly use incompressibility, but the majority of balanced cross sections are geometry-specific and therefore more restrictive.

2.3.1 Line length balancing

Line-length balanced cross sections are a subset of area balanced sections. In addition to the assumptions inherent to area balancing, line length balancing relies on the assumption that parallel folding occurs via shear parallel to bedding, making the stratigraphic horizons lines of no finite longitudinal extension. Thus, the shortening magnitude is the difference between bed length in the deformed state and the same bed in the undeformed state. This method requires a cross sectional model of the subsurface

geometry that tries to replicate the subsurface geology and is governed by generalized empirical rules to help insure viability (Bally et al., 1966; Dahlstrom, 1969; Elliott, 1983; Price and Mountjoy, 1970; Woodward et al., 1989).

Shortening values from line length balancing are commonly cited as a "minimum estimate," which is typically the only uncertainty referenced. This minimum estimate arises where the hanging wall cutoffs of emergent thrusts in a section have been eroded (Fig. 2.1). Because the geologist does not know how much bed length is missing due to erosion, the stratigraphic horizons are lined up to make the displacement as small as possible in the restored section.

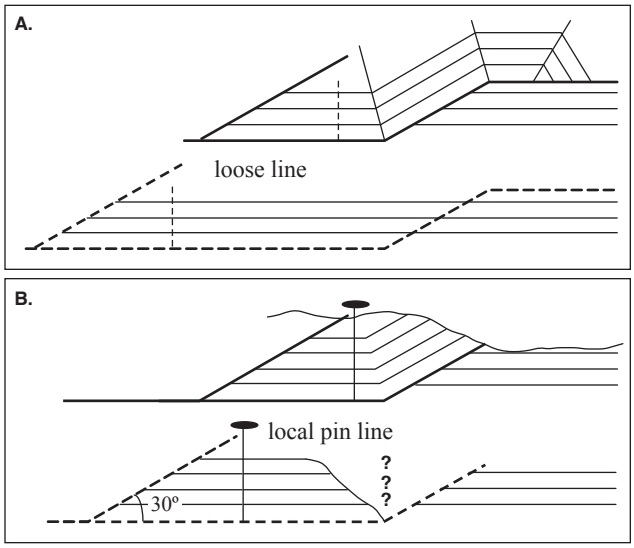

Fig. 2.1: Cross section illustrating the "minimum shortening estimate" commonly associated with line-length balanced sections. (A) shows the actual section in the absence of erosion; (B) shows the same section where the hanging wall cutoff has been eroded. The restoration in the bottom panel of (B) is a minimum because the geologist does not know how far to the right the hanging wall ramp would lie.

However, eroded hanging wall cutoffs are only one of many potential sources of uncertainty in a balanced section and thus "minimum estimate" is misleading (Allmendinger, 2004; Elliott, 1976; Sheffels, 1990). Errors may also arise due to uncertainties in depth to decollement, incorrect structural model of the subsurface, poorly known initial stratigraphy, and deformation at scales smaller than the resolution of the section (e.g., Marrett and Allmendinger, 1992). One possible way to account for variation in shortening from all but the last of these sources of error would be to draft a large suite of line-length balanced sections along the same transect, spanning the range of possible internal geometries and initial conditions in a type of hand-crafted Monte Carlo simulation. Though possible for individual structures amenable to numerical simulation (e.g., Allmendinger, 2004; Brooks et al., 2000), this approach is impractical for regional sections across many structures.

2.3.1 Area balancing

Area balancing, based only on the assumption that the cross sectional area of the modern, deformed thrust belt is equal to the area of the undeformed stratigraphic section (Chamberlin, 1910; Chamberlin, 1919b; Chamberlin, 1919a; Chamberlin, 1923; Hossack, 1979; Mitra and Namson, 1989), is a more generalized method than line length balancing. Because area balancing provides a method of calculating shortening that does not depend on one specific subsurface geometric interpretation, the method does

not provide the geometric or temporal resolution of line length balancing. However, this independence is also the greatest strength of area balancing: the method encompasses any two-dimensional kinematic fold model that fills the required area and captures all scales of deformation. This attribute of area-balanced cross sections that makes them uniquely suited to the task of determining uncertainty in shortening magnitude.

2.4 Error analysis via area balancing

The horizontal shortening in any balanced section is the difference between the initial and final widths of the section, which is not the same as the principal shortening axis (e.g., Cladouhos and Allmendinger, 1993). For area balancing, we define the initial area as a simple polygon defined by the stratigraphic thicknesses and their uncertainties at each end and the initial width, which is unknown at the start of the calculation (Fig. 2.2). Unlike the case of line length balancing, the areas in both the initial and the final (i.e., deformed) state can be calculated analytically. Thus, the errors can be propagated formally, a major advantage of this approach. We use the terms “uncertainty” and “error” interchangeably.

2.4.1 Analytical determination of shortening and error propagation

For the area of the deformed section, we use the concept of an enveloping polygon to encompass the pre-growth strata in the section. The area of any polygon can be described analytically as (e.g., Harris and Stocker, 1998):

$$A = \frac{1}{2}\sum_{i=0}^{n-1}\left(x_i y_{i+1} - x_{i+1} y_i\right), \tag{2.1}$$

where A is the area of the polygon, n is the number of vertices in the polygon, and (x_i, y_i) are the Cartesian coordinates of each vertex. The calculated uncertainty, or error, on the deformed area (δA) is a function of the uncertainty on each specific vertex (δx_i, δy_i) (Fig. 2.1A). As discussed below, these uncertainties encompass both those associated with eroded hanging wall cutoffs and depth to decollement. By assuming a Gaussian distribution of uncertainty values, we use the standard formula to propagate error through the area calculation (Bevington and Robinson, 2003; Taylor, 1997), known as the sum in quadrature:

$$\delta A = \sqrt{\left(\frac{\partial A}{\partial x_1}\delta x_1\right)^2 + \left(\frac{\partial A}{\partial y_1}\delta y_1\right)^2 + \cdots + \left(\frac{\partial A}{\partial x_n}\delta x_n\right)^2 + \left(\frac{\partial A}{\partial y_n}\delta y_n\right)^2}\,. \tag{2.2a}$$

If the errors are not random and uncorrelated, then one should use, instead, the maximum error estimate:

$$\delta A \le \left|\frac{\partial A}{\partial x_1}\right|\delta x_1 + \left|\frac{\partial A}{\partial y_1}\right|\delta y_1 + \cdots + \left|\frac{\partial A}{\partial x_n}\right|\delta x_n + \left|\frac{\partial A}{\partial y_n}\right|\delta y_n\,. \tag{2.2b}$$

In the rest of this paper, we will show the error in quadrature in equation "a" is accompanied by the maximum error estimate in equation "b".

Because the deformed area must equal the undeformed area, the initial width of the section ($W_i \pm \delta W_i$) can be calculated from the area in Eq. (2.1) and the two

stratigraphic thicknesses at the "west" and "east" ends of the section (T_W, T_E) (Fig. 2.1A):

$$A = \left(W_i T_E\right) + \left(W_i \frac{\left(T_W - T_E\right)}{2}\right) = W_i \left(\frac{T_W + T_E}{2}\right). \tag{2.3}$$

The original width is calculated by rearranging Eq. (2.3):

$$W_i = \frac{2A}{\left(T_E + T_W\right)} = 2A\left(T_E + T_W\right)^{-1}. \tag{2.4}$$

By definition, A in equations (2.3) and (2.4) must be the same as A in equation (2.1). The uncertainty for the initial width is:

$$\delta W_i = \sqrt{\left(\frac{\partial W_i}{\partial A}\delta A\right)^2 + \left(\frac{\partial W_i}{\partial T_E}\delta T_E\right)^2 + \left(\frac{\partial W_i}{\partial T_W}\delta T_W\right)^2} \tag{2.5a}$$

$$\delta W_i = \left|\frac{\partial W_i}{\partial A}\right|\delta A + \left|\frac{\partial W_i}{\partial T_E}\right|\delta T_E + \left|\frac{\partial W_i}{\partial T_W}\right|\delta T_W \tag{2.5b}$$

where δT_W and δT_E are the uncertainties on stratigraphic thicknesses and δA is the area error calculated in equation (2.2).

Finally, knowing the initial width ($W_i \pm \delta W_i$) and the final, deformed width ($W_f \pm \delta W_f$) (Fig. 2.1) allows us to calculate the shortening, S, and its uncertainty, δS, across the fold and thrust belt:

$$S = W_f - W_i \tag{2.6}$$

and

$$\delta S = \sqrt{\left(\frac{\partial S}{\partial W_i}\delta W_i\right)^2 + \left(\frac{\partial S}{\partial W_f}\delta W_f\right)^2}\,. \tag{2.7a}$$

$$\delta S = \left|\frac{\partial S}{\partial W_i}\right|\delta W_i + \left|\frac{\partial S}{\partial W_f}\right|\delta W_f \tag{2.7b}$$

We can also calculate the percent horizontal shortening and its error:

$$S_{\%} = 1 - \frac{W_f}{W_i} = 1 - W_f W_i^{-1}\,, \tag{2.8}$$

and

$$\delta S_{\%} = \sqrt{\left(\frac{\partial S_{\%}}{\partial W_i}\delta W_i\right)^2 + \left(\frac{\partial S_{\%}}{\partial W_f}\delta W_f\right)^2} \tag{2.9a}$$

$$\delta S_{\%} = \left|\frac{\partial S_{\%}}{\partial W_i}\right|\delta W_i + \left|\frac{\partial S_{\%}}{\partial W_f}\right|\delta W_f\,. \tag{2.9b}$$

To calculate the uncertainty in shortening magnitude and percentage, errors must be specified for the input parameters: the vertices of the enveloping polygon, the stratigraphic thicknesses at the two ends of the line of section, and the deformed width of the thrust belt (Fig. 2.2). The errors for the enveloping polygon, δx_i and δy_i, encompass both the uncertainties in the depth to the decollement and those associated

with any eroded hanging wall cutoffs. Independent uncertainties are assigned to each vertex such that contacts at the surface generally have negligible error but those in the subsurface have greater error, and those at eroded hanging wall cutoffs have the greatest uncertainty of all. The errors on the stratigraphic thicknesses, δT_E and δT_W, would ideally come from measured sections where available, but more commonly will come from map thicknesses, which would likely have larger errors. All other sources of error are propagated from δx_i, δy_i, δT_E, and δT_W (Fig. 2.1A).

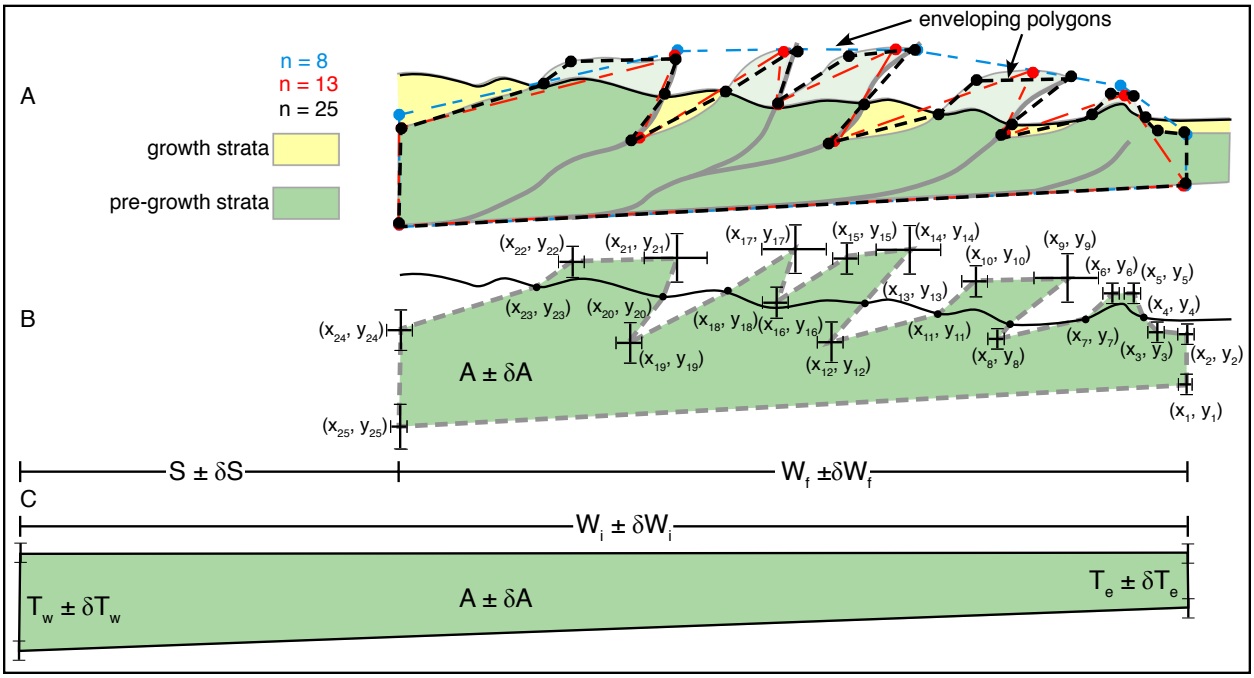

Fig. 2.2: Hypothetical area balance with attendant uncertainties. Three different "enveloping polygons" are shown in (A) with increasing number of vertices and thus increasing complexity. (B) Assignment of hypothetical uncertainties (error bars) to each of the 25 vertices in the most complex enveloping polygon. (C) The stratigraphic wedge in the initial state, as well as the horizontal shortening. Variables are the same as those used in the text.

2.4.2 Minimal polygon complexity necessary to capture accurate shortening

Using polygons to envelop the cross sectional area raises the important question of how complex the polygon must be to capture accurately the shortening for the region. One can imagine two extremes: a simple rectangle enclosing the entire deformed area or a very complex polygon with hundreds of vertices that replicates the outline of the specific line-length balanced cross section. Between these two cases lies an ideal polygon that captures the minimum complexity needed to calculate a robust, stable area estimate but is not heavily reliant on the modeled subsurface geometry. While a polygon with 5 vertices is clearly a poor estimate of the subsurface geology (Fig. 2.2), a polygon with 75 vertices would likely be overly restrained by the originally proposed line-length balanced model.

To determine the minimum number of vertices necessary for a robust shortening calculation, we iterate the analysis with increasingly complicated enveloping polygon geometries (Fig. 2.2) until the solutions for both the shortening magnitude and uncertainty stabilize (Fig. 2.4). For the Subandean test cases described in the subsequent section of this paper, the shortening solutions stabilize for polygons of approximately 20 or more vertices, far fewer than needed to capture the exact outline of the line-length balanced section on which the polygons are based. This stability is likely due to compensating errors: after 15 or 20 vertices, adding another vertex, with its associated uncertainty, does not significantly change the overall solution. However, it is true that

some crude approximation of the line-length section is also necessary, reflecting the fact that the polygons with fewer vertices invariably include a significant amount of growth strata or air that was never filled with subsequently eroded rock.

2.5 Test cases from the Subandean Belt

To demonstrate the application of our area balancing method, we use three sections from the Subandean belt of Bolivia and northern Argentina (Fig. 2.3), two dominated by emergent thrusts (McQuarrie, 2002; McQuarrie et al., 2008) and the other blind (Echavarría et al., 2003). These three sections allow us to compare the results of sections drawn by the same authors (McQuarrie, 2002; McQuarrie et al., 2008) and to compare between different authors (Echavarría et al., 2003; McQuarrie, 2002). The quality of our error analysis depends on using reliable uncertainties on the input data; one of the authors of this paper (RWA) was involved with the construction of the Echavarría cross section and Nadine McQuarrie (pers. comm., 2010) has graciously shared her insight on the uncertainties involved in the construction of her sections. We show the input parameters and uncertainties that we used in our analysis in Table 2.1 and the shortening results based on those values, compared to previous work, in Table 2.2. However, the best practice, as described below, is a rigorous assessment of errors on the input parameters during cross section construction. Thus the results presented in these test cases should be viewed as a proof of concept.

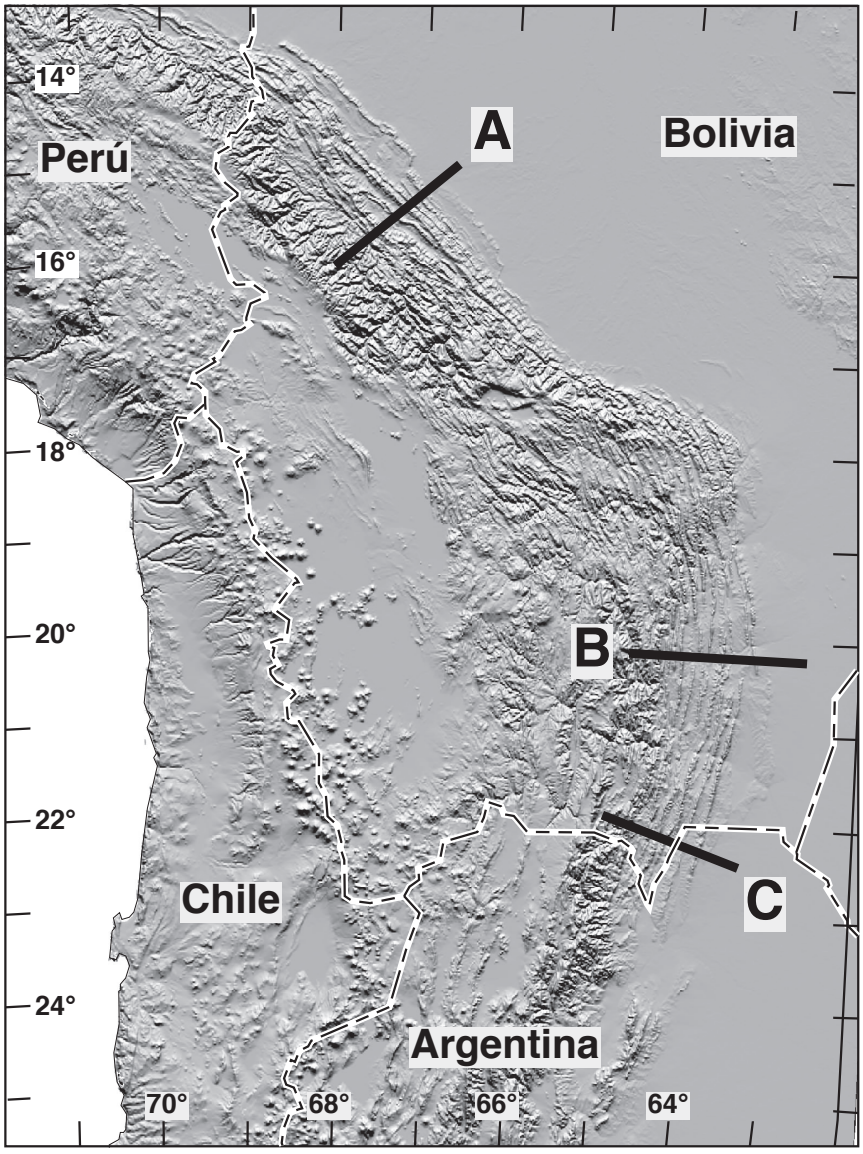

Fig. 2.3: Location map of the Central Andes showing the balanced cross-sections analyzed from the Subandean belt. Sections A and B, located in Bolivia, were published and described by McQuarrie (2002) and McQuarrie et al. (2008); section C, located in northernmost Argentina, was published by Echavarría et al. (2003). Shaded relief topography rendered from the GTOPO30 data set.

2.5.1 Bolivian sections

Our area balancing method yields 75 ± 27 km of shortening when applied to the northern Bolivia section and 64 ± 17 km for the southern section (table 2.2, Fig. 2.4). Our estimates do not include shortening on the trailing thrusts in the sections. These uncertainties on shortening have been calculated based on input error values for the deformed width, the location of each polygon vertex, and for the stratigraphic thicknesses in the undeformed state (table 2.1). To examine the effect that a single parameter (e.g., stratigraphic thickness, decollement depth, or eroded hanging wall cutoffs) has on the total uncertainty, we set all errors, except for the parameter of interest, equal to zero and then ran the analyses over again (table 2.3). Note that total error should generally be less than the sum of the individual errors for a Gaussian distribution. If the input uncertainties are not independent and uncorrelated, then the errors no longer have a Gaussian distribution and one would use the maximum error estimate, which is considerably larger (table 2.2).

Percent shortening is a more ambiguous measure because it is so highly dependent on initial and final lengths. Nonetheless we cite them here because McQuarrie et al. (2008) claimed there was a significant difference between percent shortening in the northern and southern cross sections. As shown in table 2.2, the shortening percentage values for the two regions in Bolivia are similar to those calculated via line length balancing. This is not surprising given that we used

McQuarrie's sections as the starting point for our area analysis. However, the errors that we calculate are three to five times larger than the 2% error cited by McQuarrie et al. (2008). The considerable overlap in error envelopes for the two sections (Fig. 2.4) shows that their conclusion of a coupling between tectonics and climate based on similar shortening percentages is not robust.

Table 2.1. Reference case inputs

Measured and calculated values	*Northern Bolivia*	*Southern Bolivia*	*N. Argentina*
Stratigraphic thicknesses & errors	2.1 ± 0.8 km 8.10 ± 1.2 km	5.6 ± 0.8 km 8.5 ± 0.8 km	2.9 ± 0.6 km 4.6 ± 0.4 km
Final (modern) width & errors	96 ± 1 km	113 ± 1 km	82 ± 1 km
Decollement error	± 0.75 km	± 0.75 km	± 0.5 km
Subsurface vertices error	± 0.8 km	± 0.8 km	± 0.6 km
Surface vertices errors	± 0.1 km	± 0.1 km	± 0.1 km
Eroded hanging wall errors	± 3.0 km	± 3.0 km	± 1.0 km

Table 2.2. Comparison of previous line-length balancing with area balancing results

Shortening calculation	*Northern Bolivia*	*Southern Bolivia*	*N. Argentina*
Line-length balance (McQuarrie, 2002; Echavarría et al., 2003)	66 ± 7 km 41 ± 2 %	67 ± 7 km 32 ± 2 %	45 km
Area balance ± Gaussian error (this study)	75 ± 27 km 44 ± 9 %	64 ± 17 km 36 ± 6 %	48 ± 15 km 37 ± 7 %
Area balance ± Maximum error (this study)	75 ± 72 km 44 ± 24 %	64 ± 49 km 36 ± 18 %	48 ± 44 km 37 ± 22 %

Fig. 2.4: Example of area balancing from northern Bolivia. (A) Cross section from the northern Bolivian Subandean belt, modified after McQuarrie (2002). Heavy black polygon shows the pre-growth strata used in the analysis. (B) Suite of enveloping polygons with increasing number of vertices corresponding to the data points for the northern section shown in Figure 4E. Simple polygon below represents the initial stratigraphic wedge. (C) Geologic cross section for the southern Bolivian Subandean Belt, modified after McQuarrie (2002). Heavy black polygon shows the pre-growth strata used in the analysis. (D) Suite of enveloping polygons with increasing number of vertices corresponding to the data points for the northern section shown in Figure 4E. Simple polygon below represents the initial stratigraphic wedge. (E) Plot of number of polygons in the enveloping polygon versus horizontal shortening magnitude in kilometers for both the northern and the souther sections of McQuarrie (2002). Error bars show the uncertainty at each point in the analysis; note overlap of error bars for northern and southern sections. The solution stabilizes at 20 or fewer vertices.

A.

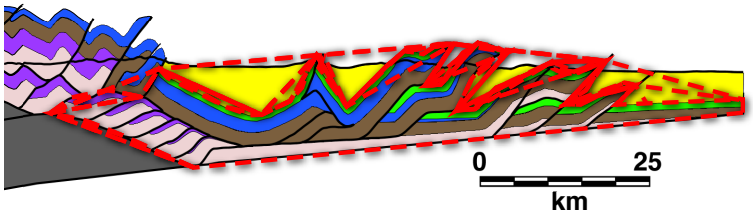
0
25
km

B.

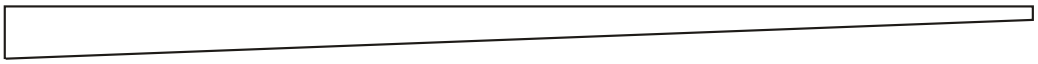

C.

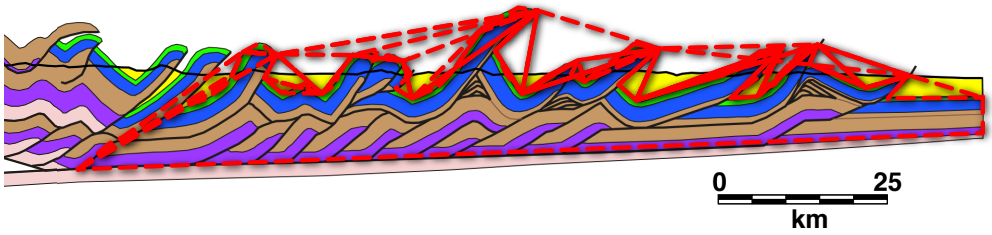
0
25
km

D.

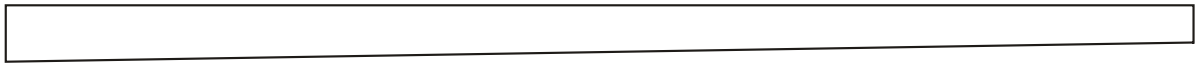

E.

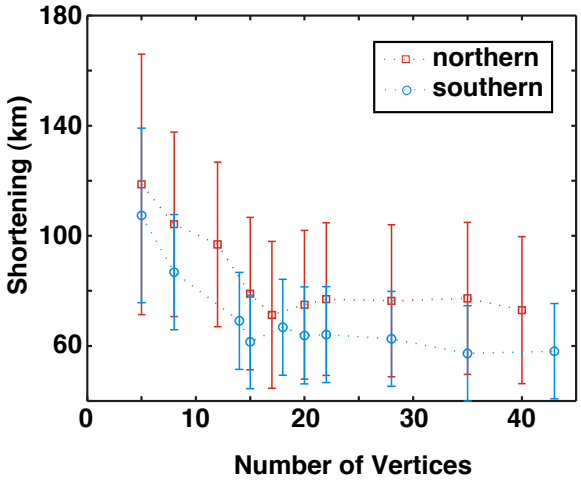
180
140
100
60
Shortening (km)
0
10
20
30
40
Number of Vertices
northern
southern

2.5.2 Argentine section

To analyze the differences in uncertainty values for sections dominated by blind thrusts as compared to emergent thrusts, we calculate shortening and uncertainty values for the section in northern Argentina (Echavarría et al., 2003). For simplicity, we balance the section to the east of the Nogalito Range (Fig. 2.5) because, west of this range, the section, as drawn, cuts into the basement thrust. We calculate 48 ± 15 km shortening for the eastern part of the section, compared to 45 km shortening determined via line length balancing (Echavarría et al., 2003). As in the case of the Bolivian sections, Table 2.3 shows the effect that each parameter has on the overall error.

The shortening and uncertainty results from area balancing for the two southernmost sections are very similar: 36 ± 6% for the Bolivian section (McQuarrie et al., 2008) and 37 ± 7% for the northern Argentine section (Echavarría et al., 2003). The percent shortening values for both sections agree with those calculated via line length balancing, and it is the similarity between the uncertainty values that is noteworthy. While the region in Argentina and southern Bolivia is well studied, with both seismic and drill hole data available (Belotti et al., 1995; Dunn et al., 1995; Sempere, 1995), the section in northern Bolivia is not as well known. However, we use similar initial uncertainty values for all three sections to demonstrate the method and not to determine definitively the uncertainty associated with each section.

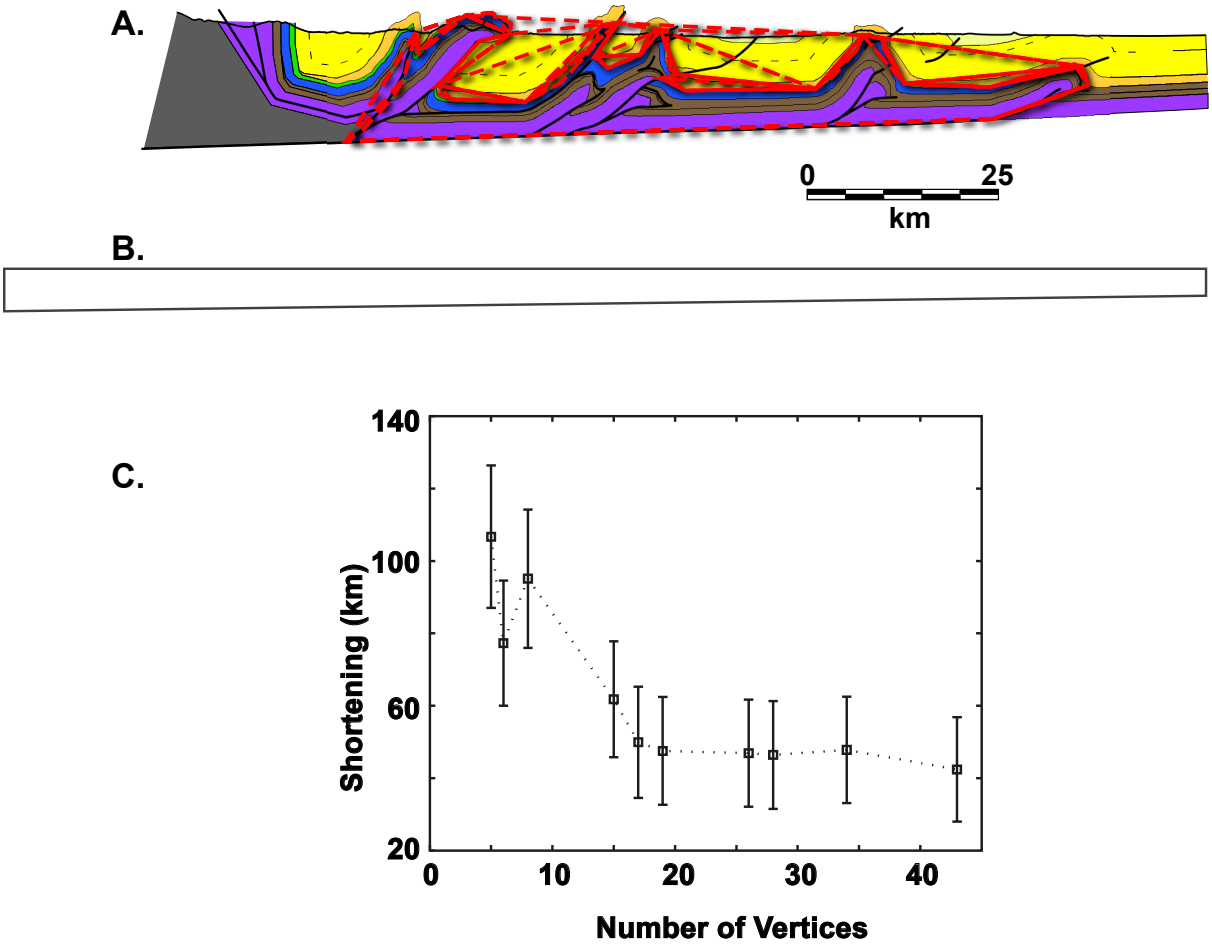

Fig. 2.5: Diagram similar to figure 4, showing the results of the analysis of Echavarría et al.'s (2003) cross section from the northern Argentine Subandean belt. (A) Geologic cross section for the southern Bolivian Subandean Belt, modified after Echavarría et al. (2003). Heavy black polygon shows the pre-growth strata used in the analysis. (B) suite of enveloping polygons with increasing number of vertices corresponding to the data points for the northern section shown in Figure 4E. Simple polygon below represents the initial stratigraphic wedge. (C) Plot of number of polygons in the enveloping polygon versus horizontal shortening magnitude in kilometers. Error bars show the uncertainty at each point in the analysis.

2.5.3 Sensitivity of Total Error to Different Parameters

As is abundantly clear from these Subandean examples, the error on stratigraphic thickness is a major source of shortening uncertainty. In all sections, 8 to 40% error in stratigraphic thicknesses on the two ends of a cross section accounts for 80% or more of the total error in shortening determination (Table 2.3). Even for a reasonably well known section, a 10% uncertainty in stratigraphic thickness contributes 50-75% of the overall shortening error. If one's only objective were to calculate shortening, significantly greater reduction in errors could be achieved through field studies necessary to improve knowledge of stratigraphic thickness than one could produce by carrying out a much more expensive program of subsurface exploration. Granted, other advantages exist to collecting data from subsurface exploration, especially the knowledge of subsurface geometry.

Table 2.3. Contributions to total error

Error	*Northern Bolivia*	*Southern Bolivia*	*N. Argentina*
Total	± 27 km	± 17 km	± 15 km
From stratigraphic thickness	± 24 km	± 16 km	± 12.5 km
From decollement	± 7 km	± 1 km	± 1.1 km
From eroded hanging wall	± 2 km	± 4 km	± 1.2 km

The relative importance of decollement depth and eroded hanging wall cutoff depend on the specific sections (Table 2.3). In a fully emergent belt with a large number of eroded hanging wall cutoffs, the contribution of this factor to the overall uncertainty would increase. In line length balancing, because one determines the initial width simply by adding up the lengths of individual beds, the uncertainty in hanging wall cutoff would translate directly into shortening magnitude uncertainty. This is not the case in area balancing. For example, the Argentine section has one major eroded hanging wall cutoff, changing the uncertainty in that cutoff from 1 to 5 km only changes the uncertainty in shortening by 1 km (from ± 15 km to ± 16 km) for the reference case.

2.6 Accurate determination of errors on input parameters

As the test cases show, accurate determination of input errors is critical. Our method does not alleviate this task but only makes it clear what the key parameters are and, once determined, how to propagate those errors through the calculation to produce realistic errors for shortening magnitude.

2.6.1 Deformed state: The enveloping polygon

Assigning uncertainty to each of the vertices in the enveloping polygon accounts for a number of different types of geological errors. While there is uncertainty inherent to choosing a specific fold kinematic model, an area balancing method eliminates this

uncertainty by accommodating all cylindrical fold models that can occupy the same area.

The vertices at the base of the polygon describe the position and uncertainty in the decollement depth and dip. The errors assigned to these vertices would depend on the source and quality of data—borehole, reflection seismic, and stratigraphic—that the geologist used to identify the decollement. If stratigraphic data are used to define the decollement depth, then the assumption that the errors are random and uncorrelated would not be valid, requiring the use of the maximum error estimate (e.g., Table 2.2) rather than assuming a Gaussian distribution. Other errors on subsurface vertices would likewise depend on the availability and quality of subsurface data. For example, is a broad syncline of growth strata imaged clearly on seismic data or is it pierced by a well? Depending on the placement of each vertex and the quality of the available data, the uncertainty associated with a specific polygon could be quite variable.

The errors on the vertices that lie above the present erosional surface present different challenges. Where the faults are largely blind, one can geometrically project the crest of an eroded anticline based on stratigraphic thickness and some basic assumptions of fold kinematic model (or range of models). The largest individual uncertainties on vertices in the deformed state probably are those associated with eroded hanging wall cutoffs, though they do not contribute that much to the overall uncertainty. Although these are accommodated via minimum shortening estimates in

line-length sections, there is a reasonable maximum projection of the hanging wall cutoff as well. If the section of interest lies close to the tip line of an emergent thrust, one could use an up-plunge projection and some model of the displacement gradient profile along a fault (Higgs and Williams, 1987; Marrett and Allmendinger, 1990; Walsh and Watterson, 1987; Walsh and Watterson, 1989) to determine where the now eroded hanging wall cutoff should lie. More commonly, we suspect, people will use their intuition as to the probable location of the cutoff and simply select a large uncertainty.

2.6.2 Initial state: the stratigraphic wedge

As we have seen, uncertainty in initial stratigraphic thickness is a major source of error that is rarely included in line-length sections. To estimate this uncertainty, as well as improve the overall shortening estimate, one might measure several stratigraphic sections at either end of the now deformed package. Alternatively, because data on balanced cross-sections are commonly projected from a corridor of finite width on either side of the section, one might use the variation in map thickness that occur along strike within that corridor.

As mentioned previously, one source of error in balanced sections is the shortening that occurs at scales below the resolution of the section (Marrett and Allmendinger, 1990; Marrett and Allmendinger, 1991; Marrett and Allmendinger, 1992). This might include initial layer parallel shortening, pervasive minor faulting and

folding, pressure solution and cleavage development, etc (e.g., Geiser, 1988; Groshong and Epard, 1994; Groshong, 1994; Hossack, 1979). Hypothetically, simply by doing an area balance, we capture this deformation as well. However, the ability to do so depends on one's ability to determine true initial stratigraphic thickness prior to the start deformation. Because we measure stratigraphic sections today, in the deformed state, it is much more difficult to ensure that deformation due to pervasive mechanisms have not been included in our determination of stratigraphic thickness.

Pressure solution and cleavage development are commonly associated with volume loss, bringing into question the plain strain and constant volume or area assumptions. Area loss balanced by area gain in another part of the section presents no particular challenges to the error propagation method described here. An average net area loss from the entire section could easily be accommodated by adding a term expressing that average area loss (and uncertainty) to eqn. (2). It would be very difficult to determine an accurate average area loss, however.

2.6.3 What is the true magnitude of the shortening?

Determining a single value of shortening magnitude for a belt is somewhat ambiguous and arbitrary, and percent shortening is even more fuzzy. Take the case of McQuarrie's section in southern Bolivia (McQuarrie, 2002; McQuarrie et al., 2008). The regional pin lines are located 10-15 km east of the thrust front, which reduces the percent shortening

by inclusion of a significant width of undeformed section, but does not affect the magnitude of shortening. More subtle, but equally important, in a line-length balanced section, different stratigraphic horizons can have different shortening magnitudes because of internal duplexing of some layers but not others (McQuarrie, pers. comm., 2010). Where one knows the structural geometry a priori, this could be very important because the initial undeformed polygon would not be a simple wedge as we have portrayed it but a more complicated polygon, with multiple steps on the internal side (Fig. 2.6). However, we usually do not know the structural geometry ahead of time and duplexes are commonly used to accommodate space problems that may actually arise from poorly known stratigraphy. Finally, the present day width of a belt is commonly determined by its width at the surface, but its maximum width at depth is longer because of the dip of the trailing thrust. McQuarrie (McQuarrie, 2002) avoided this ambiguity by defining the Subandean belt by the basement cutoff. This definition is not without problems—McQuarrie et al. (2008) use a different and more traditional definition— both because the we do not know the location of that cutoff, and because it results in provinces that overlap (i.e., the eastern boundary of the Interadean belt lies east of the western boundary of the Subandean belt). Using one measure rather than the other can change the magnitude of shortening by many kilometers, even though the shortening error does not change much because the uncertainty on final width contributes little to the overall error.

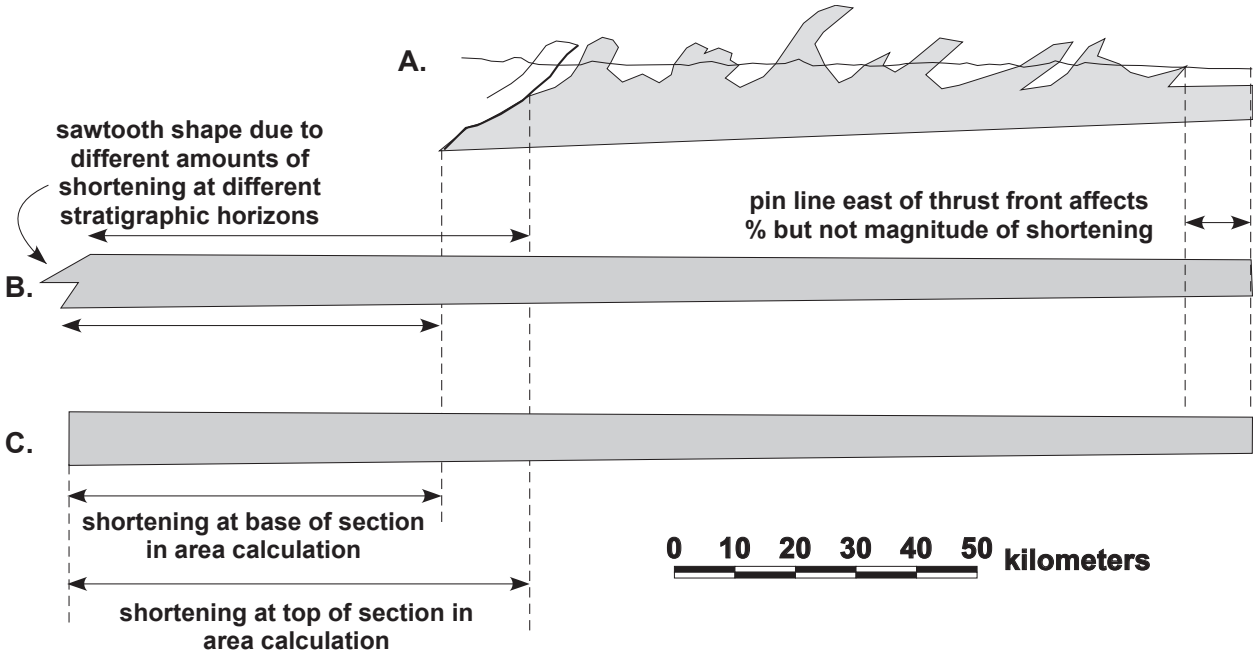

Fig. 2.6: Illustration of the ambiguities of the shortening magnitude calculation. (A) outline of the deformed pre-growth strata for the southern Bolivia cross section (McQuarrie, 2002). (B) Outline of McQuarrie's (2002) line-length reconstruction of the the section in (A). Note the sawtooth left side of the section is due to different amounts of shortening at different stratigraphic horizons. (C) The equivalent area balance of the deformed gray polygon shown in (A). Horizontal double headed arrows show different permissible values of shortening magnitude.

2.6.4 Can we determine true probabilistic uncertainties?

Ideally, one would like to be able to state the shortening at, the alpha-95 confidence level, for example. The error propagation that we describe here would allow for this but the real question is whether the input data allow for the determination of true probabilistic uncertainties, which depend on repeated measurements of the same parameter. While one can imagine approaches to determine the one or two sigma error on the depth to decollement or the stratigraphic thickness at one end of the cross section or the other, these approaches would probably require more effort than most people have traditionally put into balanced cross section construction.

What, then, is the advantage of carrying out error propagation if the probabilistic errors will not routinely be determined? Most importantly, it is the best way of quantitatively linking the uncertainty on the input parameters, even if determined only informally, to the likely error on the shortening. More specifically, error propagation provides a mechanism for investigating the effects of different types of uncertainty on the final solution. Most obvious is the previously under-appreciated effect of stratigraphic thickness, but this also applies to the relative importance of uncertainty in decollement position or eroded hanging wall cutoffs for any particular section. Finally, it provides a mechanism for specifying where one's preferred line-length solution lies within the range of plausible solutions due to all different types of fold kinematic models.

2.7 Conclusions

Calculating the magnitude of shortening in a mountain belt is the end result of a structural model that is constructed from data which have quantifiable errors. Without propagating these errors through the analysis, structural geologists have no scientifically legitimate way of determining whether two parts of an orogen have distinct shortening values and therefore that external processes, climate, or plate boundary interactions explain those differences. Likewise, other uses of structural shortening data—geodynamic modeling, paleogeographic reconstructions, etc.—are equally suspect if the uncertainty on their input data, the shortening value, cannot be quantified accurately.

Line-length balanced sections with errors assessed via area balancing are entirely complementary. Line-length balanced sections make predictions in the form of detailed geometric models of the subsurface, which can be tested and refined. The internal structural models are particularly useful for identifying and assessing potential sources of subsurfaces resources or the sequences in which the structures developed. Nonetheless, the practice of using only one line-length balanced section to calculate shortening and using only the hanging wall cutoffs to estimate uncertainty is flawed when the primary objective is a thorough estimate of orogenic shortening.

The method we have presented here is only the first step in producing a complete analysis of errors in shortening magnitude. Future improvements will account for the considerable likelihood that the initial stratigraphic geometry is more complicated than a simple wedge-shaped foreland basin. Additionally, a scheme to include basement thrusts, internal pinch-outs, and preexisting deformation would allow for the analysis of more regions. Finally, the natural progression of this work would be to expand the method into three dimension and calculate shortening estimates by volume balancing.

2.8 Acknowledgments

I very much appreciate Nadine McQuarrie's gracious sharing of her knowledge of stratigraphic data in Bolivia as well as constructive comments on an earlier draft of this paper, though she may not agree with the conclusions presented here.

2.9 References

Allmendinger, R. W., 2004. Evaluating uncertainty in balanced cross-sections: A critical step for relating thrust-belts to plateau uplift. *Geological Society of America Abstracts with Programs* 36, 49.

Bally, A. W., Gordy P. L., Stewart G. A., 1966. Structure, seismic data, and orogenic evolution of southern Canadian Rocky Mountains. *Bulletin Canadian Petroleum Geology* 14, 337-381.

Belotti, H. J., Saccavino, L. L., Schachner, G. A., 1995. Structural styles and petroleum occurrence in the Sub-Andean fold and thrust belt of northern Argentina. In: Tankard A.J. *et al.* (Eds.), Petroleum basins of South America. American Association of Petroleum Geologists, Tulsa, Oklahoma, pp. 545-555.

Bevington, P. R., Robinson, D. K., 2003. Data reduction and error analysis for the physical sciences, McGraw-Hill, New York, 320 pp.

Brooks, B. A., Sandvol E., Ross A., 2000. Fold style inversion; placing probabilistic constraints on the predicted shape of blind thrust faults. *Journal of Geophysical Research* B105, 13,281-13,301.

Chamberlin, R. T., 1910. The Appalachian folds of central Pennsylvania. *Journal of Geology* 18, 228-251.

Chamberlin, R. T., 1919a. The building of the Colorado Rockies. *Journal of Geology* 27, 225-251.

Chamberlin, R. T., 1919b. The building of the Colorado Rockies. *Journal of Geology* 27, 145-164.

Chamberlin, R. T., 1923. On the crustal shortening of the Colorado Rockies. *American Journal of Science* 6, 215-221.

Cladouhos, T. T., Allmendinger R. W., 1993. Finite strain and rotation from fault slip data. *Journal of Structural Geology* 15, 771-784.

Dahlstrom, C. D. A., 1969. Balanced cross sections. *Canadian Journal of Earth Sciences* 6, 743-757.

Dunn, J. F., Hartshorn, K. G., Hartshorn, P. W., 1995. Structural styles and hydrocarbon potential of the Sub-Andean thrust belt of southern Bolivia. In: Tankard A.J. *et al.* (Eds.), Petroleum basins of South America. American Association of Petroleum Geologists, Tulsa, Oklahoma, pp. 523-543.

Echavarría, L., Hernández R., Allmendinger R. W., Reynolds J., 2003. Subandean thrust and fold belt of northwestern Argentina: Geometry and timing of the Andean evolution. *AAPG Bulletin* 87, 965-985.

Elliott, D., 1976. The motion of thrust sheets. *Journal of Geophysical Research* 81, 949-963.

Elliott, D., 1983. The construction of balanced cross-sections. *Journal of Structural Geology* 5, 101.

Geiser, P., 1988. The role of kinematics in the construction and analys of geological cross sections in deformed terranes. In: Mitra G., Wojtal S. (Eds.), Geometrics and mechanisms of thrusting. *Special Paper 222,* Geological Society of America, Boulder, Colorado, pp. 47-76.

Groshong, R. H. J., 1994. Area balance, depth to detachment, and strain in extension. *Tectonics* 13, 1488-1497.

Groshong, R. H. J., Epard J., 1994. The role of strain in area-constant detachment folding. *Journal of Structural Geology* 16, 613-618.

Hardy, S., 1995. A method for quantifying the kinematics of fault-bend folding. *Journal of Structural Geology* 17, 1785-1788. doi:10.1016/0191-8141(95)00077-Q.

Hardy, S., 1997. A velocity description of constant-thickness fault-propagation folding. *Journal of Structural Geology* 19, 893-896.

Harris, J. W., Stocker, H., 1998. Handbook of mathematics and computational science, Springer-Verlag, New York, 1028 pp.

Higgs, W. G., Williams G. D., 1987. Displacement efficiency of faults and fractures. *Journal of Structural Geology* 9, 371-374.

Hossack, J. R., 1979. The use of balanced cross-sections in the calculation of orogenic contraction: a review. *Journal of the Geological Society* 136, 705-711. doi:10.1144/gsjgs.136.6.0705.

Kley, J., Monaldi C. R., 1998. Tectonic shortening and crustal thickness in the Central Andes; how good is the correlation?. *Geology* 26, 723-726.

Malvern, L. E., 1969. Introduction to the mechanics of a continuous medium, Prentice-Hall, Inc., Englewood Cliffs, N.J., .

Marrett, R. A., Allmendinger R. W., 1990. Kinematic analysis of fault-slip data. *Journal of Structural Geology* 12, 973-986.

Marrett, R. A., Allmendinger R. W., 1991. Estimates of strain due to brittle faulting: Sampling of fault populations. *Journal of Structural Geology* 13, 735-738.

Marrett, R. A., Allmendinger R. W., 1992. The amount of extension on "small" faults: An example from the Viking Graben. *Geology* 20, 47-50.

McQuarrie, N., 2002. The kinematic history of the central Andean fold-thrust belt, Bolivia: Implications for building a high plateau. *Geological Society of America Bulletin* 114, 950-963.

McQuarrie, N., Ehlers T. A., Barnes J. B., Meade B., 2008. Temporal variation in climate and tectonic coupling in the central Andes. *Geology* 36, 999-1002. doi:10.1130/G25124A.1.

Mitra, S., Namson J., 1989. Equal-area balancing. *American Journal of Science* 289, 563-599.

Price, R. A., Mountjoy, E. W., 1970. Geologic structure of the Canadian Rocky Mountains between Bow and Athabasca rivers -- a progress report. In: Wheeler J.O. (Ed.), Structure of the southern Canadian Cordillera. Geological Association of Canada, pp. 7-25.

Sempere, T., 1995. Phanerozoic evolution of Bolivia and adjacent regions. In: Tankard A.J. *et al.* (Eds.), Petroleum basins of South America. American Association of Petroleum Geologists, Tulsa, Oklahoma, pp. 207-230.

Sheffels, B. M., 1990. Lower bound on the amount of crustal shortening in the central Bolivian Andes. *Geology* 18 , 812-815.

Taylor, J. R., 1997. An introduction to error analysis: The study of uncertainties in physical measurements, University Science Books, Sausalito, California, 327 pp.

Walsh, J. J., Watterson J., 1987. Distributions of cumulative displacement and seismic slip on a single normal fault surface. *Journal of Structural Geology* 9, 1039-1046.

Walsh, J. J., Watterson J., 1989. Displacement gradients on fault surfaces. *Journal of Structural Geology* 11, 307-316.

Woodward, N. B., Boyer, S. E., Suppe, J., 1989. Balanced geological cross sections: An essential technique in geological research and exploration, American Geophysical Union, Washington, D.C., 170 pp.

Zehnder, A. T., Allmendinger R. W., 2000. Velocity field for the trishear model. *Journal of Structural Geology* 22, 1009-1014.

CHAPTER THREE:

Assessing the shortening history and magnitude of the Argentine Precordillera at 30ºS

3.1 Abstract

Cross sections for the Argentine Precordillera calculate shortening magnitudes that vary by up to 30% of the maximum estimates; these line-length balanced cross sections do not include rigorous uncertainty bounds. Additionally, these cross sectional models of the region indicate that the decollement from the Precordillera may project below the high Andes, requiring that thickening in the Andes involved crustal-scale structures. To try to resolve the true shortening magnitude in the Precordillera, we collected structural field data throughout the region and constructed two profiles across to establish a sequence of relative motion and to calculate shortening and uncertainty magnitudes via area balancing. The relative timing in the Precordillera indicates several periods of back-breaking thrust development across the range. Activity on the thrusts in the region is divided into three major time periods: shortening prior to 20 Ma in the western region; formation of faults in the central region as well as reactivation on the western thrusts from 11 - 4 Ma; and the formation of the eastern Precordillera and the reactivation of the central faults from 3 - 0 Ma. We calculate 117 + 40 km of shortening across the northern profile and 114 ± 47 km of shortening across the southern profile. These shortening

values both confirm the wide range of existing shortening estimates, and uphold the likelihood that the decollement projects into the thickened crust below the high Andes, requiring crustal-scale structures to accommodate their uplift.

3.2 Introduction

The structure in the Precordillera of western Argentina records a shortening history that began at ~20 Ma and continues through the present (Jordan et al., 1993a; Smalley et al., 1993; Zapata and Allmendinger, 1996b). Several cross sections through the region show a variety of shortening magnitudes and relate the shortening to the formation of the high Andes to the west (Allmendinger et al., 1990; Cristallini and Ramos, 2000; Zapata and Allmendinger, 1996b). Jordan and others (1993a; 2001) demonstrate a possible relationship between the changing geometry of the subducting Nazca slab and the shortening activity in the Precordillera. However, without rigorous methods of assessing the uncertainties on the shortening magnitudes and rates, the relationship between the Precordillera and the geometry of the Nazca slab, as well as the uplift of the high Andes, is difficult to assess.

We present new field data with revised timing implications and area balanced cross sections with uncertainty bounds across the Precordillera to assess the range of existing shortening estimates for the region. The new field data suggest modifications to the relative timing implied by existing line-length balanced sections for the area and

indicate three distinct periods of activity, including a long period of quiescence in the mid-Miocene. Our new shortening magnitudes confirm both the location of the projected decollement below the high Andes as well as the wide range of existing shortening values.

3.3 Summary of regional geology

We conducted field work throughout the Argentine Precordillera between approximately the Río Jáchal (30° S) and Gualilán (31° S) with a focus on the western and central portions of the thrust belt (Fig. 3.1). This region of the Precordillera overlies the Chilean flat slab segment of the subducted Nazca plate (Cahill and Isacks, 1992; Jordan et al., 1983) that is located at approximately 90 km depth nearly 500 km from the trench (Gans et al., 2011). Near Jáchal, the ~50 km wide fold-and-thrust belt is composed of NNE-striking faults that bring Paleozoic rocks to the surface in a series of thin-skinned faults (Allmendinger et al., 1990; Baldis and Chebli, 1969; Furque, 1979; 1984; Jordan et al., 1993a; Ortíz and Zambrano, 1981) that are paired with the thick-skinned basement-cored Quaternary folds to the east (Beer et al., 1990; Zapata and Allmendinger, 1996a; 1996b). The Precordillera is flanked by active intermontane and foreland basins: the Uspallata-Callingasta-Iglesia basin to the west and the Bermejo basin to the east. The Precordillera and associated basins occupy the volcanic gap created by the flat slab (Kay and Abbruzzi, 1996), and the Neogene and Pliocene

sediments cover the western structural boundary between the frontal Cordillera and the Precordillera map (González et al., 1999).

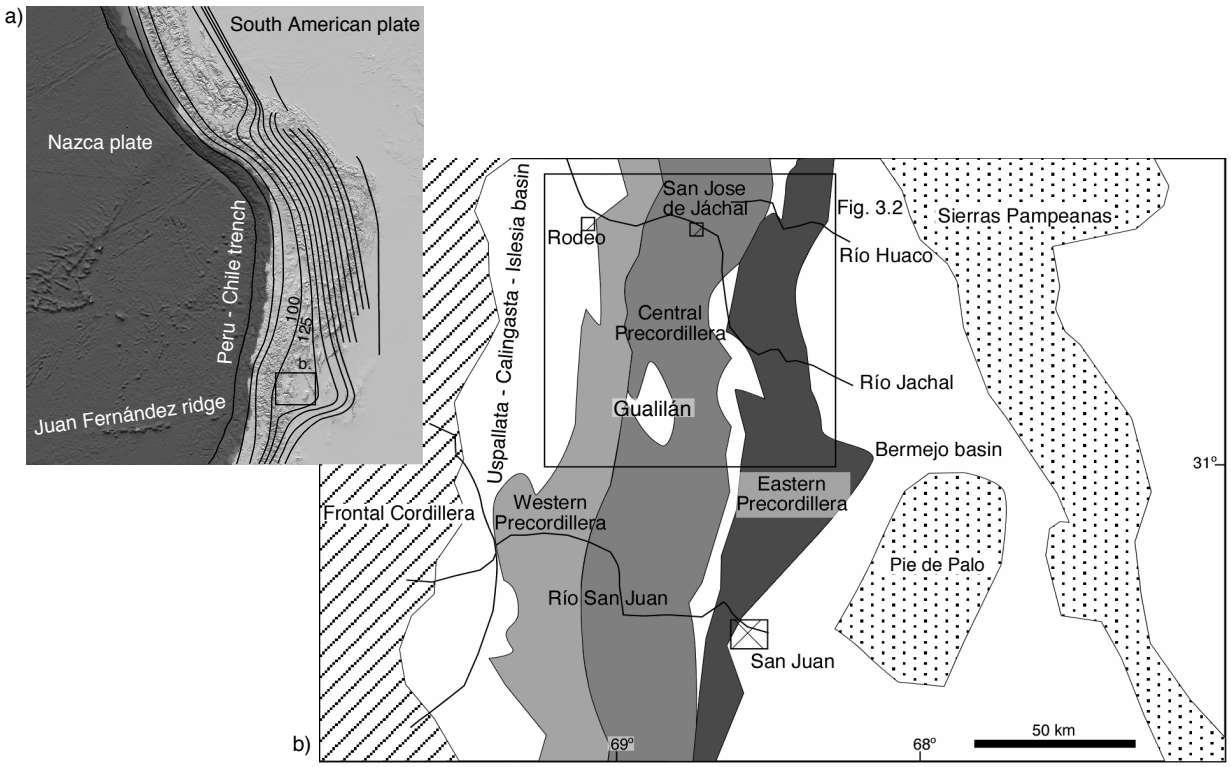

Fig. 3.1: Regional map of western South America and the Precordillera. a) DEM showing Nazca and South American plates with contours of the depth to the slab (in km) based on Cahill and Isacks (1992), as well as the location of the Juan Fernández ridge. Inset shows location of b. b) Tectonic map of the Argentine Precordillera north of San Juan. Inset shows location of Fig. 3.2.

The Precordillera is divided into three sections based on the stratigraphic units and structural styles of the faults across the region (Baldis et al., 1982; Baldis and Chebli, 1969; Ortíz and Zambrano, 1981). The western Precordillera brings Ordovician slope facies to the surface (Astini, 1998; Baldis et al., 1982; Furque, 1984; Thomas and Astini, 2003; von Gosen, 1997) and places them over Neogene sediments in the Tranca and Caracol valleys in several west-dipping thrusts (Furque, 1984; Jordan et al., 1993a). The Ordovician slope sediments are strongly folded and have undergone a lower greenschist phase metamorphism (von Gosen, 1997). The central Precordillera has a similar structural geometry but involves primarily Ordovician shelf facies carbonate rocks and overlying Paleozoic strata.

The eastern Precordillera is a series of relatively open anticlines and tight synclines of basement-cored Quaternary foreland basin material (Allmendinger et al., 1990; Bracaccini, 1946; Zapata and Allmendinger, 1996a; 1996b).These are likely the surface expressions of blind thick-skinned faults in the basement relative to pre-existing Mesozoic and older structures (Baldis and Chebli, 1969). Folding in the eastern Precordillera is younger than 2.7 Ma (Zapata and Allmendinger, 1996a) and is the location of the majority of active deformation in the Precordillera, as defined by the location of seismicity in the region, as well as near Pie de Palo (Fig. 3.1b) (Siame et al., 2005; 2006; Smalley et al., 1993).

Jordan and others (1993a) first established the timing of the formation and movement of the structures in the Precordillera and described the thrust belt as an eastward-advancing formation with reactivation likely throughout the Precordillera, and out-of-sequence motion on the Vallecito fault (Allmendinger et al., 1990). Zapata and Allmendinger (1996b) confirmed the eastward migration of motion and determined that the eastern Precordillera was the locus of deformation after 2.7 Ma. von Gosen (1997) completed a study of the Paleozoic strata in the Precordillera and determine that there was a significant period of west-verging folding and shortening in the Paleozoic, deforming units younger than Late Carboniferous. West-verging, pre-Andean folding is readily apparent in the Ordovician flysch, pillow basalts, and ultramafics from the western Precordillera. However, Alvarez-Marron and others (2006) concluded that a large component of the east-verging deformation in the Precordillera was pre-Andean (Late Tertiary) in age, and that the Neogene structures show a strong component of transpression.

Changes in the geometry of the subducting slab and changes in motion in the Precordillera are temporally correlated: Jordan and others (1993a) proposed that, although there is evidence in the western Precordillera for shortening after 21 Ma, the most significant phase of shortening in the Precordillera was approximately post-11 Ma, which is also roughly when the Nazca slab began to shallow (Kay and Abbruzzi, 1996; Yáñez et al., 2001). Yáñez and others (2001; 2002) reconstructed the plate history and the

location of the Juan Fernández ridge (Fig. 3.1a), and showed that, because the trend of the ridge and the direction of the plate convergence were nearly parallel after 10 Ma, the ridge began to subduct in a stable location beneath the Precordillera. Martinod and others (2010) suggest that the flat portion of the Nazca slab increases the coupling between the slab and the overriding plate, which may increase shortening magnitudes at the surface. If the slab began to shallow at approximately 10 Ma, changes in the slip activity on the faults in the Precordillera may be related to an increased coupling between the overriding and down-going plates.

3.4 Geology of the western and central Precordillera

3.4.1 Western Precordillera

The Tranca and Caracol faults compose the western Precordillera at the latitude of the Río Jáchal (Fig. 3.2). In the northern section of the Tranca valley, the thrust places the Ordovician Yerba Loca formation over Tertiary redbeds that Jordan and others (1993a) correlate to 21.6 Ma sandstones at other locations in the Precordillera (Fig. 3.3). An angular, locally-derived gray conglomerate overlies much of the northern end of the Tranca valley, including several exposures of the Ordovician-Tertiary fault. The gray conglomerate dates to 19.5 Ma (Jordan et al., 1993a) and its age indicates that much of the activity on the main fault was confined to after 21.6 Ma but before 19.5 Ma. At the

Fig. 3.2: Geologic map of the Precordillera showing the lithology and the locations of field data as well as the major thrusts, towns, river, and dated stratigraphic columns. Profiles A-A' and B-B' shown in Fig. 3.7. Shorter profiles shown C, D, E shown in Fig. 3.11. Based on field data was well as Cardó and Díaz (1999), Furque (1979), Furque (1984), and González et al. (1999).

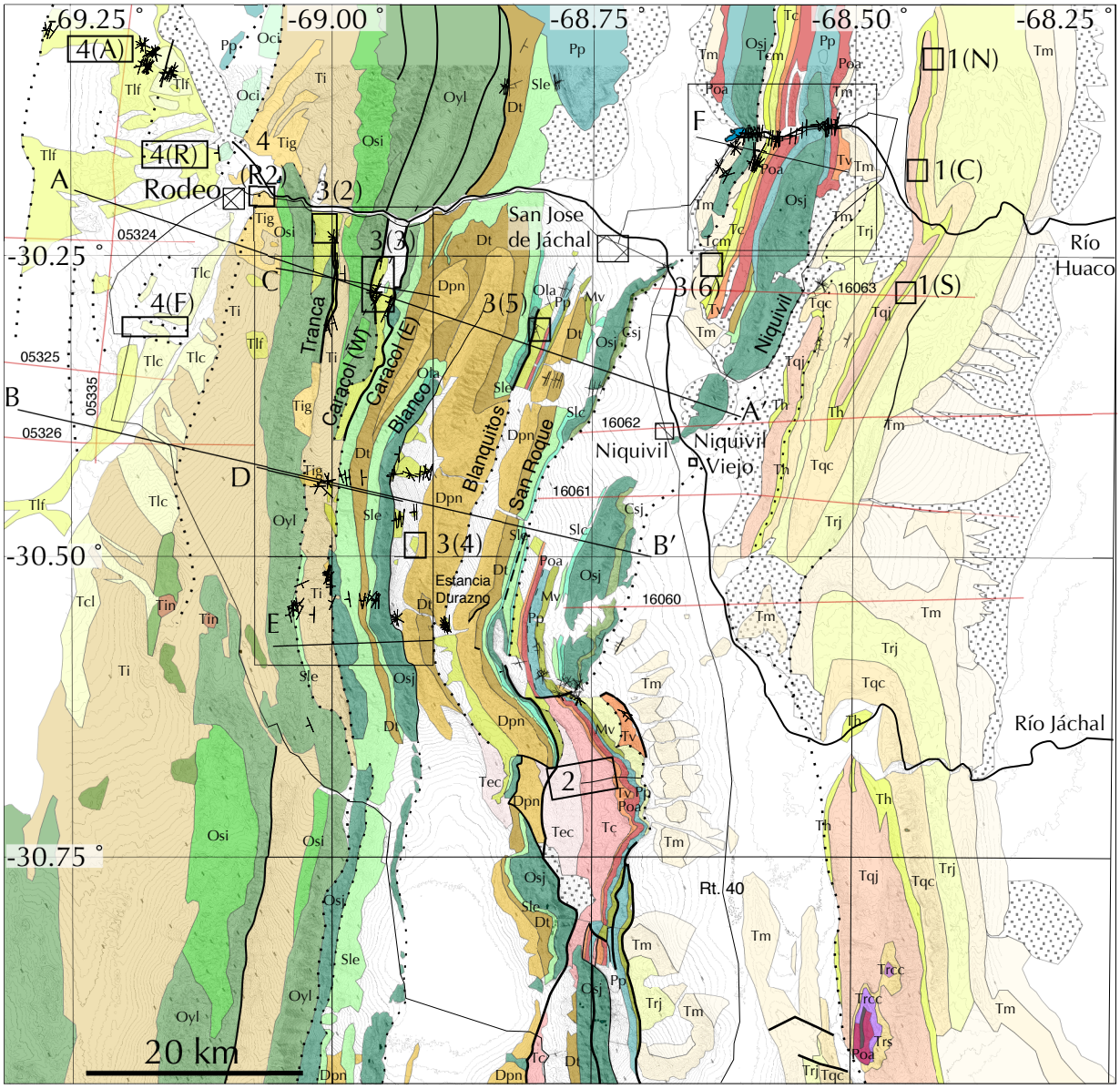

Iglesia basin sediments:

- (pls) Iglesia
- (pl) Las Flores
- (m) Tertiary intrusives
- (m) Lomas del Campanario
- (m) Iglesia Group

Fault
Covered fault
Inferred fault
River
Town
Road
05325 Location of seismic survey lines
i(X) Location of measured sections with reference

Precordillera units and Bermejo basin sediments:

- (Tr) Cañon Colorado
- (p) Ojo de Agua
- (Pp) Panacan
- (M) Volcan
- (d) Punta Negra
- (d) Talacasto
- (s) Los Espejos
- (s-o) La Chilca
- (o) Cuerpos Ingeos Basicos
- (o) Yerba Loca
- (o) Sierra de la Invernada
- (o) Los Azules
- (o) San Juan
- (c) San Roque
- (q) alluvial deposits
- (hl) active fan deposits
- (pls) relict fan deposits
- (m) El Corral
- (m) Cuculi
- (pl) Mogna
- (pl) Rio Jáchal
- (m) Quebrada del Cura
- (m) Huachipampa
- (m) Quebrada del Jarillal
- (m) Rio Salado
- (m) Cauquenes
- (m) Cerro Morado
- (ol) Vallecito

1: Beer and Jordan, 1989
2: Jordan et al., 1990
3: Jordan et al., 1993
4: Ruskin and Jordan, 2007

northernmost end of the Tranca valley, there is a secondary fault that places the 21.6 Ma redbeds over 9.4 Ma chestnut conglomerates (Fig. 3.2) (Jordan et al., 1993b).

At the northern end of the Caracol valley, east- and west-dipping reverse faults bound the east and west sides of the intermontane valley. On the western side of the valley, the west-dipping fault places Ordovician slope facies over mid-Miocene pink and green cross-bedded eolian sandstones (Jordan et al., 1993a); these units are correlated to the 13.4 Ma eolian sandstones in the Blanco valley, southern Tranca valley, and elsewhere throughout the Precordillera (Jordan et al., 1993a), and indicate that the final phase of motion on the northern end of the western Caracol valley must be younger than 13.4 Ma. The 9.4 Ma chestnut conglomerate in the Tranca valley rests unconformably on the uplifted hanging wall of the Caracol valley and is buttressed by paleotopography on the eastern side of the valley (Fig. 3.2). Near Río Jáchal, both the main west-dipping Caracol and Tranca faults dip ~60° W.

Further south in the Caracol valley, the west-dipping fault places the Ordovician facies over Tertiary redbeds similar to those in the Tranca valley. This part of the fault is separate from the northern end of the valley by left-lateral offset on a steep fault and may represent an earlier phase of motion that was similar to that of the Ordovician-Tertiary fault in the Tranca valley. At a topographic saddle, the Tranca and Caracol valleys merge and form one larger valley to the south (Fig. 3.2). The relationship

between the Tranca and Caracol thrusts is likely to be one of en echelon faults with ~25 km of overlap between the two oppositely plunging tip lines.

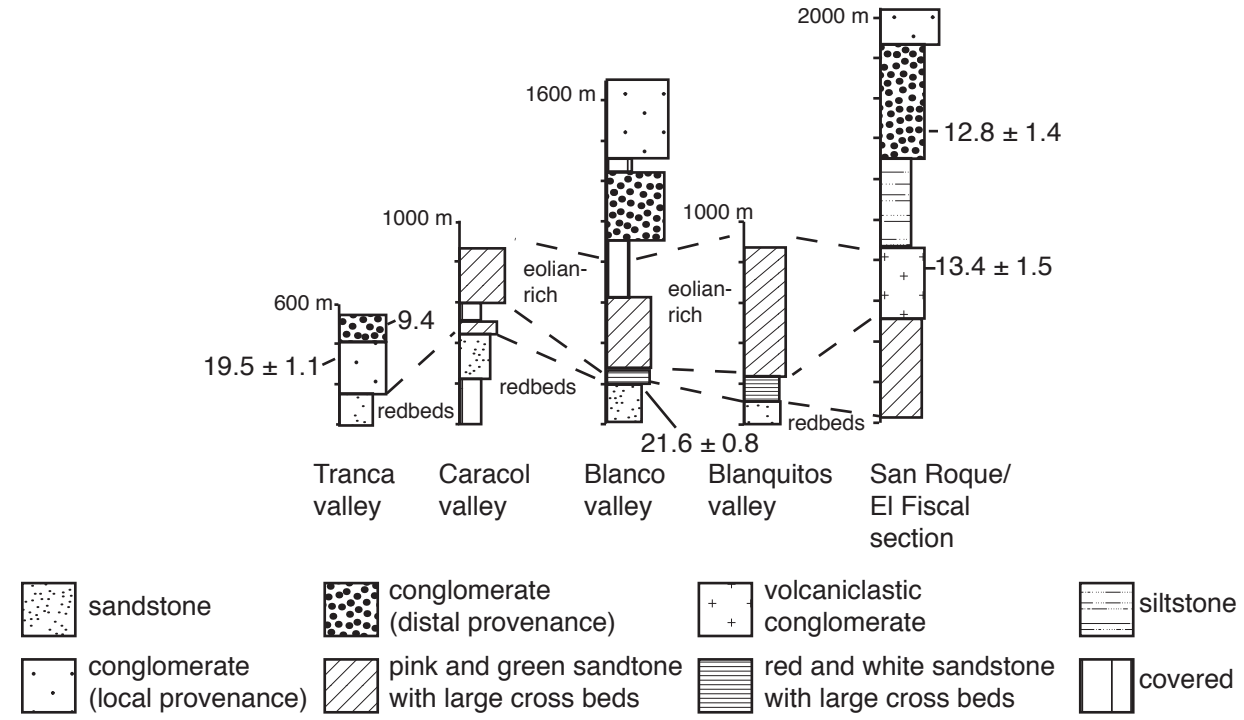

Fig. 3.3: Stratigraphic columns for the Tertiary strata in the valleys of the western and central Precordillera. Modified from Jordan et al. (1993a).

The east-dipping fault in the Caracol valley (Fig. 3.2) brings Ordovician slope and shelf facies to the surfaces and places them over early Miocene redbeds, similar to those in the Tranca valley, the southern end of the west-dipping Caracol fault, and the Blanco valley (Fig. 3.3). The eastern fault also places strongly cleaved and folded red Silurian shales (González et al., 1999; Furque, 1979) over the Tertiary units at several locations along strike. The fault dips ~60º E at most locations. Activity on this fault is not as tightly constrained as motion on the western fault, but clearly must post-date the 21.6 Ma deposition of the redbeds in the footwall.

In the southern extent of the merged Tranca-Caracol valley, the west- and east-verging faults continue to define the valley. The west-dipping fault places Ordovician rocks over Tertiary redbeds, red and pink sandstones, and in some places, over tightly folded Silurian shales (Fig. 3.2). The east-dipping fault places Ordovician rocks over the early Miocene redbeds (Fig. 3.4). The units in the footwalls of both faults are folded, and the beds dip both shallowly and steeply to the east and the west. Through most of the valley, both of the faults are covered by consolidated and unconsolidated gravels, and the gravels do not appear to be cut by the faults on either side of the valley. The older, consolidated gravels in the central part of the valley onlap and over the folded Miocene strata in the middle of the valley, and the gravels dip ~15ºW. The gravels are likely to be Pliocene in age (Cardó and Díaz, 1999), but may be as old as mid-Miocene. This gives a

latest possible age of motion on the faults of ~2 Ma, but we believe the gravels to be early Pliocene in age due to the level of consolidation.

The southern end of the Tranca-Caracol valley is filled with an unconsolidated gravel that contains large (>40 cm) clasts of Ordovician limestone, likely from the San Juan formation to the east, at 2700 – 3200 m elevation in the center of the valley. At the eastern edge of the valley, these gravels overlie a consolidated cemented gravel that contains clasts from the frontal Cordillera as well as the Precordillera. Under the unconsolidated gravels are Tertiary redbeds, as well as pink and white cross-bedded eolian sandstones. The unconsolidated gravels in the center and southern regions of the Tranca-Caracol valley are qualitatively distinct, but both overlie the fault contact. Directly under the east-dipping fault near the mouth of one of the large slot canyons on the eastern side of the valley, a conglomeratic unit contains large clasts of San Juan limestone and may represent a basal conglomerate associated with the uplift and erosion of the eastern fault.

Fig. 3.4: Geologic map of the Tranca - Caracol valley showing the location of fault strike and dip (heavy black lines) and bedding (light black lines) data. Dates show ages of indicated Neogene strata in the northern Tranca and Caracol valleys. In the Blanco valley, the fault dip is not on the Ordovician-Tertiary fault plane but is within the fault gouge. Lithology the same as for Fig. 3.2.

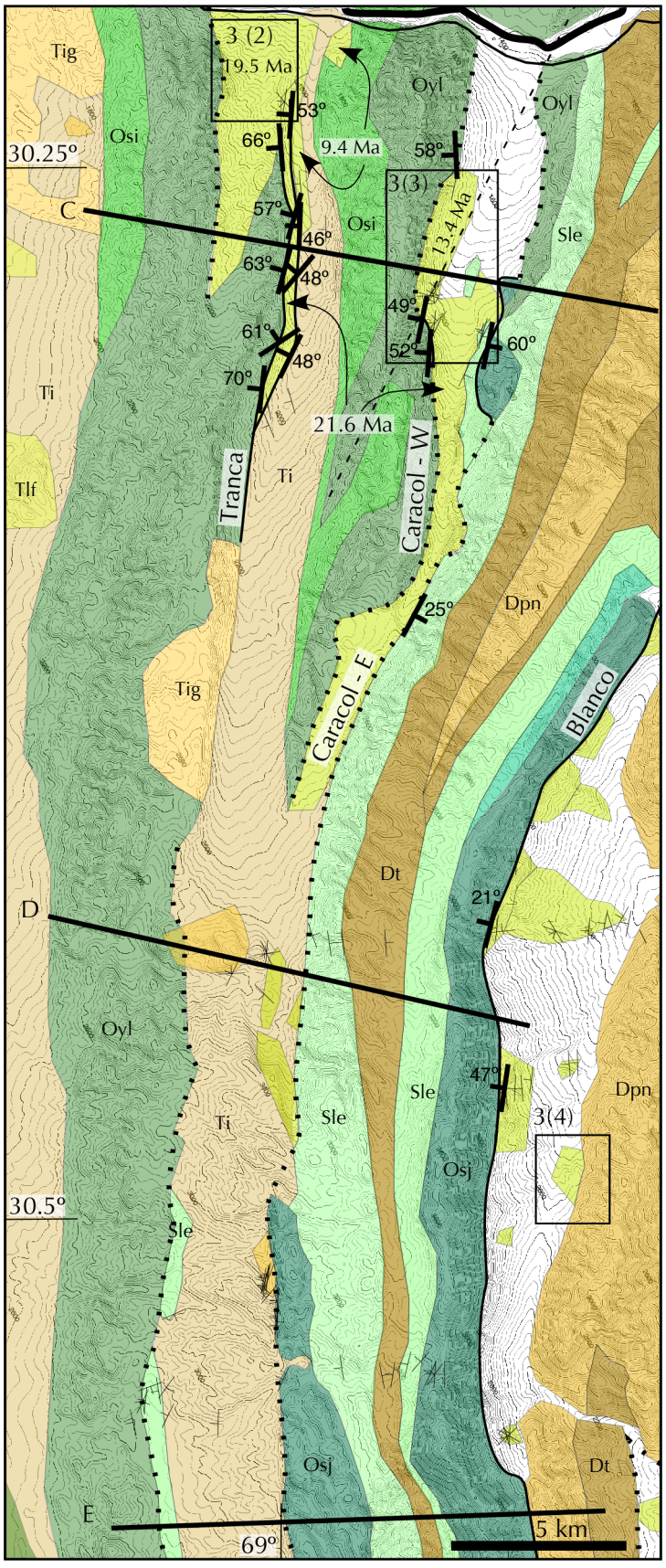
3 (2)
19.5 Ma
53º
66º
9.4 Ma
58º
3(3)
13.4 Ma
57º
46º
63º
48º
49º
61º
52º
60º
48º
70º
21.6 Ma
30.25º
C
Tig
Osi
Oyl
Oyl
Sle
Osi
Ti
Tlf
Tranca
Ti
Caracol - W
25º
Dpn
Caracol - E
Blanco
Tig
Dt
21º
D
Oyl
47º
Sle
Dpn
Ti
Sle
3(4)
Osj
30.5º
Sle
Osj
Dt
E
69º
5 km

3.4.2 Central Precordillera

The Blanco fault, which is the westernmost thrust in the central Precordillera, forms the highest topography in the Precordillera between Jáchal and Gualilán (Fig. 3.2). In the center of the Blanco valley, the fault exposes almost a kilometer of vertical relief of Ordovician limestone in the hanging wall, placing the limestone over Tertiary conglomerates in the foreland basin sequence of the Bermejo basin (Jordan et al., 1993a). At the northern end of the valley, the Tertiary sequence in the footwall is folded into an overturned syncline and a splay of the main thrust places green Devonian shales between the Tertiary and the Ordovician (Jordan et al., 19993a). The Blanco thrust does not cut across the Río Jáchal but instead the tip line plunges to the north between the valley and the river (Fig. 3.2). The main Blanco thrust fault dip is relatively steep (44° W) at the northern end of the valley near the plunging tip line, but the fault dips more gently in the central and southern parts of the valley (22° – 25° W). In the southernmost extent of the valley, the Blanco fault cuts down-section in the direction of translation across the folded hanging wall of the Blanquitos thrust, to the east, and is not strongly deformed by the folding in the Blanquitos thrust (Fig. 3.2). In the northern half of the valley, some folding of the hanging wall of the Blanco fault is likely related to motion on the Blanquitos thrust, but the folding is minor compared to the degree of folding in the Blanquitos hanging wall.

The exposures of Tertiary redbeds and sandstones in the Blanco valley are the source of the 21.6 Ma data from Jordan and others (1993a). The Tertiary sequence is relatively well exposed with a small covered interval (~300 m) in the center of the valley; nearly a kilometer of stratigraphic thickness is exposed beneath the fault. The top unit in the footwall is a conglomerate with clasts from the frontal Cordillera and the Precordillera (Fig. 3.2). While the unit immediately below the fault is not dated, the conglomerates are well above the pink and green cross-bedded eolian sandstones that are correlated to 13.4 Ma units (Jordan et al., 1993a), and the conglomerates are likely to be younger than 12 – 10 Ma.

East of the Blanco valley, the Blanquitos thrust brings Ordovician limestone and other Paleozoic units to the surface (Fig. 3.2). In the north, the fault places limestone over Tertiary units; in the south, the faults cut up-section into the Devonian shales. The hanging wall has several large amplitude folds: an anticline that is related to the lateral ramp in the hanging wall as the fault cuts up from Ordovician to Devonian rocks; a tight syncline; and a much broader anticline that forms the majority of the Blanquitos hanging wall. The southern portion of the hanging wall is not strongly deformed by the fault-fold structure in the San Roque block to its east (Fig. 3.2). The fault surface is only exposed at the northern and southern extents of the fault trace, where it dips moderately (35^{o} – 60^{o} W) and the average fault plane dips 40^{o} W. At the Blanquitos locality at the northern end of the fault (Fig. 3.2), the Tertiary units in the footwall are

strongly cross-bedded and the strata dip 40º – 60º W below a fault with an average dip of 36º W. At the southern locality of Estancia Durazno, the beds dips 55º – 70º W and the fault dips 60º W (Fig. 3.2). While the structures in the south dip more steeply than those to the north, the strata in the footwall dip more steeply than the faults in both locations. It is likely that the units in both the hanging and footwalls are folded, making the relative timing of the fault ambiguous. The Tertiary units in the footwalls are from the lower half of the stratigraphic sequence, including the redbeds as well as the pink and green eolian sandstones (Fig. 3.3) (Jordan et al., 1993a).

Farther east, the San Roque fault also brings Ordovician limestone to the surface and places the Paleozioc rocks over Tertiary conglomerates and sandstones (Fig. 3.2). Near the Río Huaco, there are several exposures of the fault contact, but it is otherwise covered along the majority of the fault trace. North of the latitude where the Río Jáchal crosses the thrust, the San Roque fault geometry is that of a standard fault-bend fold system. To the south of the Río Jáchal, there is a hanging wall anticline above a lateral ramp in the hanging wall as the fault ramps up from the San Roque limestone to the San Juan limestone. Additionally, a small splay of the fault brings an extra slice of the Devonian to the surface and is likely related to a tight fold to the south (Fig. 3.2).

In the northern valley near the Río Huaco, the San Roque footwall is composed of conglomerates of local and distal provenance in the El Fiscal section (Jordan et al., 1993a). Within the distal conglomerate, a reworked tuff contains grains with an age of

12.8 ± 1.4 Ma, making the conglomerates younger than at least the age of the grains. The conglomerates with a distal source are within the upper portion of the stratigraphic section, the top of which is approximately 9 – 8 Ma, based on magnetic stratigraphy (Jordan et al., 1993a).

The Niquivil fault is the easternmost thrust in the central Precordillera (Fig. 3.2). To the east of the Niquivil thrust, the eastern Precordillera province of basement-rooted deformation contains the Niquivil, Las Salinas, and Bermejo anticlines, which fold the Miocene and Pliocene foreland basin strata (Beer and Jordan, 1989; Jordan et al., 1993a; Zapata and Allmendinger, 1996a; 1996b). The northern section of the Niquivil thrust, near the Río Huaco, is a broad fault propagation fold that is cored with Ordovician limestone; the main fault is blind. South of the Río Huaco, motion related to the folding of the Niquivil anticline refolds and deforms the Niquivil fault (Zapata and Allmendinger, 1996a; 1996b).

Farther south, near Río Francia, the Niquivil fault brings the Ordovician San Roque formation to the surface in the core of a fault propagation fold (Fig. 3.2). At the southern end of the Niquivil fault, the strata in the hanging wall dip ~40º W. The anticlines in the eastern Precordillera are farther from the Niquivil fault near Río Francia than in the north, and there is not surface evidence of refolding of the fault related to the formation of the anticlines (Zapata and Allmendinger, 1996b). While the fault may be folded in the surface and the kink axis covered, it is likely that any structure that folds

the Niquivil thrust also folded the San Roque fault since the two hanging walls both dip approximately 40° W.

On the western and eastern sides of the Niquivil thrust near the Río Huaco, the thrust folds the Cerro Morado formation (Fig. 3.5), which dates to 13.4 Ma (Jordan et al., 1993a). The Cerro Morado formation is a locally-derived volcaniclastic unit that must have been deposited prior to, and subsequently deformed by, motion on the Niquivil thrust. Poorly consolidated conglomerates were deformed by ~1 Ma on the Vallecito thrust (Allmendinger et al., 1990), which is located between the San Roque and Niquivil thrusts. A second, gently folded conglomerate overlies the more steeply dipping conglomerates. The Niquivil thrust is still active as it has created a 10 – 15 m high fault scarp in Quaternary deposits where the fault crosses the Río Jáchal (Fig. 3.6). There is no geomorphic evidence of strike-slip offset on the scarp.

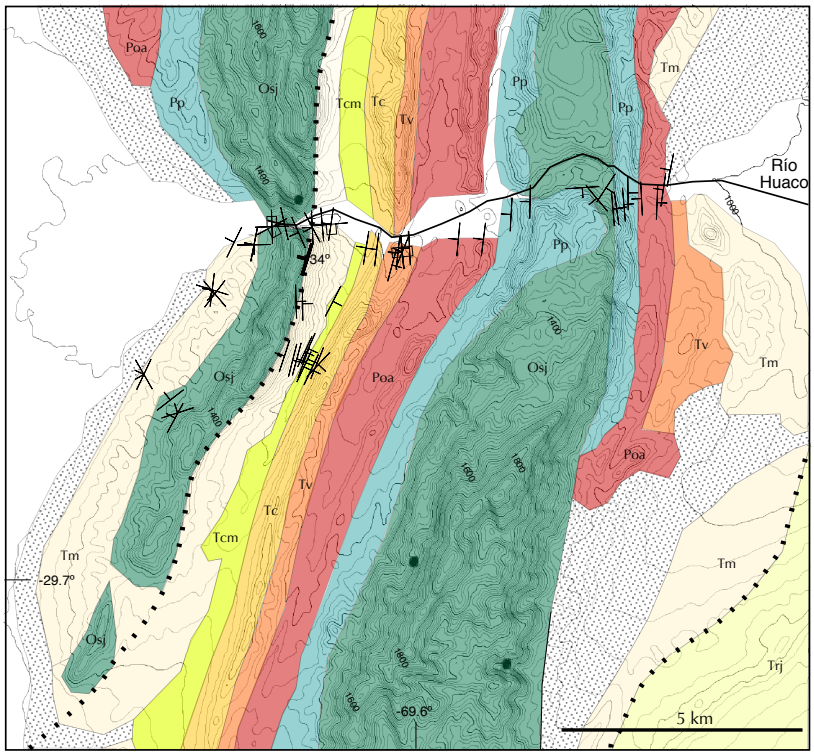

Fig. 3.5: Geologic map of the Río Huaco area showing field data. Lithology same as for Fig. 3.2.

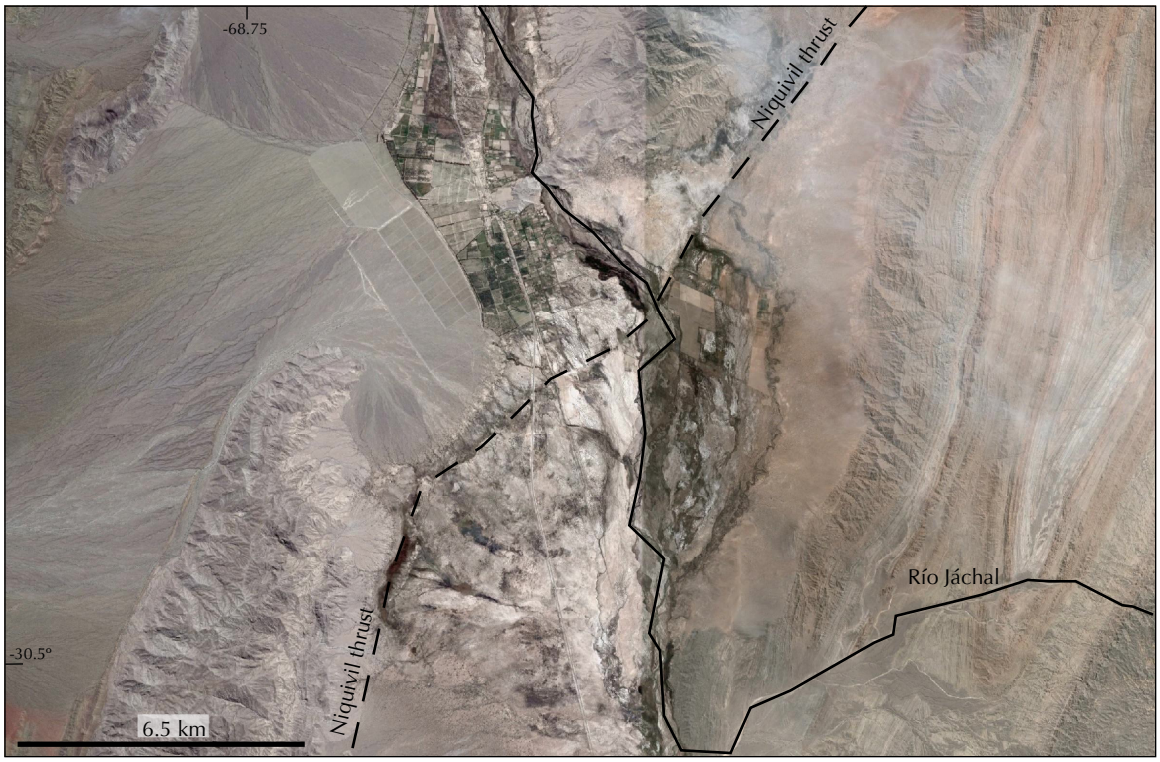

Fig. 3.6: Scene from Google Earth showing the trace of the Niquivil fault and its relationship to the Río Jáchal.

3.5 Shortening magnitudes from area balancing

We calculate shortening magnitudes across the Precordillera, as well as uncertainty bounds that are numerically propagated throughout the calculation, to establish the reasonable range of shortening values across several generations of existing cross sections in the region. Allmendinger and others (1990) and Zapata and Allmendinger (1996b) constructed line-length balanced cross sections in the Precordillera, and von Gosen (1997) and Alvarez-Marron and others (2006) contributed different

interpretations of the structures in the region, notably in the western Precordillera, but did not estimate shortening magnitudes. Cristallini and Ramos (2000) drew a cross section for the Precordillera at the latitude of the Río San Juan, approximately 100 km south of our field area. Previous cross sections yield 72 – 136 km of shortening across the entire Precordillera; while this range may simply be a result changes in shortening along strike, the lack of uncertainty estimates does not allow us to compare between the regions. Calculating shortening values that include error estimates based on measurable geologic inputs allows us to assess where shortening magnitudes from different cross sections lie in a range of estimates, as well as to determine the likely sources of uncertainty for a section.

In addition to determining a likely range of shortening values for the Precordillera, recalculating shortening with new error estimates allows us to re-examine the conundrum that Allmendinger and others (1990) introduced: the fact that Precordillera decollement projects below the high topography of the Andes, limiting the options for mechanisms to build a thickened crust and tall mountains across a brittle Neogene detachment. The lowest shortening estimate (72 km) would place the end of the decollement in the Iglesia basin, while the highest shortening value (136 km) projects the decollement west of the Chile-Argentina border. By calculating shortening magnitudes with uncertainty values, we can project the decollement to the west of the

Precordillera, with a range of possible end-point locations, to assess whether the geometry of the detachment remains a challenge with the new cross sections.

3.5.1 Area balancing

Although our new field work provides additional insight into the evolution and relative timing of the Precordillera thrusts, the new data do not allow for significantly better resolution of the subsurface geometry of the western portion of the belt. As our objective is to assess the shortening magnitudes along the thrust belt rather than the internal geometry, area balancing is ideally suited as this method does not rely on the internal complexities of the thrust belt.

To calculate the magnitude of shortening in the western and central Precordillera, we constructed cross-sectional areas along profiles A and B (Fig. 3.2) based on the surface geometry, structural relationships, and seismic reflection data (Fig. 3.7). To calculate the shortening via an area balance of the profiles, we need to constrain the surface and subsurface boundaries of the sections, as well as the stratigraphic thicknesses on both ends of the profile. For the eastern boundary and basal decollement, we used available seismic reflection data (Allmendinger et al., 1990; Zapata and Allmendinger, 1996b) to project the Niquivil thrust to the decollement; both the Niquivil hanging wall and the corresponding units in the basement are visible in the seismic data (Fig. 3.7). The depth of the decollement at the eastern margin has an uncertainty related to the conversion from travel times in the seismic data to depth. Using a range of

plausible velocities, the calculated depth and uncertainty is 15 ± 1.5 km. As the decollement is not visible in the seismic lines, we calculated the depth of the Cambro-Ordovician limestones at several locations immediately east of the Niquivil thrust and determined a dip of $2^{o} \pm 1^{o}$ W.

Fig. 3.7: Cross sectional profiles of A-A′ and B-B′. Black polygons inscribe area used in area balancing calculations. Crosses indicate the extent of the estimated uncertainties for the calculations. Dashed lines indicate the projected location of the trailing thrusts and the decollements. Area in footwall below leading thrust is included to capture shortening on the Niquivil thrust. Vertical line in Profile B below surface indicates the calculated depth to decollement based on seismic data. Lithology same as for Fig. 3.2.

Profile A:

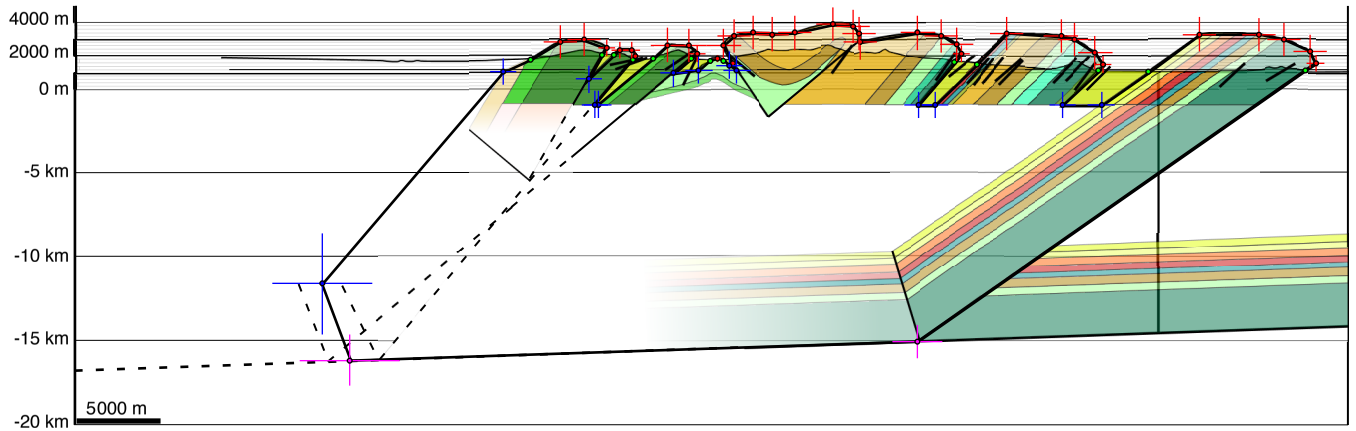

Profile B:

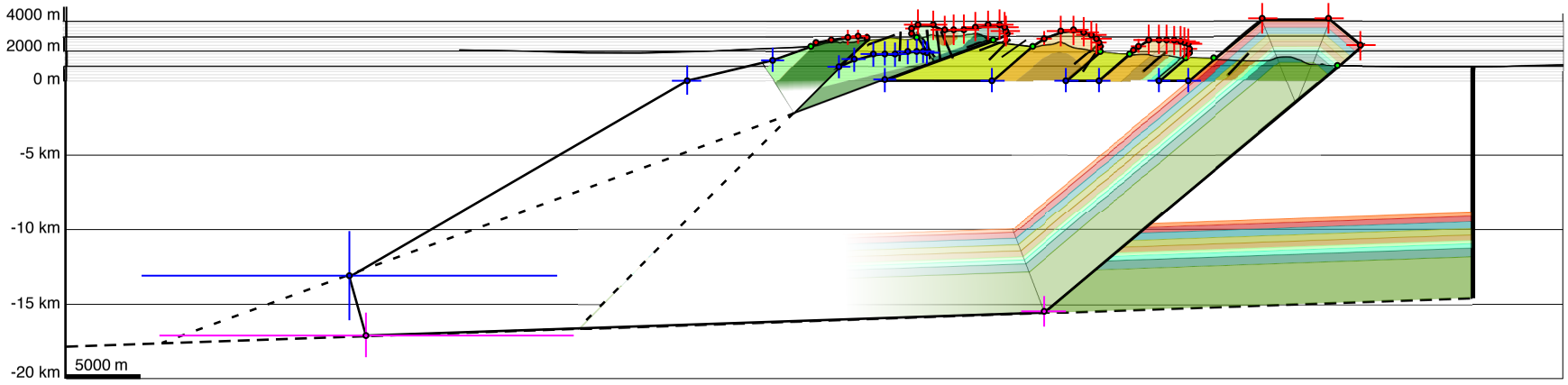

The upper boundary of the profile is both the topography of the profiles and the projection of the thrust plates into the subsurface to avoid growth strata, as well as eroded hanging wall cut-offs. Because tip lines of several faults are present along strike, we project their likely location in the air by assuming an elliptical displacement gradient function.

The most uncertain boundary of the profiles is the western limit of our deformed polygon. At the surface, the back of the Tranca hanging wall forms the western boundary of the profiles. Seismic data in the Iglesia basin do not show interpretable structures in the basement (Beer et al., 1990; Ruskin and Jordan, 2007), and the subsurface geometry of the thrust is ambiguous. We chose two extreme values: a longer cross-section based on the take-off angle of the thrusts in the central Precordillera (profile A) or on the gentler dip of the Blanco thrust (profile B), and a shorter section based on the steep dip of the Tranca thrust. The true orientation of the structure likely lies between these two different profiles, but we do not have sufficient data to constrain the western geometry.

We employ the program *AreaErrorProp*, a numerical algorithm that calculates the shortening and its associated uncertainty values through area balancing of cross sections (Judge and Allmendinger, 2011). Area balancing assumes only plane strain and that the area of the deformed section must equal the area of the initial undeformed section (Chamberlain, 1910; Hossack, 1979; Mitra and Namson, 1989). This method also

requires that one can estimate all material removed at eroded hanging wall cut-offs. Because area balancing is independent of the geometry inside the deformed polygon, the method does not provide a specific model for the evaluation of the faults in the system. Instead, area balancing encompasses all scales of faulting, does not require a specific folding model, beyond the fact that the folds must be cylindrical, and will work for any deformation style that fills the polygon.

To use this balancing method, we compiled stratigraphic thicknesses for the sedimentary rocks at both ends of the cross sections, as well as reasonable uncertainty estimates for the thicknesses. The stratigraphy at the eastern edge of the Precordillera is relatively well known (Baldis and Chebli, 1969; Furque, 1979; Jordan et al., 1993a; Limarino et al., 1987; Limarino and Cerasi, 1992; Ottone and Azcuy, 1986). Based on the published thicknesses and on surface mapping and exposures, we calculate 5275 m for the thickness of the eastern stratigraphic column for section A (table 3.1). Because the reported thickness variations are low and the values are relatively consistent with our field observations, we estimate 100 – 350 m of uncertainty for each unit based on the discrepancies between reported thicknesses and our observations. For the eastern stratigraphic column for section A, we calculate 500 m of uncertainty for the total column based the square root of the sum of the squared individual values.

Table 3.1: Stratigraphic thickness values for profile A

Stratigraphy	*Unit thickness [m]*	*Unit uncertainty [m]*	*Source*
Eastern stratigraphy			
Cauquenes (Miocene)	400	100	Furque (1979)
Cerro Morado (Miocene)	350	150	Jordan et al. (1993a)
Vallecito (Oligocene)	450	100	Jordan et al. (1993a); Limarino et al., (1987)
Ojo de Agua (Permian)	385	100	Ottone and Azcuy (1986); Burcowski and Zambrano (1990)
Panacán (Pennsylvanian)	340	100	Ottone and Azcuy (1986)
Talacasto (Devonian)	500	100	Furque (1979)
Los Espejos (Silurian)	450	250	Astini and Maretto (1996)
Ordovician limestones (San Roque & San Juan)	2400	250	Furque (1979)
total:	5275	500	
Western stratigraphy			
Devonian units	1000	1000	Limarino and Cerasi (1992)
Ordovician slope units (Yerba Loca & Invernada)	3600	500	Furque (1984)
total:	4600	2000	

In the western Precordillera, significantly less stratigraphy is exposed and the majority of the rocks at the surface show evidence of strong folding prior to the Andean orogeny (Alvarez-Marron et al., 2006; Furque, 1984; Jordan et al., 1993a; von Gosen, 1997). Several kilometers of Ordovician slope facies are mapped as the Yerba Loca and La Invernada formations in the hanging walls of the Tranca and Caracol thrusts (Furque; 1984; González et al., 1999; Cardó and Díaz, 1999). In the Iglesia basin, there are

several exposures of highly cleaved Devonian shales (Beer et al., 1990; Furque, 1984; Ruskin, 2006). Seismic reflection data do not show interpretable structures in the basement of the Iglesia basin, but there is a strong reflector, interpreted to be the top of the basement, potentially corresponding to the top of the projected back limb of the Tranca thrust (Beer et al., 1990; Ruskin and Jordan, 2007). By including only the Ordovician and Siluro-Devonian units in the western stratigraphic column, we calculate a thickness of 4600 m (table 3.1).

Table 3.2: Stratigraphic thickness values for profile B

Stratigraphy	*Unit thickness [m]*	*Unit uncertainty [m]*	*Source*
Eastern stratigraphy			
Vallecito (Oligocene)	250	100	Jordan et al. (1993a); Limarino et al., (1987)
Ojo de Agua (Permian)	400	100	Ottone and Azcuy (1986); Burcowski and Zambrano (1990)
Panacán (Pennsylvanian)	400		Ottone and Azcuy (1986); Burcowski and Zambrano (1990)
Volcan (Mississippian)	400	150	Ottone and Azcuy (1986); Burcowski and Zambrano (1990)
Talacasto (Devonian)	400	200	Furque (1979)
Los Espejos (Silurian)	200	100	Astini and Maretto (1996)
La Chilca (Silurian)	350	150	Astini and Maretto (1996)
Ordovician limestones (San Roque & San Juan)	3300	350	Furque (1979)
total:	5700	500	

Western stratigraphy			
Devonian units	1000	1000	Limarino and Cerasi (1992)
Ordovician slope units (Yerba Loca & Invernada)	3500	500	Furque (1984)
total:	4500	1200	

We assign 2000 m of uncertainty for the western column, but this is truly an estimate as there are many possible sources of variation in thickness in the western Precordillera. For example, Furque (1984) measured the thickness of the Yerba Loca formation at 1500 m, but this value does not necessarily represent the thickness of the Ordovician unit prior to Andean deformation. The many small faults and folds in the Ordovician may either predate Andean shortening or be a results of the Miocene thrusting so that any measured thickness may over- or under-estimate the true value. Additionally, while the Tranca and Caracol faults do not bring to the surface any unit younger than the Devonian shales, there is not restriction on their involvement in the subsurface. Finally, in addition to not knowing which units were involved in the motion on the Tranca thrust, the thickness of the younger units are also poorly constrained in the west. Therefore, we chose a large uncertainty value for the thickness of the western stratigraphic columns (tables 3.1 and 3.2).

The remaining required values are the individual uncertainties associated with each type of point on the enveloping polygon: surface, eroded hanging wall cut-offs, decollement, and subsurface (table 3.3). We estimate that the uncertainty on the location

of the vertices where the polygon crosses the surface of the Earth is 100 m. This value includes possible discrepancies between GPS and map locations using different data and projections, as well as graphical errors that may arise during the construction of either cross section or polygon.

Table 3.3: Input uncertainty value

Vertex	*Uncertainty*
Surface	100 m
Eroded hanging wall cut-offs	1000 m; 500 m
Decollement	East: δx = 1500 m; δy = 1000 m
	West: δx = 3000 m; δy = 1500 m
Subsurface	800 m
Modern width	3200 m

We partially constrain the uncertainty of the vertices at the hanging wall cut-offs by mapping the location in the footwall of minor vertical faults: we interpret these faults to represent fracture related to the overburden of a once present, but now eroded, hanging wall. The extent of these faults is a conservative estimate of the amount of post-thrusting erosion at a specific fault. Several footwall localities preserve these steep minor faults with vertical displacements, but many locations do not. Based on the distribution of these overburden faults, the steep dips of the main thrusts, and the narrowness of many of the valleys, we interpret the extent of the eroded hanging wall cut-offs conservatively, but assign 1000 m uncertainty values to the vertices on the eroded hanging walls. The exception to this is at the projected tips of the faults that are

less than 1000 m above the ground; for these faults, we assign 500 m of uncertainty (table 3.3).

The two vertices located on the decollement have different uncertainty values. At the eastern edge, we use seismic reflection data to interpret the decollement at 15 ± 1.5 km below the surface and to dip 2° ± 1° W. By using the seismic profiles to calculate the location of the eastern corner of the cross section and projecting the decollement beneath the Precordillera, the uncertainty on the dip of the decollement influences the lift-off location for the westernmost ramp. Using the 1° of uncertainty on the dip of the decollement and the 1500 m of uncertainty on the depth, we calculate a horizontal uncertainty of 3000 m on the projection of the decollement and a vertical uncertainty of 1500 m (table 3.3). Additionally, for the vertex on the western edge that represent the top of the stratigraphic column, we use 3000 m for both vertical and horizontal uncertainties. As a result of using the eastern corner of the polygon to locate the western corner, the locations and uncertainty values are not independent, as we discuss in the next section.

We chose to terminate the projection of the post- and syn-deformation strata at 2000 m below the surface. While this geometry may erroneously include this material in the subsurface in the area balancing polygon, these Miocene and younger strata are folded in many of the footwalls, limiting the down-dip extent of the strata. For vertices at this depth and shallower, we assign 800 m of uncertainty. A majority of the Cenozoic

strata are greater than 800 m thick, but not substantially, and this uncertainty value allows for the possibility that a larger portion of the foreland basin strata has been faulted out of the section.

Finally, for the uncertainty associated with the modern width of the cross section, the *AreaErrorProp* program calculates the current width from the location two most distal horizontal vertices. The uncertainty of the width, assuming a Gaussian distribution of the errors, is the square root of the sum of the squared values of the individual uncertainties. In this case, the uncertainty on the modern width is 3200 m, based on the horizontal uncertainties in the leading vertex (100 m) and the trailing vertex (3000 m).

3.5.2 Shortening magnitude

For each profile, we constructed polygons with increasing numbers of vertices and compared the calculated shortening magnitude to the complexity of the polygon to determine the minimum number of vertices needed to capture the shortening value without relying heavily on the modeled subsurface geometry (Fig. 3.8). Judge and Allmendinger (2011) suggested that the critical number is approximately 20 vertices, but we find that, in the case of the Precordillera, the magnitude of shortening does not significantly change between polygons with 5 and 70 vertices (Fig. 3.8) because the variation in the area is insignificant compared to the subsurface area. The specific

Fig. 3.8: Area balancing calculations for both profiles. a) and d) Restored wedges based on stratigraphic thicknesses and initial width calculated in area balance. b) and e) Polygons used for area balancing. Vertices and associated uncertainties shown, as well as the numerical values. c) and f) Plot showing shortening magnitude v. number of vertices for both the short and long profiles, as well as the value for the intermediate polygon.

a)

Profile A:

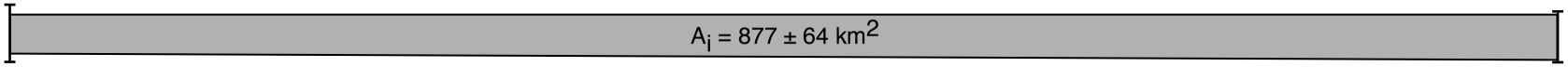

T_w = 4600 ± 2000 m

T_e = 5275 ± 500 m

b)

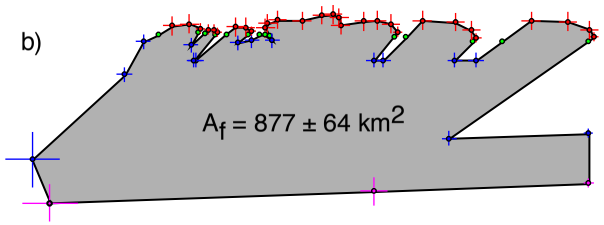

Surface:	δx = δy = 100 m
Normal subsurface:	δx = δy = 800 m (δx = δy = 3000 m)
Eroded hanging wall:	δx = δy = 1000 m (δx = δy = 500 m)
Decollement:	east: δx = 1.5 km; δy = 1.5 km west: δx = 3 km; δy = 2 km

c)

Shortening = 117 ± 40 (91) km

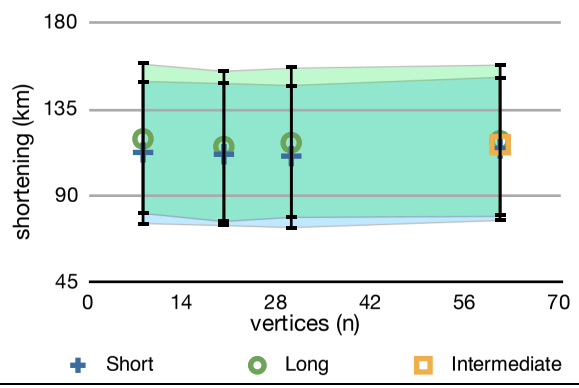

d)

Profile B:

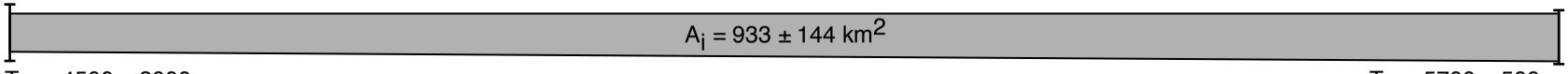

T_w = 4500 ± 2000 m

T_e = 5700 ± 500 m

e)

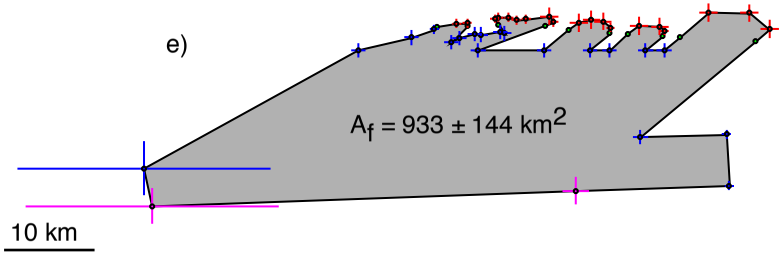

Surface:	δx = δy = 100 m
Normal subsurface:	δx = δy = 800 m (δx = 14 km; δy = 3000 m)
Eroded hanging wall:	δx = δy = 1000 m (δx = δy = 500 m)
Decollement:	east: δx = 1.5 km; δy = 1.5 km west: δx = 14 km; δy = 2 km

f)

Shortening = 114 ± 47 (118) km

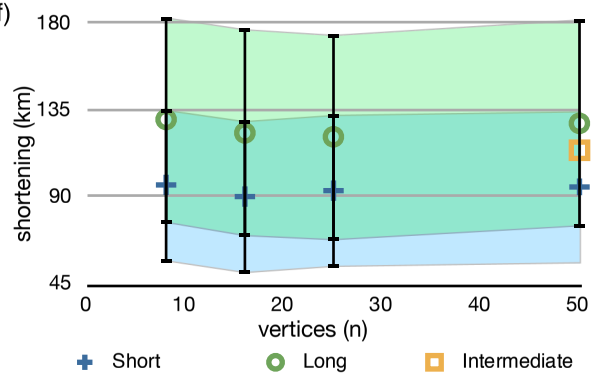

geometry of the Precordillera is responsible for this effect: the decollement is deep enough that the large cross-sectional area is not greatly impacted by changes near the surface.

For section A, area balancing yields 117 ± 40 km of shortening across the western and central Precordillera; section B shows 114 ± 47 km of shortening. For both of these polygons, we use an intermediate location for the trailing vertex on the decollement. This intermediate location is between the two extreme profile options outline above, and includes a horizontal uncertainty large enough to allow the vertex to be at either end position. While we consider the two profiles based on the surface geology to be more likely than the intermediate position, this method includes the wide range of possible geometries that may exist beneath the Iglesia basin.

Our calculated shortening magnitudes are similar to other values calculated for the Precordillera in the same region: 95 km along a similar cross section (Allmendinger et al., 1990) and 136 km farther south (Cristallini and Ramos, 2000). Allmendinger and others (1990) also computed a shortening value based on a generic area balance and estimated 72 km of shortening for the western and central Precordillera. The two largest differences between the previous estimates and our are the modeled dip of the trailing thrust in the western Precordillera, and the amount of syn- and post-deformation sediment that exist in the hanging wall of the Niquivil thrust. In both instances, the area

of our cross section is larger than that of the earlier cross sections, making our shortening magnitude estimate larger.

3.5.3 Error estimates

The uncertainty value of ± 40 km that we calculate is the Gaussian estimate, which assumes that all of the input uncertainty values are unbiased and uncorrelated. While we have tried to honor these assumptions, there are both obvious and subtle ways we violate these rules. For example, we used seismic reflection data to establish only the geometry of the decollement and not to calculate the stratigraphic thicknesses so as to avoid any correlation between the location of the structures and the initial wedge thickness. However, because the position of the western decollement vertex is influenced by the criteria used to determine the position of the eastern vertex, the uncertainties of these values are correlated. Furthermore, the location of the top of the western stratigraphic column is dependent not only on the location of the decollement but also on the stratigraphic thicknesses, which correlates with the uncertainty on the vertex to the other two values. Finally, while we have worked to have unbiased assessments of the uncertainties for the vertices, achieving this is difficult. For example, we assign 100 m of uncertainty for the vertices located at the surface of the Earth; others may consider this value optimistically low or conservatively high.

For these reasons, we also report the calculated maximum uncertainty values of 117 ± 91km for profile A and 114 ± 118 km for profile B. 114 ± 118 km is probably an

overly conservative value—we would not expect 4 km of extension across the thrust belt. Therefore, we expect that the more realistic uncertainty value would lie between the Gaussian and maximum estimates. Because there are relatively few uncertainty values that are correlated, though they are some of the largest values, it is possible that the realistic uncertainty estimate is closer to the Gaussian value for this case.

Our shortening values are larger than those calculated from the existing line-length balanced section, and the large uncertainty values we calculate suggest several possible interpretations. First, there is significant uncertainty on the thickness of the stratigraphic column in the western Precordillera. Because the stratigraphic thicknesses have a first-order impact on the shape of the undeformed wedge, the uncertainty on those values has a very strong impact on the overall shortening value and uncertainty. We estimate almost 40% uncertainty on the western stratigraphy, and it is possible that we have calculated a shortening value based on a wedge that is far too thin; a thicker initial column in the west would reduce the shortening value.

It is also possible that we have included a small component of non-Andean deformation in the wedge, which would over-estimate the shortening magnitude, as well. Alvarez-Marron and others (2006) suggest that a majority of the deformation observed in the Precordillera is Paleozoic in age and that there is only a minor component of Cenozoic over-printing of the older shortening. While others have noted the pre-Andean deformation in the Ordovician rocks in the western Precordillera

(Ramos et al., 1984; 1986; von Gosen, 1997), the deformation in these units is different from the Andean deformation in two important ways. First, the majority of the folds and faults in the Ordovician rocks are west-verging structures while the thrusts in the Precordillera are east-verging. Secondly, the Ordovician units have undergone slight greenschist metamorphism contemporaneous with the creation of the west-verging structures; the Precordillera faults are all brittle structures that show no evidence of metamorphism beyond cataclastic grain-size reduction to form fault gouge. These distinctions between the localized pre-Andean deformation and the pervasive Andean deformation indicate that any inclusion of pre-Andean deformation in the thrust belt is unlikely. However, as discussed previously, any pre-Andean deformation of the Ordovician rocks may make it more difficult to determine the true thickness of these units in the west.

3.6 Timing of thrust activity

The oldest phase of motion in the Precordillera is likely the formation of the Tranca and Caracol faults in the western Precordillera (Fig. 3.9). The Tranca fault that places Ordovician over Miocene redbeds must be younger than the 21.6 Ma units in its footwall (Jordan et al., 1993a). The Caracol fault, which is en echelon with the Tranca fault, may shorten during this period as well, but the evidence of this motion is not as well constrained. This early phase of motion, especially for the Tranca thrust, is likely to

Fig. 3.9: Sequence of motion on the 8 main thrusts in the Precordillera. Vertical scale is age in millions of years; horizontal scale is oriented west-east. Modified from Jordan et al. (1993). Jordan et al. (1993b), Zapata and Allmendinger (1996b), and Jordan et al. (2001).

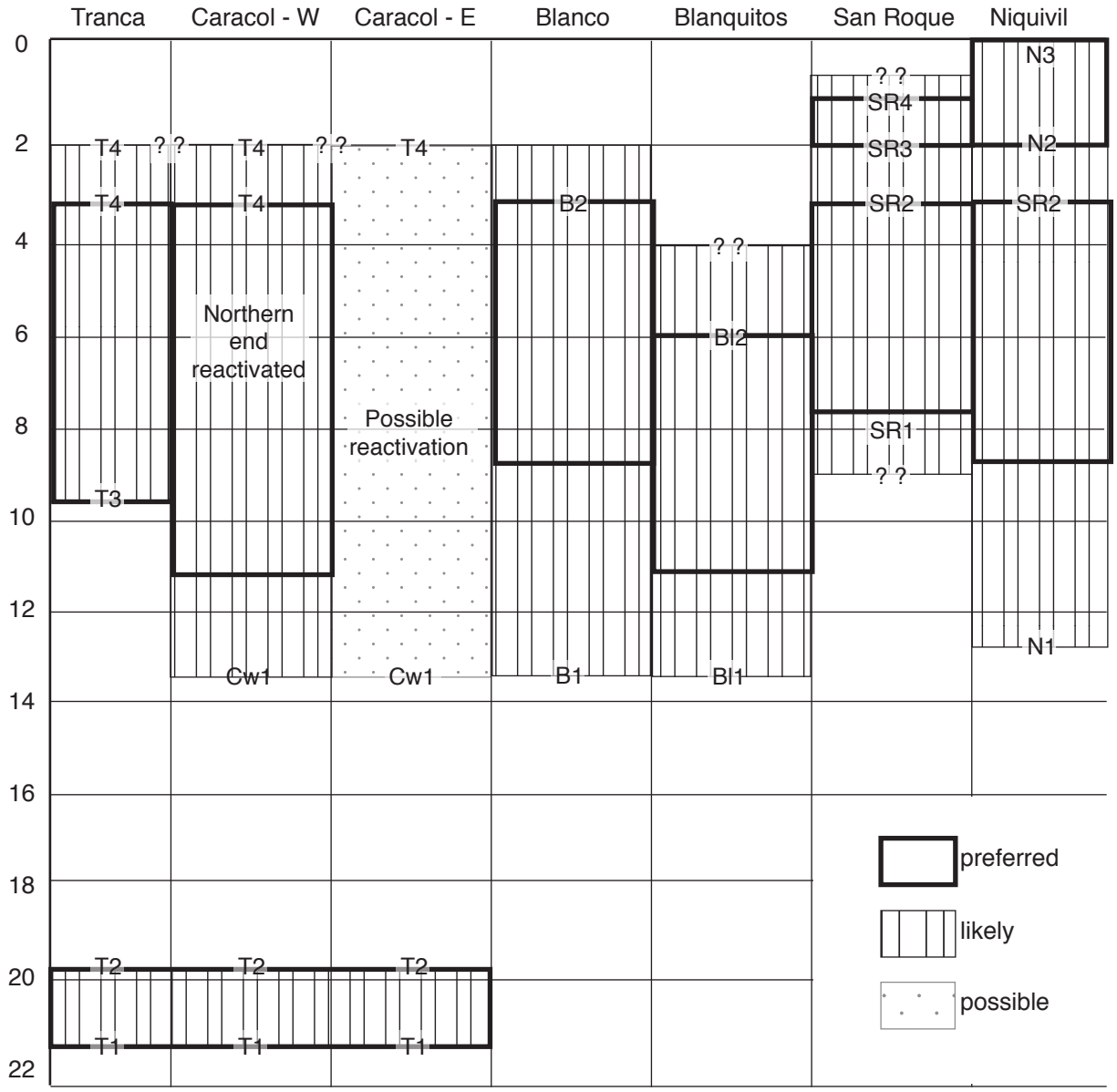

T1: Redbeds in footwalls of Tranca and Caracol thrusts (21.6 Ma)

T2: Gray conglomerates in Tranca valley (19.5 Ma)

T3: Chestnut conglomerates in Tranca footwall and on eroded Caracol hanging wall (9.4 Ma)

T4: Gravels in Tranca-Caracol valley, undisturbed by motion on the thrust faults (4 - 2 Ma)

Cw1: Eolian beds in Caracol footwall at north end and in Tranca-Caracol valley throughout (13.4 Ma)

B1: Motion on Blanco younger than units in footwall (13.4 Ma)

B2: Likely age of youngest conglomerates over east Caracol fault and top of Blanco (4 - 2 Ma).

Bl1: Eolian beds in Blanquitos footwall (13.4 Ma)

Bl2: Tertiary section in Blanquitos footwall lacks conglomerate unit. Does not deform Blanco.

SR1: Top of El Fiscal section in footwall (~8 Ma)

SR2: Deposition of Mogna facies (~5 Ma) on hanging walls of San Roque and Niquivil thrusts

SR3: Rotation of limestone conglomerates on hanging wall

SR4: Quiescence related to deposition of gravels

N1: Cerro Morado fm. on both sides of thrust (12.8 Ma)

N2: Motion on Niquivil folds Mogna f. related to motion in the La Pareja basin (2.0 Ma)

N3: Motion on Vallecito fault and modern scarps (~1 Ma)

be the most significant phase of motion on the fault based on the thickness of the gouge in the fault zone and the distance between the decollement and the surface. A period of quiescence followed and allowed for the erosion of the hanging wall and the subsequent deposition of the gray conglomerate against the fault surface at 19.5 Ma (Jordan et al., 1993a). The fault contact in the Tranca valley shows evidence of minor reactivation after the conglomerates were deposited, but the main phase of motion was likely finished by the time of deposition. The structural relationships of the southern half of the western fault in the Caracol valley are similar: Ordovician slope facies overlie 21.6 Ma redbeds in the footwall of the fault.

At the northern end of the Caracol valley, there are 13.4 Ma pink and green eolian sandstones in the footwall of the west-dipping fault, indicating that there was a significant phase of motion after the deposition on the sands. Uplift of the western Caracol fault after 13.4 Ma is consistent with the deposition of the chestnut conglomerate (9.4 Ma; Jordan et al., 1993b) onto the uplifted and eroded hanging wall of the Caracol fault. The discrepancy between the ages of the units in the footwall between the northern and southern ends of the Caracol fault suggests the final phase of motion on the northern part of the Caracol fault is younger than for the southern section. The data do not distinguish between whether this along-strike variation resulted from a reactivation of the northern portion or simply a later phase of initial motion on the northern half of the Caracol fault.

The timing of the motion of the eastern Caracol fault is less clear than that of the western fault (Fig. 3.9); at the northern end, the fault places Ordovician shelf facies over the 21.6 Ma redbeds, which is the geometry as on the southern end of the western fault. However, uplift on the eastern fault would break up the foreland basin to the east of the Tranca and Caracol faults. The apparent continuity of the oldest Miocene sediments in the basins in the western and central Precordillera suggest that the uplift of the eastern Caracol fault may post-date the deposition of the pink and green cross-bedded sandstones at 13.4 Ma (Jordan et la., 1993a). However, is also possible that motion on the eastern fault initiated at the same time as the other faults in the western Precordillera and that similar sediments were deposited in individual basins.

The western Precordillera is likely connected to the central Precordillera through the syncline in the hanging wall of the eastern Caracol fault that also forms the hanging wall of the Blanco fault. The Ordovician unit at the base of these thrusts is not the slope facies present in the hanging walls of the Tranca and Caracol faults at the northern ends of the valleys but is the shelf-facies San Juan limestone. The division between these facies is believed to be an approximately north-south striking feature with shelf facies to the east and slope facies to the west. The shelf-slope break between the Ordovician facies is not exposed at the surface, and this location must occur somewhere between the Tranca-Caracol fault to the west and the east-dipping Caracol fault. At the latitude

of profile B and to its south, the shelf facies are exposed at the base of the syncline in the Caracol and Blanco faults.

The Blanco fault has a relatively shallow dip in the center and southern portions of the valley (20° – 25° W), which is substantially gentler than the dips of the western Precordillera (~60° W). The synclinal structure between the eastern Caracol fault and the Blanco fault resolves the problem by allowing the Blanco fault to act as a break-out fault that is independent of the west-dipping faults in the western Precordillera. In this model, the western Precordillera becomes a thin-skinned triangle zone and the Blanco fault was formed during a phase of motion that was after 13.4 Ma, the age of the units in the Blanco footwall (Fig. 3.9).

The timing of the formation of the duplexes in the triangle zone that comprises the western Precordillera is unclear. These duplexes may have formed any time after the deposition of the 13.4 Ma sandstones in the center of the southern portion of the Tranca - Caracol valley. The formation of the duplexes would have rotated both the western and eastern Caracol faults, and likely the Tranca fault, as well. Both the Tranca and Caracol faults dip more steeply than their original orientation, but there is little to constrain the timing of these rotations.

The next significant phase of motion is likely the formation of the Blanquitos fault to the east of the Blanco valley (Fig. 3.9). The 13.4 Ma eolian sandstones are in both the hanging and footwalls of the Blanquitos fault, constraining the initial phase of

motion to be younger than the eolian beds. Additionally, the large anticline-syncline pairs in the hanging wall do not strongly fold the hanging wall of the Blanco fault, suggesting that the majority of the deformation on Blanquitos occurred before the Blanco fault reached the surface.

Motion on the Niquivil thrust, to the east of the Blanquitos fault, is difficult to constrain. Fault motion is bracketed by the 12.8 Ma Cerro Morado formation near the northern end of the anticline produced by motion on the fault (Jordan et al., 1993a); the volcaniclastic unit is on both sides of the anticline and was folded by motion on the thrust. The deposition of the Mogna facies (Zapata and Allmendinger, 1996a) at ~5 Ma, which was rotated after its deposition, implies a period of quiescence before 5 Ma. Though the fault motion is necessarily younger than 12.8 Ma and older than 5 Ma, there is little else to constrain the initiation of motion on the fault. The relationship between the hanging walls of the Niquivil thrust and the San Roque thrust is ambiguous: the two hanging walls have similar dip angles. This similarity may imply that the San Roque fault formed first and that the material to the west of the Niquivil thrust was a hanging wall flat that was rotated when the Niquivil fault moved later; alternatively, the Niquivil thrust may have formed first and then the San Roque fault formed, out of sequence, and was not rotated by the Niquivil fault.

Between ~9 – 8 Ma, the Blanco fault formed and placed the limestone over the conglomerates in the footwall; motion on the Blanco thrust must post-date the 13.4 Ma

units in the footwall. Because the strata that correlate to the 13.4 Ma data come from a unit that is almost a kilometer below the thrust, movement may have been significantly later than 13.4 Ma. Motion on the Blanco fault may have been continuous or intermittent, but it is possible that the motion on the Blanco fault was related to the reactivation of both the Tranca and Caracol faults after the deposition of the 9.4 Ma conglomerates in the Tranca valley. Additionally, because the hanging wall of the Blanco fault cuts across the Blanquitos hanging wall (Fig. 3.9), the last phase of motion on the Blanco fault must post-date the formation of the motion on the Blanquitos thrust. Jordan and others (2001) interpreted the minimum duration of motion in the western Precordillera to be through ~9 – 8 Ma, which matches the timing of motion in the Tranca valley to place the redbeds over the 9.4 Ma chestnut conglomerates and to rotate the chestnut conglomerate on the Caracol hanging wall.

These final phases of motion in the western Precordillera and the formation of the Blanco fault likely impacted the drainage systems throughout the Precordillera. There are extensive gravel units throughout the western Precordillera and on the syncline between the Caracol and Blanco thrusts that help to confine the final stages of motion on the Tranca, Caracol, and Blanco faults (Fig. 3.10). The gravels in the Tranca - Caracol are poorly consolidated but are now heavily incised. There are at least two qualitatively distinct gravels in the central portion of the valley: the older gravel dips ~30° W and has large clasts from the western Precordillera;

Fig. 3. 10: DEM showing extent of high-elevation gravels in the western Precordillera based on field mapping and satellite imagery, including Google Earth and LandSat data.


-69º
-30º
50 km

the younger gravel dips ~15° W and is much finer grained. The younger of these gravels is not cut by motion on the faults, signaling that motion had ceased at these locations by some time before the Pliocene (Cardó and Díaz, 1999). On the crest of Cerro Blanco and in the syncline between the Caracol and Blanco faults, there are extensive gravels surfaces that are now incised. These gravels appear younger than the undated but likely Pliocene gravels in the Tranca - Caracol valley, and we interpret the gravels to indicate that the final stage of uplift of the Blanco fault ended by ~4 – 1 Ma.

The relative activity between the Blanco and Niquivil thrusts is ambiguous; there is no direct relationship between the two faults. It is possible that the two faults moved during the same period, but we do not have data to conclude simultaneous motion. Were the Niquivil fault to have formed and moved before the Blanco fault, this would represent the accretion of the Niquivil thrust plate to the toe of the wedge and then internal thickening of the thrust belt as Blanco moved. Alternatively, if the Blanco fault stopped moving before slip on the Niquivil fault, this would represent a typical foreland-breaking fault sequence.

Between the Blanquitos and Niquivil thrusts, the San Roque thrust folded eolian beds in its hanging wall and must post-date the deposition of the sandstones at 13.4 Ma. At the northern end of the fault, the magnetic polarity of the sediments in the footwall indicate that the top of the section is 9 – 8 Ma, indicating that the last phase of motion was likely after 8 Ma. There is evidence in the form of rotated conglomerates on the

hanging wall of the San Roque thrust that there was some minor reactivation in the last ~5 Ma, but that there was not likely much motion after the rotation of the 5 Ma conglomerates.

Both the Niquivil and San Roque thrusts show evidence of reactivation in the past 3 Ma. Before approximately 5 Ma, both faults experienced a period of quiescence while the Mogna facies was deposited. Seismic reflection data in the Bermejo basin indicate that the eastern Precordillera formed after 2.6 Ma (Zapata and Allmendinger, 1996b), and this motion faulted and refolded the Niquivil thrust near its tip line, and folded the Mogna facies on its hanging wall. The San Roque fault was reactivated or refolded by the Niquivil thrust after ~3 Ma, folding the limestone conglomerates on the hanging wall (Zapata and Allmendinger, 1996a). Motion likely ceased on the San Roque thrust by ~1 Ma, when the Vallecito fault moved between the two ridges (Allmendinger et al., 1990). The Niquivil thrust is likely still active: there is a ~10 meter fault scarp at the toe of the Niquivil fault that uplifts an active alluvial fan, indicating that the fault is either still active or moved recently (Fig. 3.6).

3.7 Discussion

3.7.1 Geometric relationships in the Precordillera

Our new field data make several changes to the existing, generalized cross sections of the Precordillera at the latitude of the Río Jáchal (Alvarez-Marron et al., 2006; von

Gosen, 1997), and make some modifications to the line-length balanced sections from Allmendinger and others (1990). By connecting the eastern Caracol thrust to the Blanco thrust through a syncline, we modify the interpretations of von Gosen (1997) and Alvarez-Marron and others (2006), and build on the interpretations of Allmendinger and others (1990). Additionally, we connect the Tranca and Caracol faults to each other, if not physically than in origin. This connection of the entire western Precordillera in the form of a triangle zone and its relationship to the Blanco thrust, forming as a break out fault at the toe of the triangle zone, is a new interpretation.

We also modify the sequence of formation of the faults in the central Precordillera. Our preferred interpretation is that the Blanquitos fault formed and moved after 11 Ma, followed by the formation of the Blanco thrust likely some time after 9 – 8 Ma. These two thrusts have definitive cross-cutting relationships and show an out-of-sequence relationship because the Blanco fault formed after the Blanquitos material as added to the wedge (Fig. 3.11). Any of the faults in the central Precordillera may have moved between ~11 Ma and ~5 Ma and motion may have been simultaneous or alternating across the faults, as long as the Blanco fault moved following the formation of the Blanquitos fault. Given the relief across the Blanco thrust and the elevation of the hanging wall, as well as the relatively young gravels at its summit, it is possible that the last phase of motion on the Blanco fault was as recent as the Pliocene.

Fig. 3.11: Profiles C, D, and E from Fig. 3.4 showing the near-surface structures in the Tranca - Caracol valley. Lithology is the same as for Fig. 3.2.

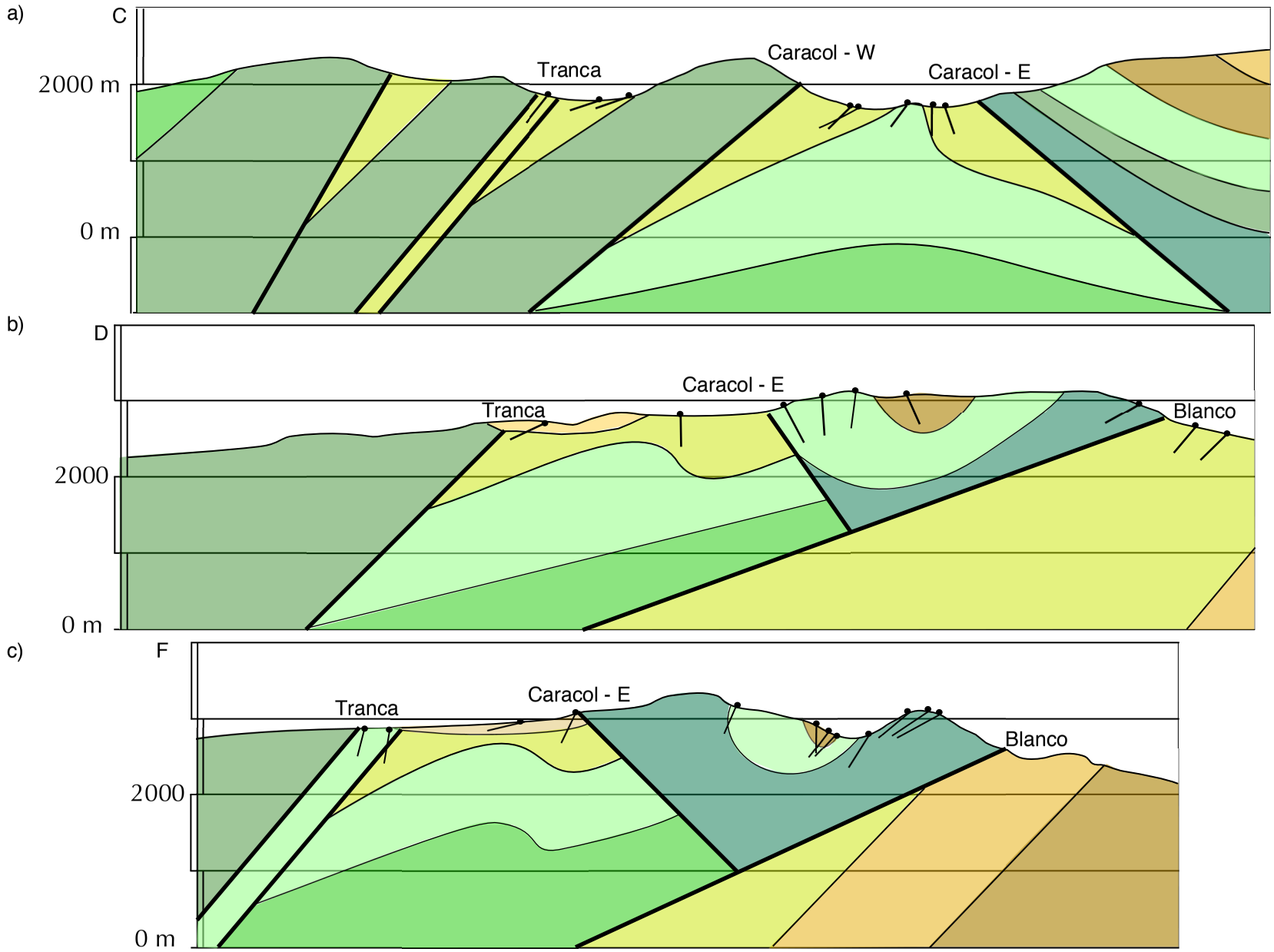
a)
C
2000 m
0 m
Tranca
Caracol - W
Caracol - E
b)
D
2000
0 m
Tranca
Caracol - E
Blanco
c)
F
2000
0 m
Tranca
Caracol - E
Blanco

3.7.2 Three periods of motion on the Precordillera

There is strong evidence that the motion on the thrusts in the Precordillera was confined to three distinct periods of motion: prior to 19.5 Ma, with motion confined to the western Precordillera; from 11 – 3 Ma, when fault motion switched to the central Precordillera with reactivation in the western Precordillera; and from 3 – 0 Ma, when the eastern Precordillera formed and the central Precordillera was both reactivated and folded by the eastern Precordillera. These constraints on timing agree well with earlier interpretations of the motion on the Precordillera: Jordan and others (1993a; 2001) found a similar gap in motion between ~19 Ma and ~14 Ma, and Zapata and Allmendinger (1996a) showed a reduction in slip rate between approximately 4 and 3 Ma.

We interpret the motion on the faults in the Caracol valley to be slightly younger than the age from Jordan and others (1993a; 2001). Because the 9.4 Ma chestnut conglomerate in the Tranca valley has a buttressed unconformity relationship with the hanging wall of the east-verging Caracol fault at the north end of the Tranca valley, one interpretation of this relationship is that the Caracol hanging wall must have been uplifted and eroded before 9.4 Ma. Additionally, because the same fault has 13.4 Ma sandstones in its footwall, the fault likely moved between 13.4 Ma and 9.4 Ma. However, the 20° W dips of the beds of the chestnut conglomerate indicate that the Caracol hanging wall were likely rotated some time after their deposition. Given the western source of the chestnut conglomerate and their likely initial dip to the east, these

beds may have been rotated more than 20°. While the Caracol thrust likely was passively rotated above the duplexes in the triangle zone to the east, the initial uplift and erosion of the hanging wall likely occurred after 13.4 Ma. This period prior to the reactivation of the Caracol thrust was likely a period of significant quiescence from 19.5 Ma to 12 – 11 Ma.

The second significant change in shortening in the Precordillera occurred at 4 – 3 Ma. During this shift, the majority of motion transferred from the central to the eastern Precordillera and there was only minor reactivation in the central thrusts after this transition. Zapata and Allmendinger (1996a) also showed this switch in activity at approximately the same time: Fig. 18 shows a significant reduction in slip rate in the central Precordillera after 4 Ma followed by a sharp increase in motion in the eastern Precordillera starting after 2.6 Ma

The time periods that we document are temporally correlated to the major changes in the slab geometry of the subducting Nazca plate. Yáñez and others (2001; 2002) suggested that the slab began shallowing at ~10 Ma, and Kay and Abbruzzi (1996) documented the last phase of magmatism in the Precordillera at 4.7 Ma, indicating that the slab was likely horizontal by approximately 5 Ma. The increase in shortening activity that we see in the central Precordillera at 11 Ma may be related to the increased coupling along the interplate surface between the shallow slab and the South American plate (Martinod et al., 2010). The decrease in shortening after 4 Ma may be related to a

decrease in plate convergence velocity: Somoza (1998) reported a 25% decrease in velocity between the Nazca and South American plates at 4.9 Ma. While the temporal shifts are not perfectly correlated, the three periods of shortening may be related to changes in the slab geometry and velocity.

3.7.3 Shortening magnitudes and decollement length

Calculating the magnitude of shortening across the Precordillera highlights two significant outcomes: 1) the calculated decollement projects ~115 km west of the Niquivil thrust, placing it below the high elevation of the Andes, and 2) the majority of the shortening in the Precordillera occurred after ~20 Ma. While von Gosen (1997) and others report evidence of shortening and folding in the Paleozoic units of the Precordillera, Alvarez-Marron and others (2006) extended this to suggest that the majority of the shortening is pre-Andean. The basis of this claim is that the strata from the Late Carboniferous and younger are not strongly deformed above the older Paleozoic rocks, and that there is evidence of oblique motion on faults in the western Precordillera.

While we agree that there was pre-Andean deformation throughout the region, we also document several areas where units from the Pennsylvanian and Permian are folded equally as strongly as the lower Paleozoic units in the hanging walls of the major thrusts in the Precordillera (Fig. 3.2). The Neogene and Quaternary strata in the hanging

walls typically have a conformable relationship with the underlying Paleozoic strata, indicating that the most significant phase of thin-skin thrusting impacted the Paleozoic and Cenozoic units equally. Additionally, von Gosen (1997) reported that most of the structures in the Paleozoic units in the western Precordillera verge to the west, as is the case at Cerro Viento along the Río Jáchal transect, while all but one of the thrusts in the Precordillera verge to the east. Because the strata throughout the Precordillera are folded equally in the hanging walls of the thrusts, and because the Paleozoic structures have an opposite sense of vergence from the brittle faults, we believe that our field data show that the majority of shortening in the Precordillera is Andean in age.

The shortening magnitudes that we calculate using an area balancing method (1117 ± 40 km and 114 ± 47 km) are in good agreement with the shortening estimates derived from line-length balanced cross sections in the Precordillera. Allmendinger and others (1990) calculated 95 km of shortening for a cross section at a latitude similar to our profile A, and they performed a generic area balance to calculate ~72 km of shortening, excluding shortening on the Tranca and Niquivil thrusts. Zapata and Allmendinger (1996b) extended the cross sections to include the eastern Precordillera, adding ~16 km of shortening across the thrust belt. To the south, along the Río San Juan, Cristallini and Ramos (2000) calculated 136 km of shortening, including motion on the eastern Precordillera.

While the agreement between the different models suggests that the cross sections are robust, the shortening value still requires that the decollement project ~115 km to the west of the Niquivil thrust scarp, which is directly below the high topography of the Andes (Fig. 3.12). The location of the decollement beneath the Frontal Cordillera in the Andes is bolstered by broad-band receiver function data that shows a strong reflector at approximately the same location and dip as our projected decollement (Gans et al., 2011; Gilbert et al., 2006).

If the decollement truly extends 115 km to the west of the central Precordillera, this requires ~115 km of shortening in the middle and lower crust. Accomplishing this shortening would require that the ramp into the basement needed to produce the crustal thickening associated with the main peaks of the Andes be still farther west. Including the uncertainty on our calculated shortening values (± 40 km for profile A; ± 47 km for profile B) shows a wide range of possible locations for the ramp into the basement. At the extreme low value of the Gaussian uncertainties, the decollement still projects beneath the Frontal Cordillera; at the high end of the uncertainty values, the ramp would be well under Chile. Any ramp into the basement located at the end of the decollement would still require some additional method for thickening the crust below the Principal Cordillera (Fig. 3.12).

Allmendinger and others (1990) also encountered this problem and proposed two possible models for thickening the crust: a crustal-scale wedge that utilizes the

Precordillera decollement as part of the footwall flat, or a lower crustal duplex that utilizes the decollement as part of the roof thrust of the duplex. These two models

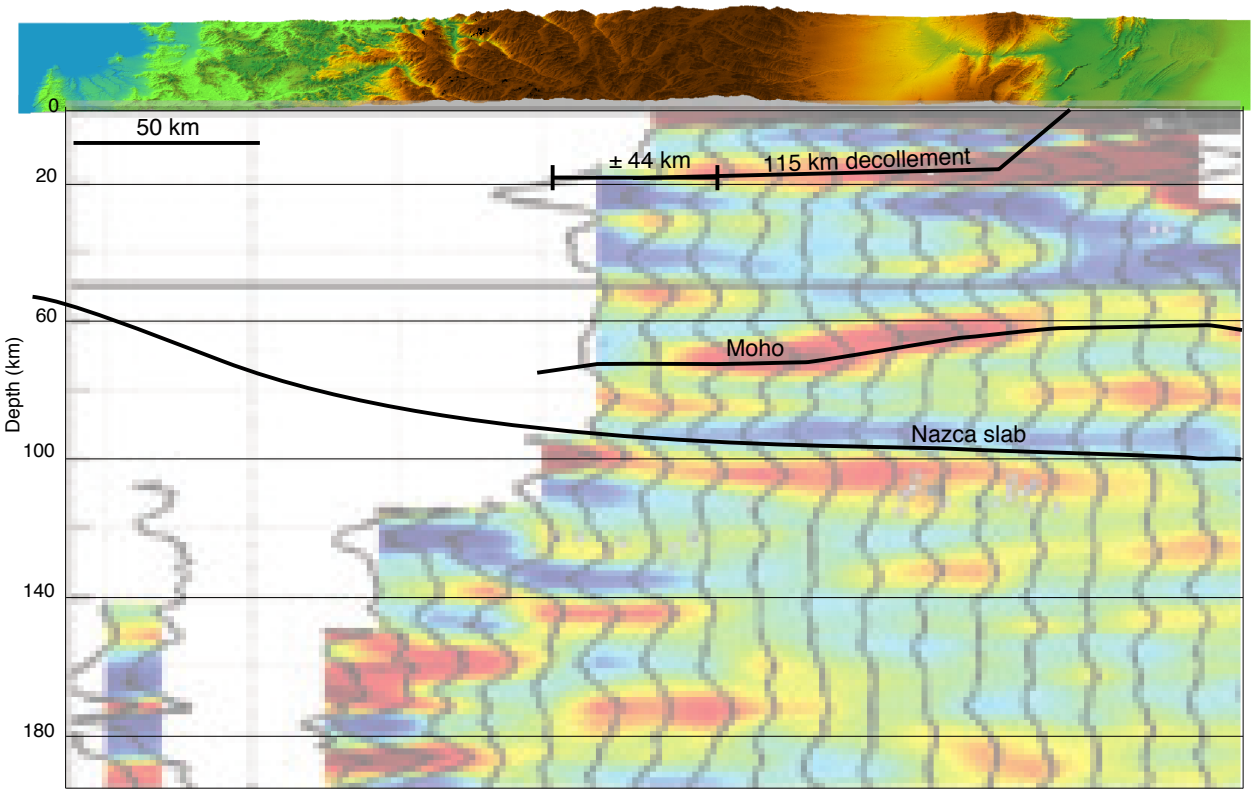

Fig. 3.12: Perspective DEM looking north along the Precordillera, Andes, Chilean coast, and Pacific ocean. Subsurface receiver function data from Fig. 4 in Gans et al. (2011) along their "X-Line 15" which crosses the Precordillera in our study area. The interpreted location of the Nazca slab and the Moho are from Gans et al. (2011). The location of the decollement and its uncertainty band are projected below the Niquivil thrust and to the west. The decollement corresponds to the location of a strong boundary in the receiver function data. Few structures are observable below the high Andes, though other profiles from Gans et al. (2011) reveal several strong boundaries below the Andes at relatively shallow depths (15 – 20 km).

account for the ~100 km of shortening in the Precordillera and ~55 km of shortening in the Principal Cordillera (Allmendinger et al., 1990). Our decollement location agrees with these models but does little to distinguish between the two. Receiver function data from beneath the Precordillera and Principal Cordillera are equivocal with regard to the two models; there is evidence for neither a crustal scale wedge nor a lower crustal duplex below the Andes (Gans et al., 2011; Gilbert et al., 2006).

3.8 Conclusions

Our new field data reveal several geometric and temporal refinements to the existing cross section in the Precordillera at 30ºS, and we calculate shortening estimates with rigorous uncertainty estimates along two sections in the region. Based on our field data and calculations, we present the following conclusions.

1) The sequence of motion on the major faults in the Precordillera is not as tightly constrained as previously described. The Blanco fault likely moved in the Pliocene or Quaternary, and evidence in the form of river incision through a 10+ m scarp suggests that the Niquivil thrust was recently or is currently active. While the Precordillera was previously interpreted as an in-sequence fold-and-thrust belt (Jordan et al., 1993a), we present broader evidence of out-of-sequence motion in the central Precordillera.

2) There were three distinct periods of motion in the Precordillera that are roughly divided by motion on the western, central, and eastern Precordillera sections. Prior to 19.5 Ma, motion was restricted to the western Precordillera. After a period of quiescence, the central Precordillera formed and shortened between 11 – 3 Ma, with some reactivation in the western Precordillera. After 3 Ma, the majority of motion occurred in the eastern Precordillera and as minor reactivation on the San Roque and Niquivil thrusts in the central Precordillera. These periods of motion are temporally correlated to changes in the geometry of the slab as well as plate convergence velocity.

3) In order to more accurately constrain the timing of motion and reactivation in the western Precordillera, obtaining data on the age of the deposition of the gravels in the Tranca - Caracol valley would be useful. Three distinct gravels need dates for the age of their deposition: the gravels that are undeformed by motion on the Tranca and Caracol thrusts in the central region of the valley; the high elevation gravels that cross the Caracol fault at ~3200 m; and the gravels that lie in the syncline between the Caracol and Blanco faults.

4) We calculate 117 ± 40 km and 114 ± 47 km of shortening across the Precordillera via area balancing. These shortening values agree with estimates calculated from existing line-length balanced sections (76 – 136 km). Additionally, we provide uncertainty

bounds on our estimates that allow for the realistic comparison of cross sections in the Precordillera as well as between the Precordillera and other regions in the Andes.

5) The decollement for the Precordillera projects ~115 km to the west, which is well below the high topography of the Principal Cordillera. The uncertainty estimates describe a range of possible locations for a basement ramp, all of which are below the high elevations in the Andes. The location of the decollement continues to require an explanation for how to significantly thicken the crust above and below a thin-skinned detachment.

3.9 References

Allmendinger, R. W., Figueroa, D., Snyder, D., Beer, J., Mpodozos, C., Isacks, B. L., 1990. Foreland shortening and crustal balancing in the Andes at 30ºS latitude. *Tectonics* 9, 789-809.

Alvarez-Marron, J., Rodriguez-Fernandez, R., Heredia, N., Busquets, P., Colombo, F., Brown, D., 2006. Neogene structures overprinting Palaeozoic thrust systems in the Andean Precordillera at 30ºS latitude. *Journal of the Geological Society, London* 163, 949-964.

Astini, R. A., 1998. Stratigraphical evidence supporting the rifting, drifting and collision of the Laurentian Precordillera terrane of western Argentina. In: R. J. & Rapela, C. W. (Eds.), The Proto-Andean Margin of Gondwana. Geological Society, London, Special Publications 142, pp. 11–33.

Astini, R. A., Maretto, H. M., 1996. Analisis estratigrafico del Silurico de la Precordillera Central de San Juan y consideraciones sobre la evolucion de la cuenca. *XIII Congreso Geológico Argentino y III Congreso de Exploración de Hidracarburos Acts I*, 351-368.

Baldis, B. A. J., Beresi, M. S., Bordonaro, O., Vaca, A., 1982. Sintesis evolutiva de la Precordillera Argentina. *V Congreso Latinoamericana de Geologia Actas* 4, 399-445.

Baldis, B. A. J., Chebli, G., 1969. Estructura profunda del área central de la Precordillera sanjuanina. *IV Jornadas Egológicas Argentinas* I, 47-66.

Beer, J. A., Allmendinger, R. W., Figueroa, D. E., Jordan, T. E., 1990. Seismic stratigraphy of a Neogene piggyback basin, Argentina. *AAPG Bulletin* 74, 1183-1202.

Beer, J. A., Jordan, T. E., 1989. The effects of Neogene thrusting on deposition in the Bermejo basin, Argentina. *Journal of Sedimentary Research* 59, 330-345.

Bracaccini, O., 1946. Contribución al conocimiento geológico de la Precordillera Sanjuanino-Mendocina (primer parte). *Boletín de Informaciónes Petroleras* 258 (Buenos Aires), 81-105.

Burcowski, F., Zambrano, J. J., 1990. Carbonifero y Permico de San Juan. *Decimo Primer Congreso Geológico Argentino, San Juan*, 78-99.

Cahill, T., Isacks, B. L., 1992. Seismicity and shape of the Nazca plate. *Journal of Geophysical Research* 97, 17503-17529.

Cardó, R., Díaz, I. N., 1999. Hoja Geológica 3169-I: Rodeo (versión Preliminar), Provincia de San Juan. *Servicio Geológico Minero Argentino Boletín No. 272*.

Chamberlin, R. T., 1910. The Appalachian folds of central Pennsylvania. *Journal of Geology* 18, 228-251.

Cristallini, E. O., Ramos, V. A., 2002. Thick-skinned and thin-skinned thrusting in the La Ramada fold and thrust belt: crustal evolution of the High Andes of San Juan, Argentina (32ºSL). *Tectonophysics* 317, 205-235.

Furque, G., 1979. Descripción geológica de la hoja 18 c, Jáchal, Provincia de San Juan. Buenos Aires, Argentina, Servicio Geológico Nacional, Boletín 164, 79 pp.

Furque, G., 1983. Descripción geológica de la hoja 19 c, Ciénega de Gualilán, Provincia de San Juan. Buenos Aires, Argentina, Servicio Geológico Nacional, Boletín 193, 111 pp.

Gans, C. R., Beck, S. L., Zandt, G., Gilbert, H., Alvarado, P., Anderson, M., Linkimer, L., 2011. Continental and oceanic crustal structure of the Pampean flat slab region, western Argentina, using receiver function analysis: new high-resolution results. *Geophysical Journal International* 186, 45-58, doi: 10.1111/j.1365-246X. 2011.05023.x.

Gilbert, H., Beck, S., Zandt, G., 2006. Lithospheric and upper mantle structure of central Chile and Argentina. *Geophysical Journal International* 165, 383-398, doi: 10.1111/j.1365-246X.2006.02867.x.

González, P., Furque, G., Caballé, M., 1999. Hoja Geológica 3169-II: San Jose de Jáchal, Provincia de San Juan. *Servicio Geológico Minero Argentino*.

Hossack, J. R., 1979. The use of balanced cross-sections in the calculation of orogenic contraction: a review. *Journal of the Geological Society* 136, 705-711. doi:10.1144/gsjgs.136.6.0705.

Jordan, T. E., Isacks, B. L., Allmendinger, R. W., Brewer, J. A., Ramos, V. A., Ando, C. J., 1983. Andean tectonics related to geometry of subducted Nazca plate. G*eological Study of America Bulletin* 94, 341-361.

Jordan, T. E., Allmendinger, R. W., Damanti, J. F., Drake, R. E., 1993a. Chronology of motion in a complete thrust belt: The Precordiller, 30–31ºS, Andes mountains. *Journal of Geology* 101, 135-156.

Jordan, T. E., Drake, R. E., Naeser, C. W., 1993b. Estratigrafia del Cenozoico Medio en la Precordillera a la latitud del Río Jáchal, San Juan Argentina. *XII Congreso Geológico Argentino y II Congreso de Exploración de Hirdocarburos, Actas II*, 132-141.

Jordan, T. E., Schlunegger, F., Cardozo, N., 2001. Unsteady and spatially variable evolution of the Neogene Andean Bermejo foreland basin, Argentina. *Journal of South American Earth Sciences* 14, 775-798.

Judge, P. A., Allmendinger, R. W., 2011. Assessing uncertainties in balanced cross sections. *Journal of Structural Geology* 33, 458-467, doi:10.1016/j.jsg.2011.01.006.

Kay, S. M., Abbruzzi, J. M., 1996. Magmatic evidence for Neogene lithospheric evolution of the central Andean "flat-slab" between 30ºS and 32ºS. *Tectonophysics* 259, 15-28.

Limarino, C. O., Sessarego, H. L., López Gamundi, O. R., Gutierrez, P. R., Césari, S. N., 1987. Las formaciones Ojo de Agua y Vallecito en el area de la Cienaga, oeste de Huaco, provincia de San Juan: Estatigrafia y paleoambientes sedimentarios. *Revista de la Asociación Geológica Argentina* 42, 153-167.

Limarino, C. O., Cerasi, S. N., 1992. Reubicación estratigráfica de la Formación Cortaderas y definición Grupo Angualasto (Carbonífero inferior, Precordillera de San Juan). *Revista de la Asociación Geológica Argentina* 47, 61-72.

Martinod, J., Husson, L., Roperch, P., Guillaume, B., Espurt, N., 2010. Horizontal subduction zones, convergence velocity and the building of the Andes. *Earth and Planetary Science Letters* 299, 299-309, doi:10.1016/j.epsl.2010.09.010.

Mitra, S., Namson J., 1989. Equal-area balancing. *American Journal of Science* 289, 563-599.

Ortíz, A., Zambrano, J. J., 1981. La provincia geológica Precordillera oriental. *VIII Congreso Geológico Argentina Actas 3*, 59-74.

Ottone, E. G., Azcuy, C. L., 1986. El perfil de la Quebrada La Delfina, Provincia de San Juan, Argentina. *Revista de la Asociación Geológica Argentina* 41, 124-136.

Ramos, V. A., Jordan, T. E., Allmendinger, R. W., Kay, S. M., Cortés, J. M., Palma, M. A., 1984. Chilenia: un terreno alóctono en la evolución paleozoica de los Andes Centrales. *IXº Congreso Geológico Argentina, Actas II*, 84-106.

Ramos, V. A., Jordan, T. E., Allmendinger, R. W., Mpodozis, C., Kay, S. M., Cortés, J. M., Palma, M. A., 1986. Paleozoic terranes of Central Argentine–Chilean Andes. *Tectonics* 5, 855-880.

Ruskin, B. G., 2006. Sequence stratigraphy and paleopedology of nonmarine foreland basins: Iglesia basin, Argentina and Axhandle basin, Utah. PhD thesis, Cornell University.

Ruskin, B. G., Jordan, T. E., 2007. Climate change across continental sequence boundaries: Paleopedology and lithofacies of Iglesia basin, northwestern Argentina. *Journal of Sedimentary Research* 77, 661-679.

Siame, L. L., Bellier, O., Sebrier, M., 2006. Active tectonics in the Argentine Precordillera and western Sierras Pampeanas. *Revista de la Asociación Geológica Argentina* 61, 604-619.

Siame, L. L., Bellier, O., Sébrier, M., Araujo, M., 2005. Deformation partitioning in flat subduction setting: Case of the Andean foreland of western Argentina (28ºS–33ºS). *Tectonics* 24, TC5003, doi:10.1029/2005TC001787.

Smalley, R. J., Pujol, J., Régnier, M., Chiu, J.-M., Chatelain, J.-L., Isacks, B. L., Araujo, M., Puebla, N., 1993. Basement seismicity beneath the Andean Precordillera thin skinned thrust belt and implications for crustal and lithospheric behavior. *Tectonics* 12, 63-76.

Somoza, R., 1998. Updated Nazca (Farallon)—South America relative motions during the last 40 My: implications for mountain building in the central Andean region. *Journal of South American Earth Sciences* 11, 211-215.

Thomas, W. A., Astini, R. A., 2003. Ordovician accretion of the Argentine Precordillera terrane to Gondwana: a review. *Journal of South American Earth Sciences* 16, 67-79.

von Gosen, W., 1997. Early Paleozoic and Andean structural evolution in the Río Jáchal section of the Argentine Precordillera. *Journal of South American Earth Sciences* 10, 361-388.

Yáñez, G. A., Ranero, C. R., von Huene, R., Díaz, J., 2001. Magnetic anomaly interpretation across the southern central Andes (32º-34ºS): The role of the Juan Fernández Ridge in the late Tertiary evolution of the margin. *Journal of Geophysical Research* 106, 6325-6345.

Yáñez, G., Cembrano, J., Pardo, M., Ranero, C., Selles, D., 2002. The Challenger–Juan Fernández–Maipo major tectonic transition of the Nazca–Andean subduction system at 33–34ºS: geodynamic evidence and implications. *Journal of South American Earth Sciences* 15, 23-38.

Zapata, T. R., Allmendinger, R. W., 1996a. Growth stratal records of instantaneous and progressive limb rotation in the Precordillera thrust belt and Bermejo basin, Argentina. *Tectonics* 15, 1065-1083.

Zapata, T. R., Allmendinger, R. W., 1996b. Thrust-front zone of the Precordillera, Argentina: A thick-skinned triangle zone. *AAPG Bulletin* 80, 359-381.

CHAPTER FOUR:

Strain partitioning and shortening rates in the Argentine Precordillera: A comparison of shortening rates and slab geometry

4.1 Abstract

The surface expression of flat slab subduction has been documented over the past ~30 years, but the dynamics between the subducting slab and the over-riding crust remain relatively poorly understood. In many locations, there may be as few as 10 – 20 km between the top of the slab and the bottom of the continental crust, depending on the depth of the slab and the thickness of the over-riding crust; this proximity suggests that there is the potential for coupling between the plates. To test the influence of the shallowing slab on deformation at the surface, we show fault slip data and shortening rates for faults throughout the Argentine Precordillera that span the time period over which the Nazca slab shallowed. While the shortening directions vary little since ~20 Ma, well before the slab began to shallow, we find evidence for strain partitioning between the thrusts in the Precordillera and steep dextral faults in the Iglesia basin. We also show that shortening rates in the Precordillera increased sharply at ~9 – 8 Ma, following the initiation of the shallowing of the Nazca slab at ~10 Ma. We interpret the temporal correlation between the shallowing of the slab and the increased shortening rates to support a model of interplate dynamics where the increased surface area

between the plate encourages locking at the plate boundary and transfers strain to the foreland fold-and-thrust belt.

4.2 Introduction

The geometry and history of the evolving central Chilean flat slab is relatively well known, as is the deformation history of the over-riding South American plate, but relatively little is known about the potential coupling between the down-doing and over-riding plates in shallow subduction zones. Barazangi and Isacks (1976) originally defined the shape of the subducting Nazca slab, and its shape has been refined several times since (e.g. Anderson et al., 2007; Cahill and Isacks, 1994; Gans et al., 2011). The slab likely began to shallow by ~10 Ma and reached its current configuration by ~4.5 Ma (Kay and Abbruzzi, 1996; Yáñez et al., 2001; 2002). Shortening at the surface progressed from west to east in the Argentine Precordillera fold and thrust belt (Allmendinger et al., 1990; Baldis et al., 1982; Jordan et al., 1993; Jordan et al., 2001; Ortíz and Zambrano, 1981), and the most recent phase of motion is localized on the eastern faults and thick-skinned basement uplifts of the Sierras Pampeanas (Coughlin et al., 1998; Jordan et al., 1993; Jordan et al., 2001; Zapata and Allmendinger, 1996) (Fig. 4.1). The common expression of modern and relict (e.g. Laramide Rocky Mountain foreland) regions of shallow subduction at the surface includes the absence of arc volcanism, thick-skinned uplifts in the foreland, and an increase in the seismic energy in the overriding plate

(Cross and Pilger, 1982; Gutscher et al., 2000; Jordan and Allmendinger, 1986; Kay and Abbruzzi, 1996; Kay et al., 1988).

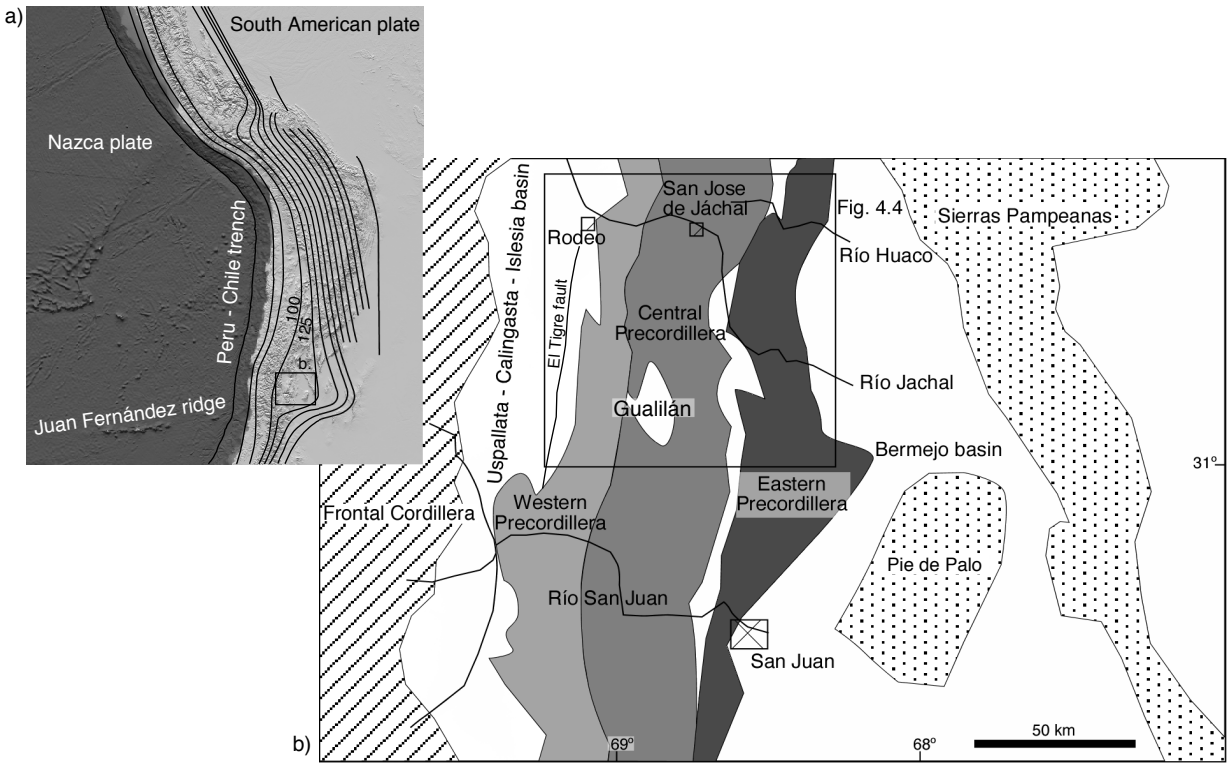

Fig. 4.1: Regional map of western South America and the Precordillera. a) DEM showing Nazca and South American plates with contours of the depth to the slab based on Cahill and Isacks (1992), as well as the location of the Juan Fernández ridge. Inset shows location of b. b) Tectonic map of the Argentine Precordillera north of San Juan. Inset shows location of Fig. 4.4.

Despite our knowledge of plate motions and deformation related to shallow subduction, our understanding of the interplate dynamics comes primarily from analog and numerical modeling (e.g. Dominguez et al., 1998; Espurt et al., 2008; Hampel et al., 2004; Martinod et al., 2010; van Hunen et al., 2002). In addition to providing insight into the geodynamic solutions to supporting the horizontal component of the shallow slabs, these models also support the observed increase in shortening at the surface (Jordan and Allmendinger, 1986; Jordan et al., 1993; Siame et al., 2005). The results from Martinod and others (2010) suggest that the increased surface area between the plates as the slab shallows results in increased frictional locking along this surface, yielding the observed and modeled increases in shortening at the surface. However, previous work in the Argentine Precordillera did not include shortening directions on the major faults not rigorous shortening estimates to related the shortening in the upper plate to the changing geometry of the down-going slab.

We present fault slip data and estimated shortening rates throughout the Precordillera to investigate the relationship between the Nazca slab and deformation patterns in the over-riding South American crust. The fault slip data are on faults from 21 Ma to younger than 2.6 Ma, spanning the time over which the Nazca slab transitioned from a relatively steep subduction angle to horizontal. We find that the shortening directions changed very little as the slab shallowed, but that shortening activity and rates increased sharply ~1 – 2 Ma after the slab began to shallow. We also

find evidence for strain partitioning between the down-dip motion on the thrusts in the Precordillera and dextral offset on the El Tigre and other steep faults in the Iglesia-Calingasta valley. We interpret the increased shortening activity to suggest that there was an increased coupling between the plates as the slab shallowed, slowing the plate convergence rate and transferring shortening from the plate boundary to the foreland thrust belt.

4.3 History of the Precordillera and the Nazca slab

4.3.1 Deformation history of the Precordillera

The Argentine Precordillera at ~30ºS evolved since ~21 Ma from a thin-skinned fold-and-thrust belt in the western and central region (Allmendinger et al., 1990; Baldis and Chebli, 1969; Jordan et al., 1993; Ortíz and Zambrano, 1981) to a thick-skinned train of open anticlines at its eastern edge (Allmendinger et al., 1990; Smalley et al., 1993; von Gosen, 1992; Zapata and Allmendinger, 1996). The two westernmost fault valleys comprise the western Precordillera, where the decollement is within the slope facies of the Ordovician units, while the thrusts of the central Precordillera bring Cambro-Ordovician limestones to the surface; the footwalls for both regions are foreland basin strata (Baldis et al., 1982; Furque, 1979; 1983; Jordan et al., 1993) (Fig. 4.1). Basement sourced faults in the eastern Precordillera fold the thick foreland sediments in the Bermejo basin that are as young as 2.7 Ma (Zapata and Allmendinger, 1996) and active

faults scarps are present at the eastern margin of the central Precordillera and active seismicity characterizes the Sierras Pampeanas.

The first phases of motion began in the western Precordillera between 21.6 and 19.5 Ma (Jordan et al., 1993). After a period of relative quiescence, significant shortening activity resumed after ~13 Ma (Jordan et al., 1993; 2001; Judge, 2012) on multiple faults throughout the newly-formed central Precordillera and as reactivation of faults in the western Precordillera. The most intense period of shortening was from ~11 – 3 Ma, with the majority of motion from 3 – 0 Ma occurring as shortening in the eastern Precordillera and minor reactivation on the eastern thick-skinned thrusts (Jordan et al., 1993; Judge, 2012; Zapata and Allmendinger, 1996).

Several cross sections through the Precordillera at differing latitudes depict different interpretations of the shortening in the region. Allmendinger and others (1990) drew a line-length balanced section and calculated 95 km of shortening across the western and central Precordillera. Zapata and Allmendinger (1996) added 7 – 21 km of shortening based on their cross sections through the eastern Precordillera. Across two sections in the Precordillera, one of which was at approximately the same latitude of that from Allmendinger et al. (1990), Judge (2012) calculated ~115 ± 45 km of shortening for the western and central portions of the Precordillera based on an area balancing method. To the south, near San Juan, Cristallini and Ramos (2000) calculated 136 km of shortening through the entire Precordillera. While there is a variety of shortening

magnitude estimates for the Precordillera, all values fall within the uncertainty estimates from Judge (2012).

4.3.2 The geometry of the Nazca slab

The evolving geometry of the subducting Nazca slab has been assembled primarily using magnetic lineations in the oceanic crust and magmatism in the over-riding South American plate. Prior to ~10 Ma, the Nazca slab subducted at a relatively steep angle below the Argentine Precordillera (Kay and Abbruzzi, 1996; Yáñez et al., 2001; 2002). During this period, the subducting portion of the aseismic Juan Fernández ridge was oblique to the plate convergence direction (Fig. 4.2) and this obliquity forced the ridge-trench intersection to sweep southward along the coast (Yáñez et al., 2002). At ~10 Ma, a bend in the ridge aligned the trend of the portion of the ridge near the trench with the convergence direction, stabilizing the subduction location at the coast to the west of the Precordillera (Yáñez et al., 2001; 2002).

The subduction of aseismic ridges and oceanic plateaus is frequently invoked to explain shallow subduction, and the Juan Fernández ridge is no exception. Gutscher and others (2000) compared ridge location and flat slab subduction along the South American coast as well as other subduction zones and determined that the buoyancy of the thickened crust has a first-order impact on the subduction angle of the

down-going slab. While Barazangi and Isacks (1976) first identified the central Chilean low-angle

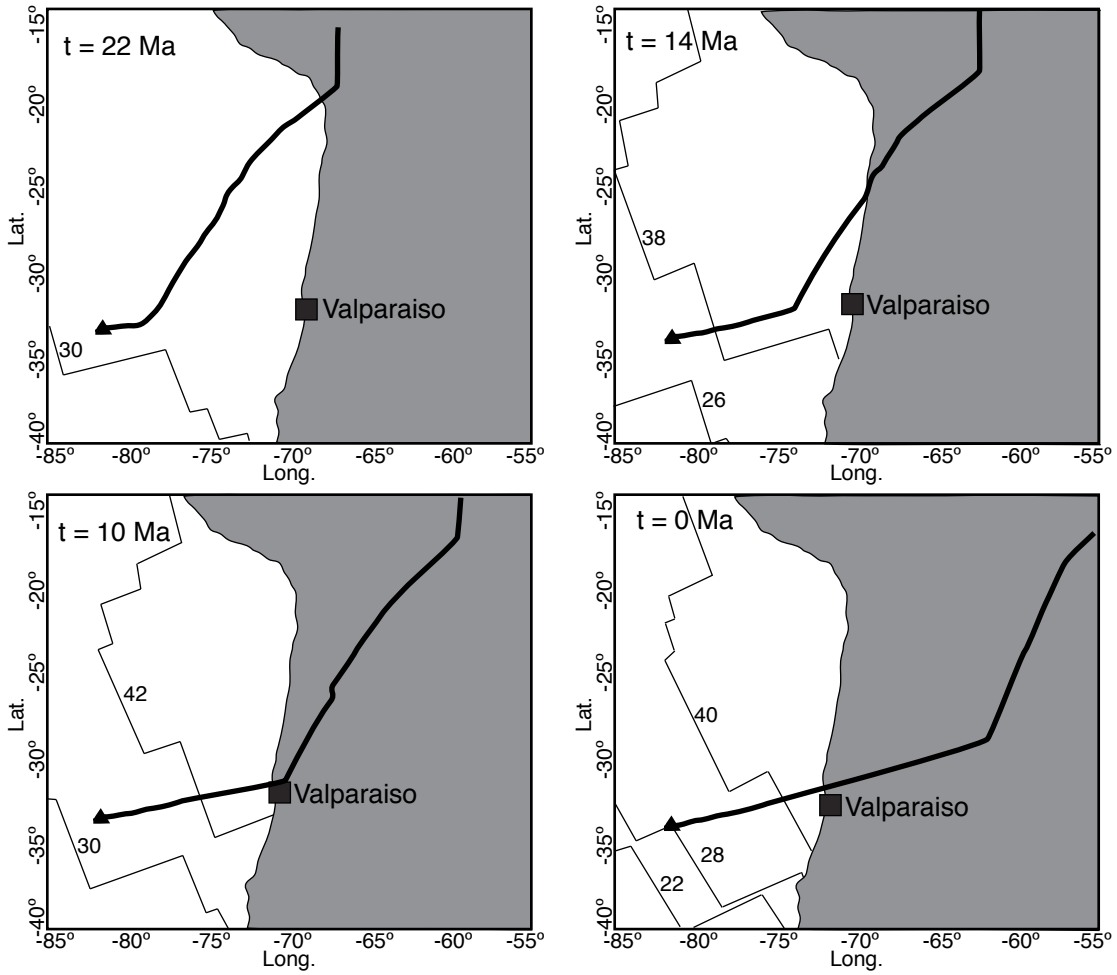

Fig. 4.2: Sequence showing progressive location of the Juan Fernández ridge (heavy black line) as it was subducted below the South American continent (shaded gray). The thin black lines show the location and number of sea-floor spreading magnetic lineations. The intersection location between the coast of Chile and the ridge moves southward until ~10 Ma.

subduction zone, the recent work by Gutscher and others (2000), von Hunen and others (2002), and Yáñez and others (2001; 2002) have strongly linked the Juan Fernández ridge to the region of shallow subduction.

If we assume that shallow subduction begins when the Juan Fernández ridge is overridden by the South American plate, we can calculate a minimum amount of time needed for the ridge to impact the Precordillera. The corner of the ridge reaches the trench at ~11 Ma, when the convergence rate between the plates was 10.9 cm/yr (Somoza, 1998; Yáñez et al., 2002); the distance from the trench to the center of the modern Iglesia basin is ~350 km. At the specified convergence rate, it would take approximately 3 million years for the ridge to reach the western edge of the Precordillera, suggesting that we would expect to see the impact of the shallowing slab after ~8 Ma.

Currently, the slab forms a horizontal bench, 80 – 100 km below the Precordillera, that extends ~400 km east from the trench (Anderson et al., 2007; Gans et al., 2011). The last phase of magmatism in the Principal Cordillera was at ~10 Ma, and magmatism ceased completely in the Precordillera by ~4.6 Ma (Kay and Abbruzzi, 1996). The lack of magmatism and the absence of the volcanic line above the shallow slab suggest that the mantle wedge was removed during the flattening of the slab.

In addition to the lack of magmatism above a shallow slab, the main feature associated with horizontal subduction are thick-skinned basement uplifts (Cross and

Pilger, 1982; Jordan and Allmendinger, 1986; Jordan et al., 1983; Pilger, 1981). Beyond these two features at the surface, there are relatively few predictions for how shallowing subduction impacts deformation in the upper plate. Gutscher and others (2000) document an increase in shallow seismicity, as well as greater seismic energy release above regions of low-angle subduction. In addition, Espurt and others (2008) use analog models to predict increased shortening rates above a shallow slab, which is consistent with field students of the region above the Chilean flat slab (Jordan and Allmendinger, 1986; Ramos et al., 2002; Siame et al., 2005).

4.4 Fault populations and kinematics

We collected fault slip data throughout the Precordillera to describe the strain field in the region as the Nazca slab shallowed from a 30° subduction angle to horizontal over the past ~10 Ma. Because the Precordillera experienced shortening over the entire period of the slab shallowing, we can test to see if shortening magnitude or direction evolved over time. Faults in the western Precordillera initiated at ~20 Ma (Jordan et al., 1993), the easternmost fault in the central Precordillera has an active 10 – 15 m scarp (Judge, 2012), and the anticlines in the eastern Precordillera are likely still deforming based both on crustal seismicity and GPS velocities (Smalley et al., 1993; Brooks et al., 2003); this span of time allows us to compare fault populations both temporally and spatially.

In the field, we measured fault plane orientation, the units in the hanging and footwalls, and determined a slip direction and sense for each fault. We used both striae and fault zone foliation to determine the slip sense and direction, with a preference for striae. We also used offset markers, such as clasts and bedding plates, to determine the sense of motion on the faults (e.g. Petit, 1987). We attempted to assign a quality rating to our fault slip data, especially if the data were notably above or below average quality, which helped to determine the reliability of a fault population. We group fault populations based on field locality and the lithologic units involved in each fault, as well as the relative amount of strain accommodated by the fault.

We analyze the fault slip data using averaged fault plane solutions for the fault populations throughout the Precordillera. We used *FaultKin 5*, which used algorithms described in Marrett and Allmendinger (1990) and Allmendinger and others (2012) to calculate the average fault plane and infinitesimal strain axes for the fault populations (Cembrano et al., 2005; Claypool et al., 2002; Marrett and Allmendinger, 1990). The calculation involves determining the principal axes of infinitesimal extension (X) and contraction (Z) for each fault population based on the individual fault orientation, slip direction, sense of motion, and, when available, weighting information such as the quality of the slip indicator or the displacement across the fault. In addition to the fault populations we describe in the field, for some locations we break the fault population apart when there are clear subsets of orientations of fault plane and slip direction to

highlight these differences; we do not ascribe temporal significance to the different subsets.

We present the fault populations throughout the Precordillera based on the timeline established by Judge (2012), who divided activity in the region into three time periods (Fig. 4.3 b). Prior to ~20 Ma, shortening was confined to the western Precordillera (Fig. 4.4), based on the ages of the sediments in the intermontane valleys and the geometry of the faults. After a period of quiescence, shortening resumed in the Precordillera at ~11 Ma when the major faults in the central Precordillera formed and there was also reactivation of the faults in the western Precordillera. This time period is

Fig. 4.3: Detailed shortening rate from 22 – 0 Ma in the Precordillera along profiles A and B. Gray regions show preferred timing of motion and reactivation in specific faults. Inset figure shows averaged slip rates and uncertainty bands for the three periods of activity: 21.6 – 19.5 Ma; 11 – 3 Ma; 3 – 0 Ma. Open black boxes show maximum duration of slip on each fault. Modified from Judge (2011).

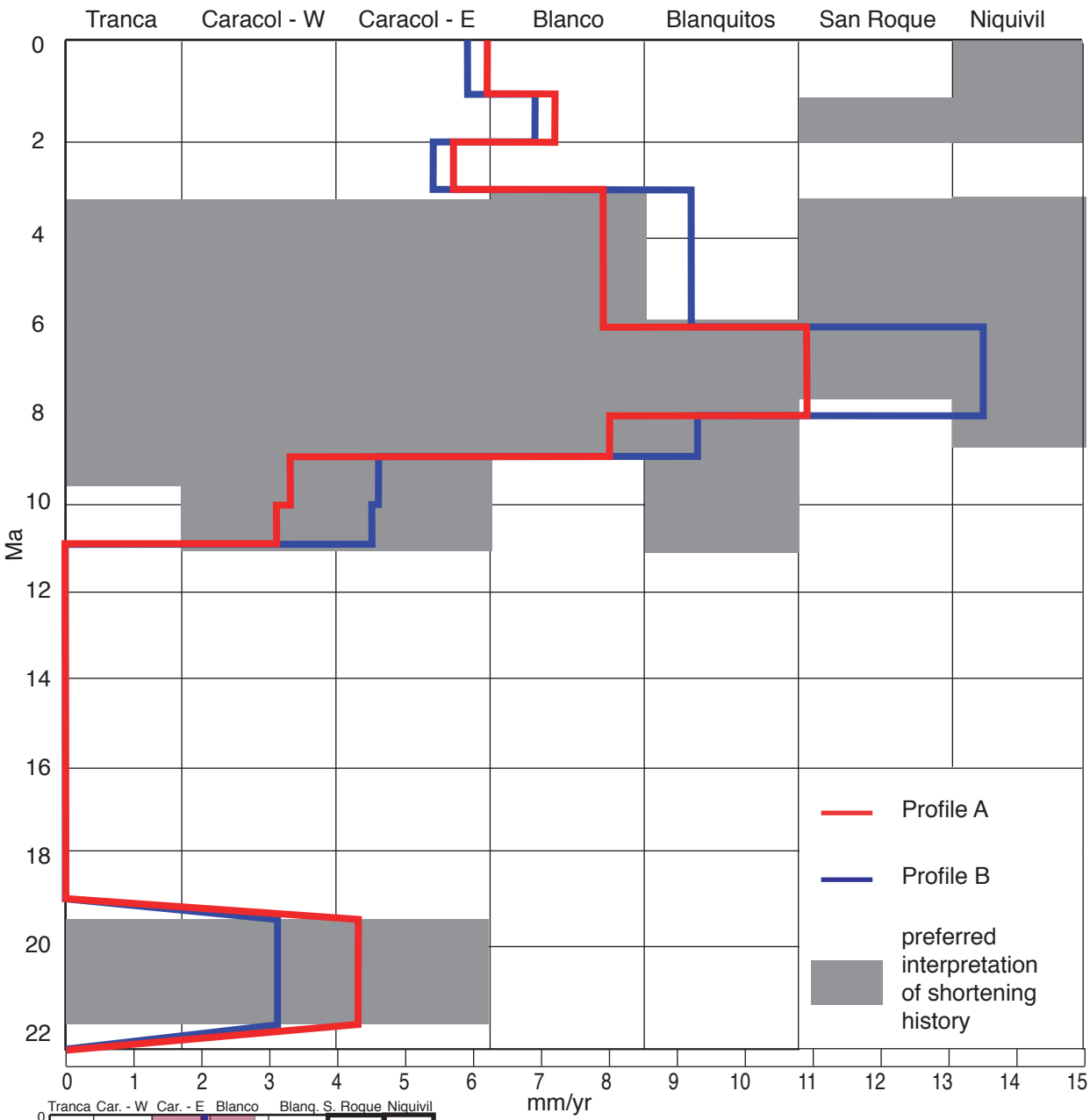

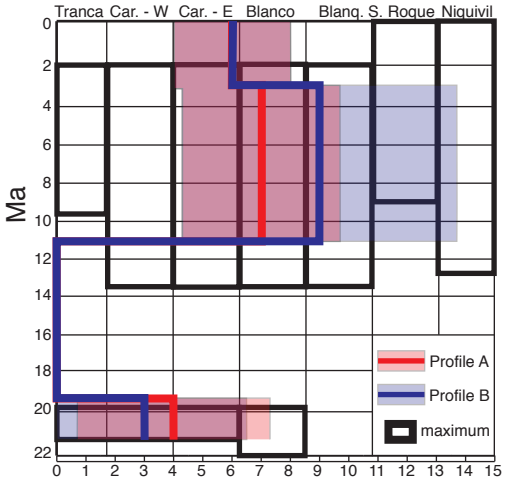

mm/yr

Averaged shortening rates [mm/yr]:

	Profile A	Profile B
3 – 0 Ma	6 ± 2	6 ± 2
11 – 3 Ma	7 ± 2.7	9 ± 4.7
21 – 19 Ma	4 ± 3.3	3 ± 3.5

Fig. 4.4: Geologic map of the Precordillera at ~30ºS. The profiles used to calculate shortening rates are along A-A′ and B-B′. Inset shows location of Fig. 4.9. Modified from Judge (2012).

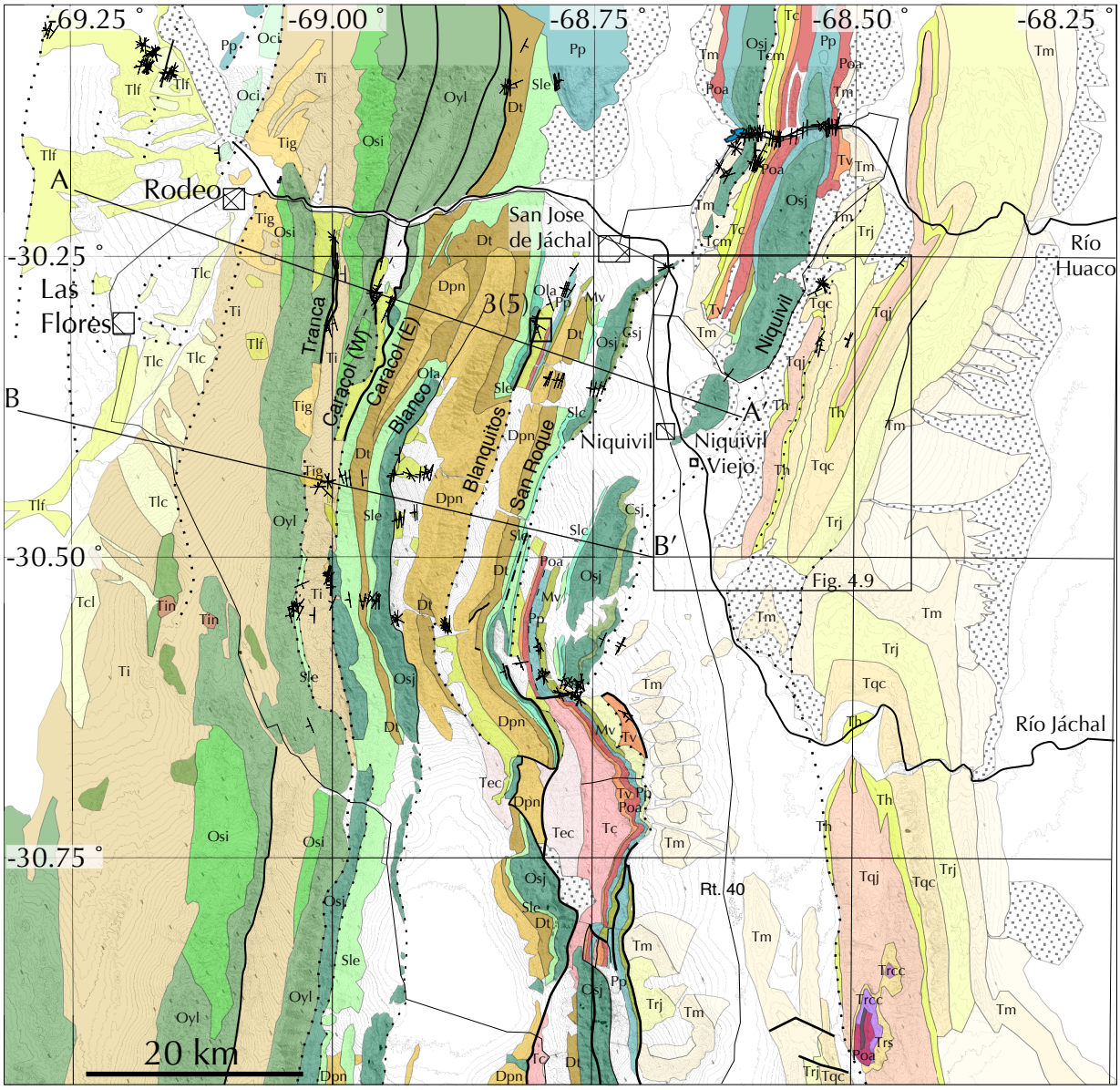

Iglesia basin sediments:

- (pls) Iglesia
- (pl) Las Flores
- (m) Tertiary intrusives
- (m) Lomas del Campanario
- (m) Iglesia Group

Fault
Covered fault
Inferred fault
River
Town
Road

Precordillera units and Bermejo basin sediments:

- (Tr) Cañon Colorado
- (p) Ojo de Agua
- (Pp) Panacan
- (M) Volcan
- (d) Punta Negra
- (d) Talacasto
- (s) Los Espejos
- (s-o) La Chilca
- (o) Cuerpos Ingeos Basicos
- (o) Yerba Loca
- (o) Sierra de la Invernada
- (o) Los Azules
- (o) San Juan
- (c) San Roque
- (q) alluvial deposits
- (hl) active fan deposits
- (pls) relict fan deposits
- (m) El Corral
- (m) Cuculi
- (pl) Mogna
- (pl) Rio Jáchal
- (m) Quebrada del Cura
- (m) Huachipampa
- (m) Quebrada del Jarillal
- (m) Rio Salado
- (m) Cauquenes
- (m) Cerro Morado
- (ol) Vallecito

defined by the ages of the stratigraphy in the footwalls of the faults, the geometry of the thrusts, and rotated conglomerates in the hanging walls. Finally, from ~3 – 0 Ma, the easternmost faults in the central Precordillera were reactivated and some were likely deformed during the formation of the anticlines in the eastern Precordillera after 2.7 Ma (Zapata and Allmendinger, 1996).

4.4.1 21.6 – 19.5 Ma

The fault populations preserved from the earliest time period are all from the western Precordillera, in the Tranca and Caracol valleys (Jordan et al., 1993) (Fig. 4.5). The three dominant faults in these valleys are the west-dipping Tranca fault, and the west- and east-dipping Caracol faults (table 4.1). These faults place Ordovician slope and shelf facies over 21.6 Ma redbeds (Jordan et al., 1993). In both the Tranca and Caracol valleys, the faults typically have a 2 – 5 m thick damage zone with sharp boundaries between the gouge and the hanging and footwalls. There is significant damage within the Tertiary units, likely due to the competency contrast between the shales and sandstones in the hanging wall that have undergone slight greenschist metamorphism (von Gosen, 1997) and the siltstones in the footwall. There is frequently a well-defined fault-zone foliation in the gouge.

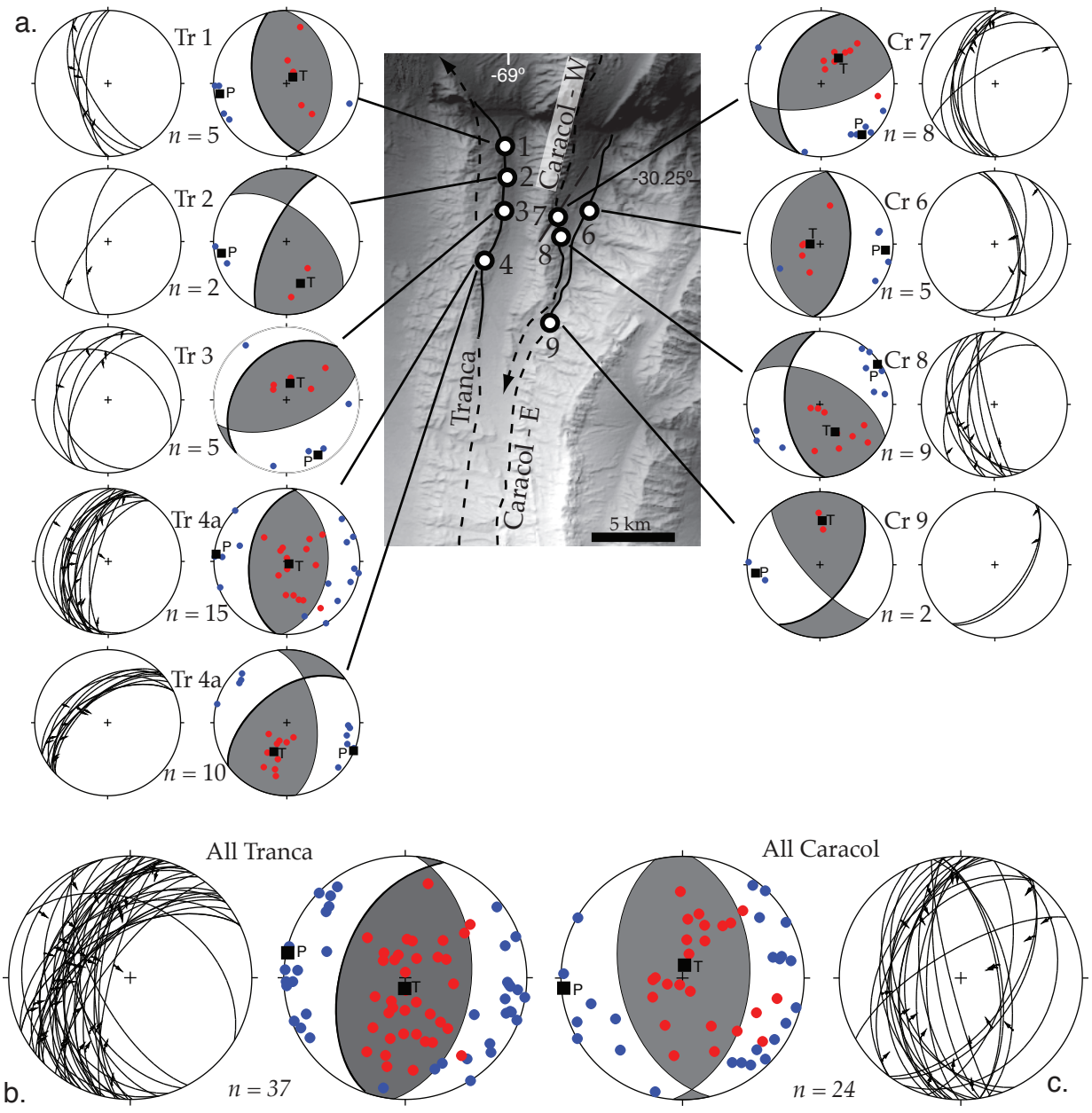

Fig. 4.5: a.) DEM of the western Precordillera showing field locations of faults active from 21.6 – 19.5 Ma in the Tranca and Caracol valleys. Stereonets show the fault slip data for each site and the fault plane solution shows the average fault plane and P axis for each fault population. b.) Stereonet shows all fault data for the Tranca valley and its fault plane solution. c.) Stereonet shows all fault data for the Caracol valley and its fault plane solution.

Table 4.1: Fault populations in the Precordillera

Site	*Coordinates (Lat. - Long.)*	*HW / FW*	*n*	*P trend*	*P plunge*	*T trend*	*T plunge*
25 - 20 Ma:							
Tranca							
1	-30.23, -69.01	Ord / T	5	262	8	41	80
2	-30.26, -69.00	Ord / T	2	260	10	162	40
3	-30.28, -69.01	Ord / T	5	150	15	11	71
4a	-30.30, -69.01	Ord / T	15	276	2	139	87
4b	-30.30, -69.01	Ord / T	10	113	2	205	54
Caracol							
6	-30.28, -68.95	Ord / T	5	95	12	272	78
7	-30.29, -68.97	Ord / T	8	141	12	33	55
8	-30.39, -68.97	Ord / T	9	55	4	151	55
9	-30.36, -68.98	Ord / T	2	263	12	2	39
11 - 3 Ma:							
Tranca							
1a	-30.23, -69.01	Gc / T	10	277	2	50	87
1b	-30.23, -69.01	T/ Cc	1	248	23	113	59
2	-30.26, -69.00	T / Cc	4	257	10	108	79
3	-30.28, -69.01	T / Cc	2	296	18	73	66
4	-30.30, -69.01	T / Cc	14	108	9	231	73
Caracol							
5	-30.25, -68,97	T / Cc	5	92	32	260	58
Blanco							
10	-30.43, -68.93	T / T	3	69	53	295	28
11	-30.43, -68.95	Ord / T	1	103	24	282	66
12	-30.47, -68.95	Ord / T	2	294	5	39	70
13	-30.55, -68.95	T / T	10	53	14	281	70
Blanquitos							
14	-30.30, -68.82	Ord / T	4	123	13	356	71
15	-30.31, -68.81	T / T	9	302	6	72	80
16	-30.32, -68.82	T / T	2	68	49	303	26
Estancia Durazno							

Site	*Coordinates (Lat. - Long.)*	*HW / FW*	*n*	*P trend*	*P plunge*	*T trend*	*T plunge*
17	-30.55, -68.90	Ord / T	2	130	12	31	38
18	-30.56, -68.90	T / T	6	122	30	14	28
San Roque							
19	-30.15, -68.61	Ord / T	1	121	12	343	74
20	-30.16, -68.61	T / T	2	342	26	120	57
21	-30.17, -68.61	T / T	12	317	1	225	73
Niquivil							
22	-30.14, -68.54	Ord / Ord	1	282	5	102	85
Río Francia							
23	-30.61, -68.79	Pal / Pal	3	171	42	287	26
24	-30.62, -68.78	Pal / T	14	48	7	281	79
25	-30.62, -68.77	T / T	5	190	8	292	58
26	-30.63, -68.73	T / T	11	29	7	215	83
27	-30.60, -68.77	Ord / T	1	156	25	31	51
3 - 0 Ma:							
Río Francia							
28	-30.62, -68.74	Q / T	5	30	29	217	61
Niquivil Anticline							
29	-30.32, -68.55	T / T	9	299	32	205	6

Within the Tranca valley, there are four main fault populations based on the natural spacings in the measurement locations. While there is variety in the slip directions between the fault populations, the faults fit together into a single group, and the population is dominated by north-striking faults that dip moderately to the west with down-dip slip (Fig. 4.5 b). In contrast, the faults in the Caracol valley do not cluster together as well as those from the Tranca valley. The fault population at Cr 8 (Fig. 4.5) more closely resembles the faults from the Tranca valley, while the faults at Cr 7 have a

stronger component of oblique motion. The diversity in fault orientation and slip direction may be related to the interactions between the south-plunging tip line of the Caracol fault and the steep fault in the Caracol valley that shows left-lateral separation (Fig. 4.5).

The fault plane solutions for the individual populations also show a diversity in fault orientation and shortening direction (Fig. 4.5). However, the averaged solutions for the two valleys show similar results. The averaged fault plane solutions for both valleys are north-striking reverse faults that dip moderately to the west (Fig. 4.5 b, c). The P axes plunge shallowly to the west and the individual infinitesimal strain axes cluster relatively well in the Tranca valley but are more scattered for the Caracol faults.

4.4.2 11 – 3 Ma

While the preserved fault populations from the earliest time period represent the main thrusts, the faults that were active from ~11 – 3 Ma vary widely in scale and can be found within and between several different units. The main thrust faults that place Cambro-Ordovician limestones over Miocene units form the dominant topographic and structural features in the central Precordillera (Fig. 4.6), much like in the western Precordillera. The fault populations associated with the major features are north-striking reverse faults that dip gently to moderately to the west (e.g. Tr4 and B11 in Fig. 4.6). The orientations of the slip directions on the major faults vary, but the dominant

trend is toward the east. The most significant deviation from this pattern is at Río Francia (RF 24 and RF 27 in Fig. 4.6), where the structures are likely folded.

The minor faults in the Precordillera are secondary faults within the Tertiary units (e.g. B13 and Bl15 in Fig. 4.6) in the footwalls of the major faults. A small minority

Fig. 4.6: DEM of Precordillera showing location of field locations of fault populations active from 11 – 3 Ma. Each field location shows the fault slip data on a stereonet and as the average fault plane solution and P axes for the population. Dark gray solutions represent the major fault populations; intermediate gray solutions show the minor fault populations throughout the region; and light gray solutions show the steep, overburden faults at SR20 and Bl16.

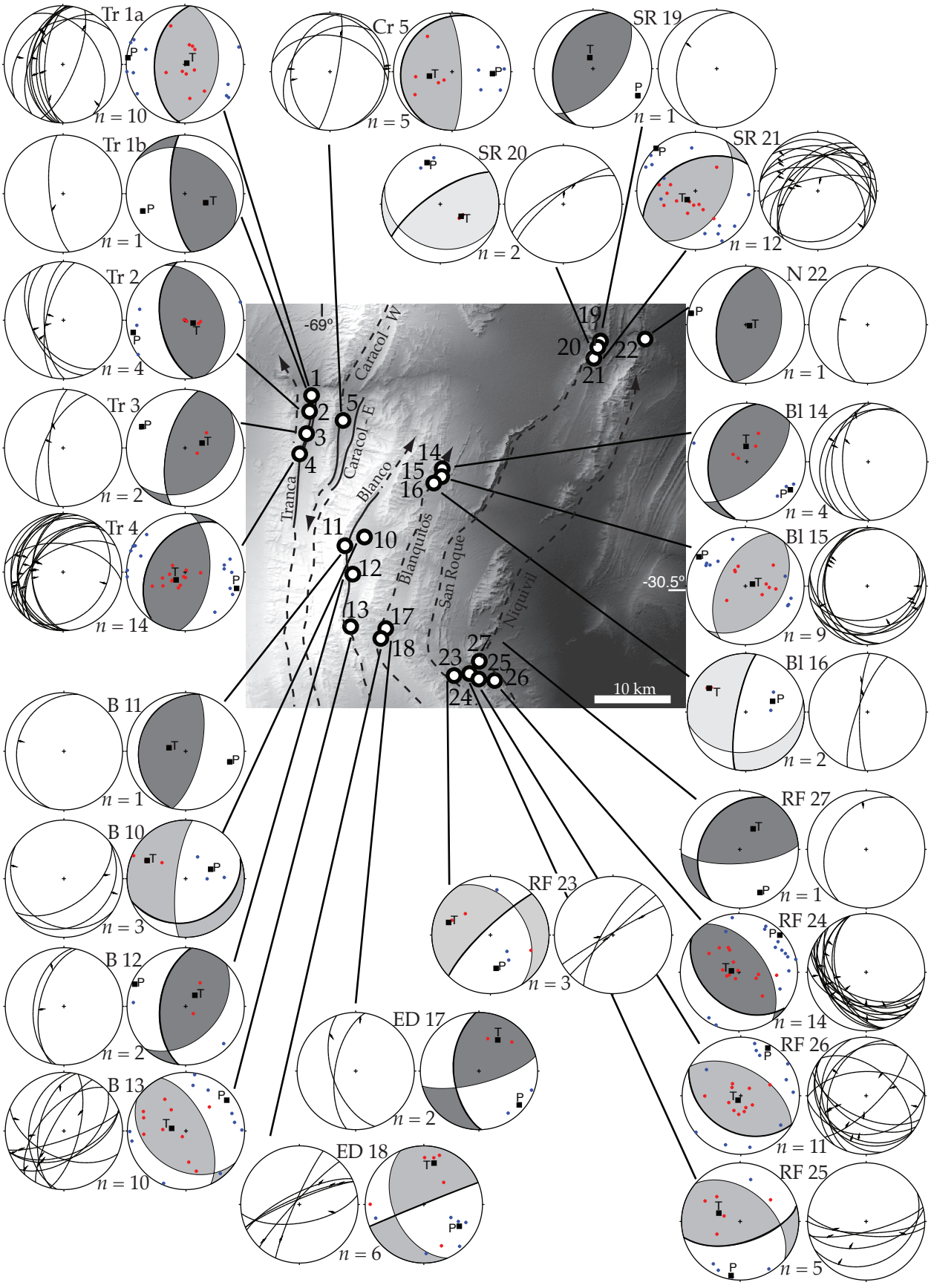
Tr 1a
n = 10
Cr 5
n = 5
SR 19
n = 1
Tr 1b
n = 1
SR 20
n = 2
SR 21
n = 12
Tr 2
n = 4
N 22
n = 1
Tr 3
n = 2
Bl 14
n = 4
Tr 4
n = 14
Bl 15
n = 9
Bl 16
n = 2
B 11
n = 1
B 10
n = 3
B 12
n = 2
B 13
n = 10
RF 27
n = 1
RF 23
n = 3
RF 24
n = 14
ED 17
n = 2
RF 26
n = 11
ED 18
n = 6
RF 25
n = 5
-69°
-30.5°
10 km
Caracol - W
Caracol - E
Blanco
Tranca
Blanquitos
San Roque
Niquivil
1
2
3
4
5
10
11
12
13
14
15
16
17
18
19
20
21
22
23
24
25
26
27

of these faults dip to the west, but there is a wide diversity of fault orientation in the smaller populations. The secondary faults are generally steeper than the faults in the major populations and show a wider variety in slip direction. The variety of fault and slip orientation in the minor faults likely represent the details in the local strain field, and may also be reactivated, pre-existing structures in the footwalls.

The third group of faults, also in the footwalls of the major faults, are high-angle faults that have steeply plunging slip indicators. Some faults fracture and vertically offset pebbles. These faults are located between 200 and 500 m to the east of the modern fault traces, and we interpret these minor structures to be related to the vertical load of a now eroded hanging wall. The overburden faults are most prominent at the San Roque (SR20) and Blanquitos (Bl16) thrusts (Fig. 4.6).

The fault plane solutions for the major populations active after 11 Ma have an average solution that strikes to the north and dips moderately to the west with a reverse sense of motion (Fig. 4.7). The average P axis plunges shallowly to the east but the individual axes trend widely around the average axis. The minor fault populations vary widely and do not group cohesively into one representative population.

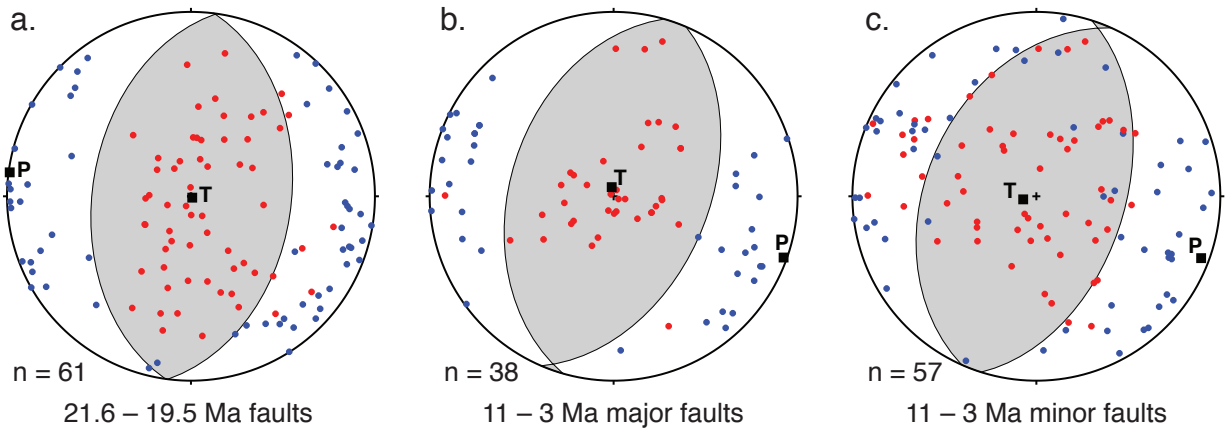

Fig. 4.7: Stereonets comparing the orientation of the fault plane solutions and the P axis orientations of fault populations. a.) Faults active in the western Precordillera from 21.6 – 19.5 Ma. b.) Major faults active in the western and central Precordillera from 11 – 3 Ma. c.) Minor faults active in the western and central Precordillera from 11 – 3 Ma.

4.4.3 3 – 0 Ma

Faults that formed within the past 3 million years (Fig. 4.8) are confined to the eastern edge of the central Precordillera and the thick-skinned anticlines of the eastern Precordillera. The faults from Río Francia (RF28), which is part of the thin-skinned central Precordillera, are between Tertiary redbeds and consolidated Quaternary gravels. None of the strain axes from the fault populations in the Río Francia valley agree with the faults elsewhere in the Precordillera, likely related to the local structural heterogeneities. A left-lateral tear fault in the valley offsets the uplifted Paleozoic strata by ~1 kilometer. Additionally, there is a regional lineament that connects the tear fault to the intersection of anticlines in the eastern Precordillera; the two easternmost major

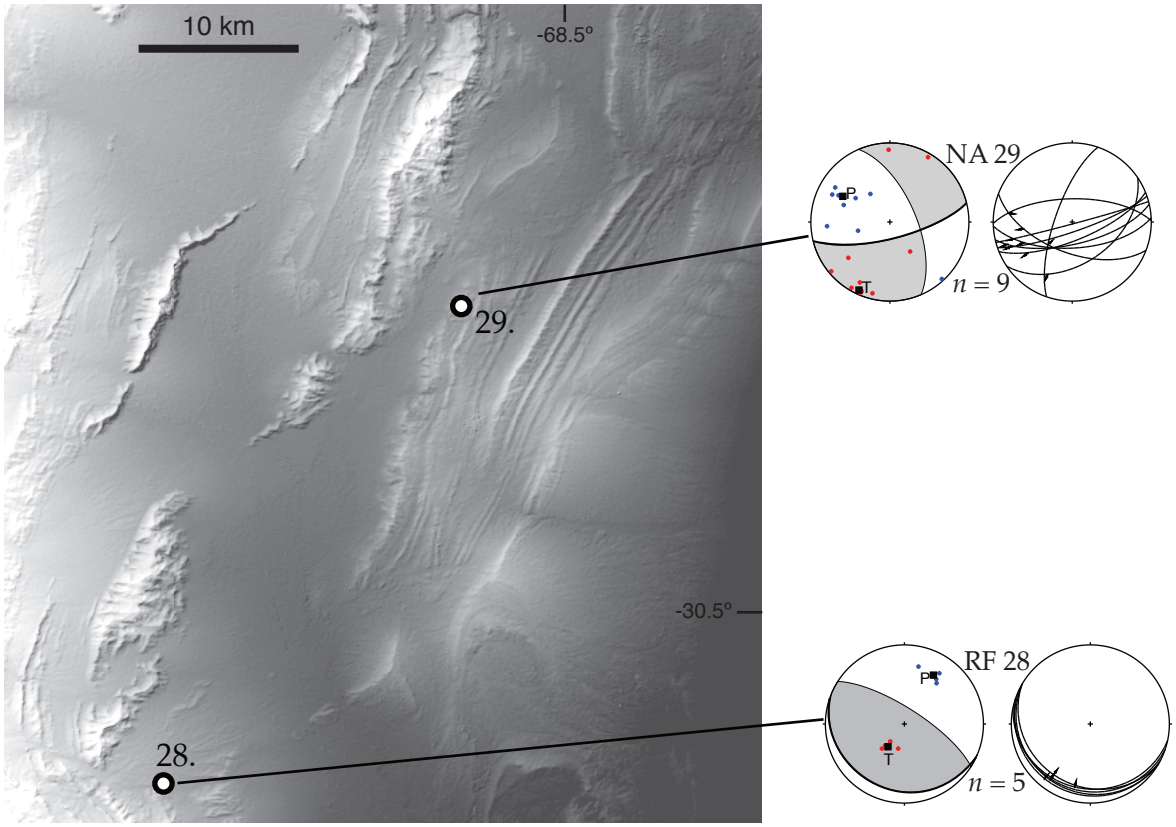

Fig. 4.8: DEM of central and eastern Precordillera showing the field locations of the youngest fault populations. Stereonets show the fault slip data for each location and the average fault plane solution with the P axes for the populations.

thrust faults in the central Precordillera are not continuous across the lineament. These regional structures impact the local strain field and render the fault populations in the area disconnected from the larger strain field throughout the Precordillera.

The faults from within the Niquivil anticline (NA29 in Fig. 4.8) are within the folded foreland basin strata in the eastern Precordillera. The steep right-lateral faults we measured off-set the anticline and are part of a much larger suite of faults that covers a significant portion of the Niquivil anticline (Fig. 4.9). While access to a majority of these faults is limited, we measured dextral faults at the northern end of the anticline. This population shows a set of steep dextral faults with relatively horizontal slip directions. To compare these measured faults to the larger population, we used Google Earth to digitize the fault traces throughout the anticline and determine the apparent sense of motion based on the offset of marker beds by the faults. These fault traces show both left- and right-lateral motion and are mutually cross-cutting with an inter-fault angle of 56^{o}, strongly suggesting that these faults are Coulomb shear fractures (Fig. 4.9). The fault plane solution for the right-lateral faults shows steep fault planes with a north-west trending P axis. This solution is consistent with the larger fault population throughout the anticline, and the shortening direction is consistent with the major fault populations in the Precordillera.

Fig. 4.9: Geologic map of the Niquivil anticline and the Niquivil thrust front. Red lines represent digitized steep faults with light-lateral apparent offset; green lines represent digitized steep faults with left-lateral apparent offset. a.) Rose diagram of the right-lateral faults showing dominant trend. b.) Rose diagram of the left-lateral faults showing dominant trend. c.) Fault plane solution of the right-lateral faults measured in the northern end of the anticline from Fig. 7. Lithology same as for Fig. 4.4.

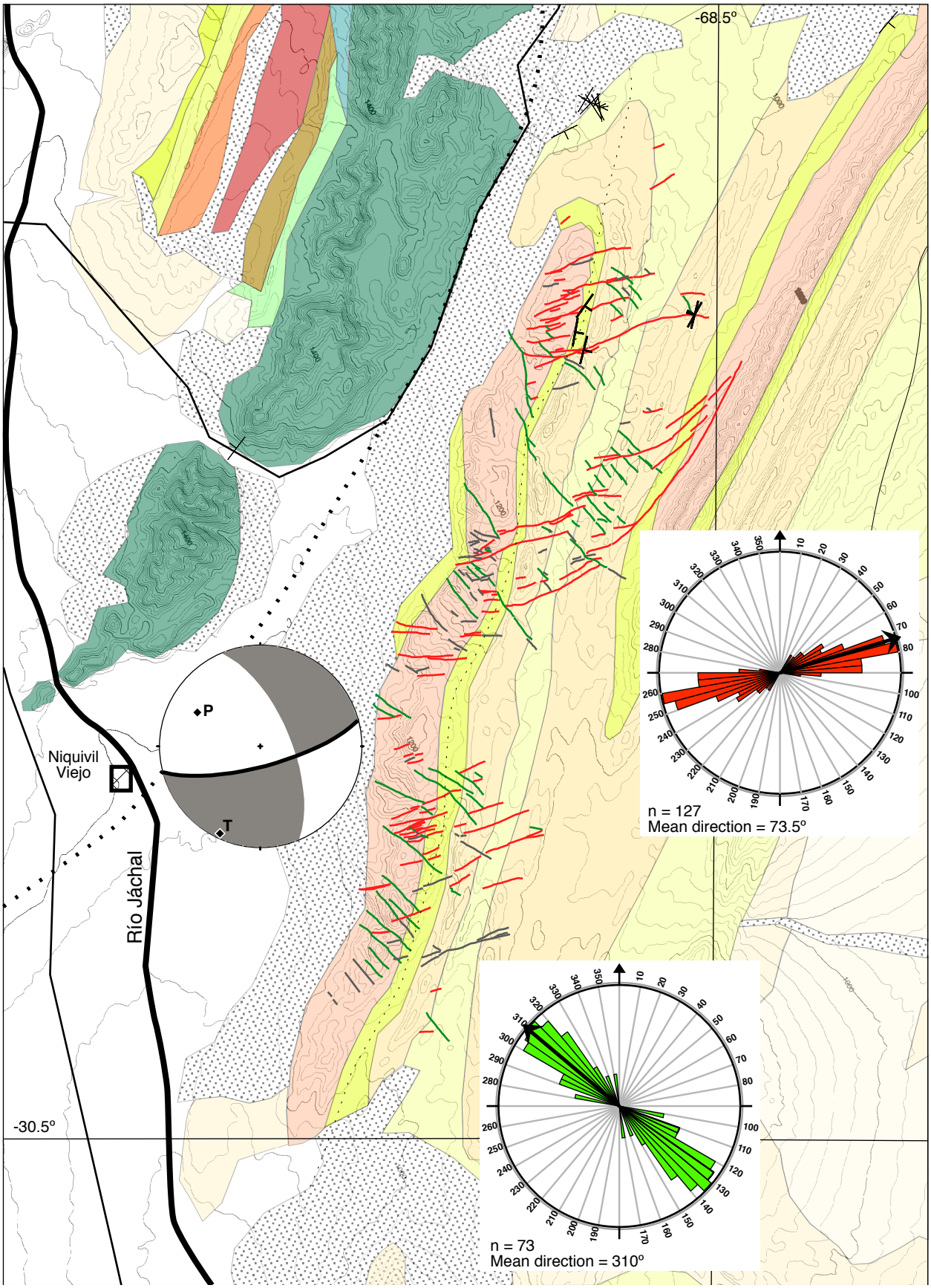
-68.5º
-30.5º
Niquivil
Viejo
Río Jáchal
P
T
n = 127
Mean direction = 73.5º
n = 73
Mean direction = 310º

No significant difference exists between the major fault populations from the two earlier time periods. The fault plane solutions are all north-striking thrust faults that dip moderately to the west and the individual shortening axes trend WNW – ESE, but there is a significant spread in the orientation of the axes. The averaged P axes for the populations trend WNW and the individual axes show a similar range of orientation for both time periods. Additionally, the shortening direction calculated for the faults in the Niquivil anticline agrees with the orientation of the P axes from the two previous time periods.

4.5 Shortening activity and rates in the Precordillera

To determine how shortening activity and rates evolved in the Precordillera since ~20 Ma, we calculated shortening rates across two profiles in the western and central Precordillera. We start by calculating the shortening magnitude of the faults in the Tranca - Caracol valley in the western Precordillera in profile B (Fig. 4.10). We chose to begin the calculation in the western Precordillera because it is the region with the best temporal constraints on the shortening history and section B has better physical constraints on the subsurface geometry. The timing of the motion on the Tranca and Caracol thrusts is constrained to be after 21.6 ± 0.8 Ma but before 19.5 ± 1.1 Ma based on the age of the redbeds in the footwalls and the conglomerates covering the fault in the hanging wall (Jordan et al., 1993). Using cross sections from Judge (2012) and the area

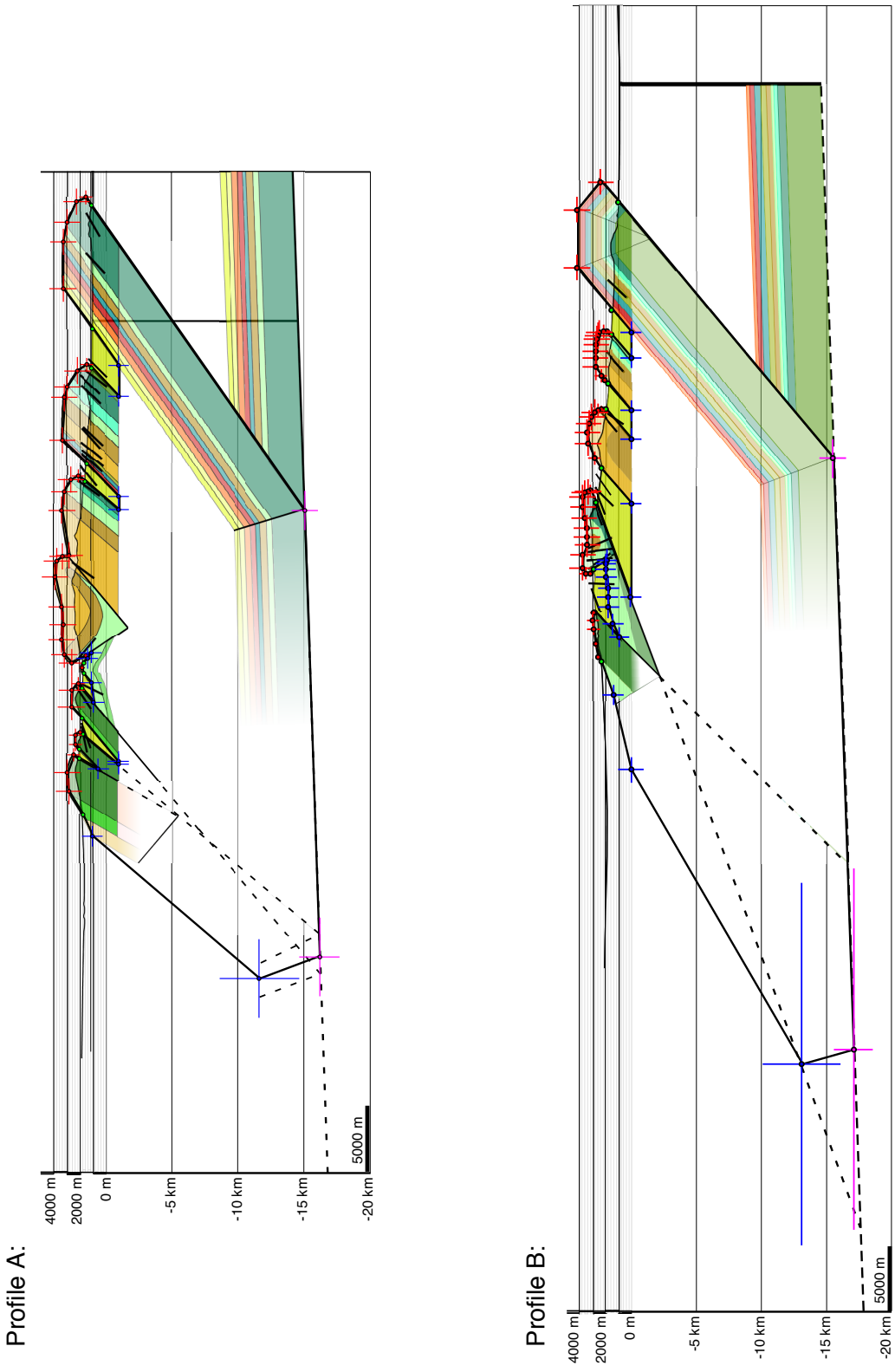

Fig. 4.10: Profile cross sections along A-A′ and B-B′ in Fig. 4.4. Lithology same as for Fig. 4.4. Modified from Judge (2012).

balancing program *AreaErrorProp* based on the algorithms in Judge and Allmendinger (2011), we determine the shortening for the western Precordillera. We calculate 7.2 ± 6 km of shortening in the region, not including any possible motion on the related Blanco fault. The shortening magnitude likely includes some reactivation on both the Tranca and Caracol faults as well as the formation of the fault that places the Tertiary redbeds over a younger conglomerate (Jordan et al., 1993). We estimate the reactivation and younger shortening to be approximately 1 km total based on the orientations and thicknesses of the post-19.5 Ma sediments in the valleys. If the shortening in the western Precordillera was 6.2 ± 6 km for the 2.1 ± 1.4 million years the faults were active, then the shortening rate is ~ 3 ± 3.5 mm/yr along profile B during the earliest period of activity, assuming a Gaussian distribution of the uncertainties.

The geometry and period of activity of the majority of the western Precordillera is relatively unknown. The timing of the potential duplexing between the Tranca and Caracol thrusts is unknown, as is the geometry of the ramp connecting the western Precordillera to the decollement at depth. For our shortening rate calculations, we excluded a majority of the motion on the western Precordillera ramp to avoid the ambiguous timing and geometry of motion. Excluding the remainder of the motion on the western ramp does not significantly change the results or interpretations of the shortening rate calculations. If the remaining ~30 km of horizontal shortening occurred before 19.5 Ma, we would have no method to independently determine a shortening

rate for the ramp and would assume that the shortening rate was ~3 mm/yr, as we calculated for the surface-breaking faults. Were we to include the 30 km in the period of shortening after 11 Ma, the shortening rates for that period would increase significantly but would not change the resulting pattern of shortening rates we calculate for the Precordillera.

To calculate the remaining averaged shortening rates for profile B as well as all of the rates for profile A, we sum the horizontal displacements for each major thrust and divide by the period of motion over which the faults were likely active (table 4.2). We include both distance and temporal uncertainties in the shortening rates based on the potential period of activity as well as the uncertainty in the geometry of the faults. Additionally, the values of the shortening uncertainties are likely to underestimate the true uncertainty of the shortening magnitude given the difficulty in assess the magnitude of initial and reactivated motion on the faults.

We also determined more detailed shortening rates for one million year increments from 22 – 0 Ma (Fig. 4.3). We determined these fates based on the total shortening for each thrust, the duration of activity for each thrust, and which thrusts were active during each increment. We do not include uncertainty estimates for the detailed shortening rates—the rates and uncertainty in table 4.2 and Fig. 4.3b show that the rates may not be distinct. The detailed and averaged rates show similar patterns of

motion from ~21 – 19 Ma, followed by quiescence, and then increased shortening after 11 Ma.

Table 4.2: Averaged shortening rates for profiles A and B

Fault	*horizontal shortening [km]*	*uncertainty [km]*	*rate [mm/yr]*	*Profile from Zapata & Allmendinger, 1996 for eastern Precordillera*
Profile A:				
21.6 – 19.5 Ma:				
Tranca:	4.5	2		
Caracol:	4.5	2		
Total:	**9**	**3**	**4 ± 3.3**	
11 – 4 Ma:				
Tranca:	[0.5]	0.5		
Caracol:	[0.5]	0.5		
Blanco:	6	2		
Blanquitos:	14.8	1		
San Roque:	14.2	2		
Niquivil:	22.6	2		
Total:	**58.6**	**4**	**7 ± 2.7**	
3 – 0 Ma:				
San Roque:	[1]	0.5		
Niquivil:	[1]	0.5		
Eastern Precordillera:	17.1	2		CC2
Total:	**19.1**	**2**	**6 ± 2**	
Profile B:				
21.6 – 19.5 Ma:				
Western Precordillera:	6.2	6		
Total:	**6.2**	**6**	**3 ± 3.5**	
11 – 4 Ma:				

Fault	*horizontal shortening [km]*	*uncertainty [km]*	*rate [mm/yr]*	*Profile from Zapata & Allmendinger, 1996 for eastern Precordillera*
Western Precordillera:	[1]	1		
Blanco:	8	2		
Blanquitos:	21.7	1		
San Roque:	21.1	2		
Niquivil:	16.8	2		
Total:	**68.6**	**4**	**9 ± 4.7**	
3 – 0 Ma:				
San Roque:	[1]	0.5		
Niquivil:	[1]	0.5		
Eastern Precordillera:	16.25	2		CS3
Total:	**18.25**	**2**	**6 ± 2**	

4.5.2 Shortening rates and directions through time in the Precordillera

The shortening rates show three periods of motion in the Precordillera. Fig. 4.3b shows the calculated average shortening rates for profiles A and B, as well as the uncertainties for the rates. There is good agreement between the two profiles for both the magnitude of the rates as well as the changes between the three time periods. Both profiles show a relatively low shortening rate (3 – 4 mm/yr) between 21.6 and 19.5 Ma due to the motion on the faults in the western Precordillera. At 11 Ma, the shortening rate for both profiles increases as the Blanco, Blanquitos, San Roque, and Niquivil faults formed and the existing faults in the western Precordillera were reactivated. The shortening rate for profile A increased from 4 ± 3.3 mm/yr to 7 ± 2.7 mm/yr at 11 Ma. Profile B underwent an increase from 3 ± 3.5 mm/yr to 9 ± 4.7 mm/yr at the same period. Finally, at ~3 Ma,

the shortening rate for both profiles decreased to 6 ± 2 mm/yr. These rates include shortening due to the formation of the anticlines in the eastern Precordillera (table 4.2) from Zapata and Allmendinger (1996). The profiles show identical averaged shortening rates for the last 3 million years of activity, a slight to moderate decrease from the previous period.

The detailed shortening rates indicate that the greatest increase in shortening rates occurred not 11 Ma but between 9 – 8 Ma. After the period of quiescence from 19 – 11 Ma, the reactivation of the western Precordillera and the formation of the many new faults in the central Precordillera increased the shortening rate throughout the region and peaked between 8 – 6 Ma at 10.9 – 13.5 mm/yr. The period of maximum shortening was flanked by moderate shortening rates, and the most recent phase of deformation (3 – 0 Ma) reflects the formation of the eastern Precordillera. These rates are similar to those calculated by Jordan and others (2001) but slightly lower, likely based on our exclusion of the majority of the shortening in the western Precordillera.

We do not explicitly calculate slip velocities for the fault populations throughout the Precordillera but instead we present the average shortening direction for each fault populations as a vector that is scaled to the averaged shortening rate (Fig. 4.11). By plotting the shortening direction in map view based on their period of activity, two patterns become evident. The first is that the majority of the shortening directions are perpendicular to the major structures and do not change direction over the three time

periods. Secondly, there are many more faults active in the 11 – 3 Ma period over a wide area, and the shortening magnitudes are largest for this time period, as well.

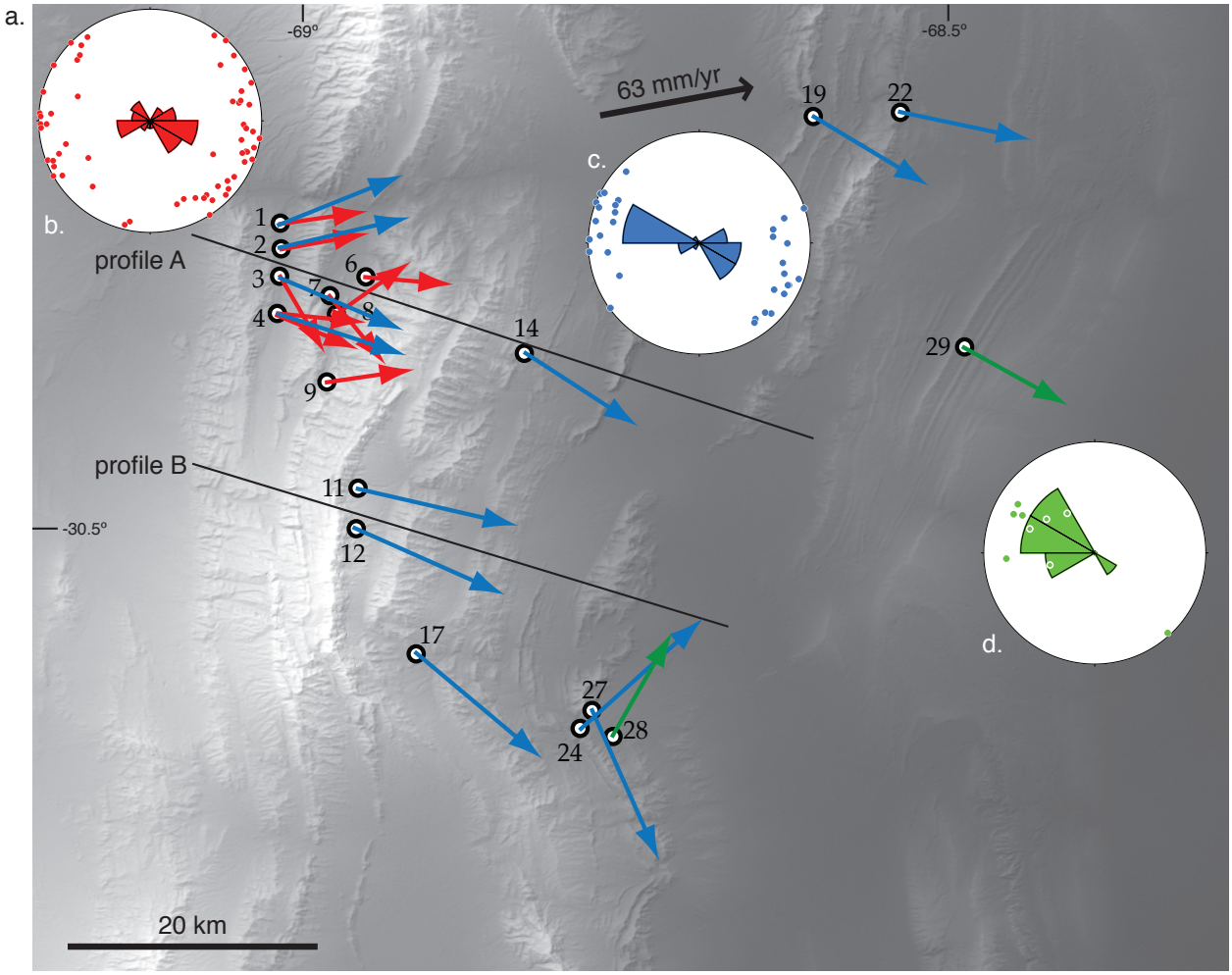

Fig. 4.11: a.) DEM showing the location of the major fault populations from the three time periods. Arrows trend in the direction of the average P axis for each population and is scaled to the average shortening rate from Fig. 4.3. Colors are coordinated to stereonet insets. b.) Stereonet and rose diagram of the individual P axes from the faults in the western Precordillera active from 21.6 – 19.5 Ma. c.) Stereonet and rose diagram of the individual P axes from the major fault populations in the western and central Precordillera active from 11 – 3 Ma. d.) Stereonet and rose diagram of the individual P axes for the faults in the Niquivil anticline.

4.6 Discussion

The results of our fault slip analysis and determination of slip rates throughout the Precordillera reveal spatial and temporal relationships between changes in the Nazca slab geometry and shortening in the crust.

4.6.1 Convergence and shortening directions since 20 Ma

Two main results arise from our analysis of the fault slip data in the Precordillera: first, shortening directions have not changed significantly since 21 Ma even as the Nazca slab shallowed; second, the shortening directions are rotated clockwise relative to the plate convergence direction but are perpendicular to the main structures throughout the Precordillera. These two results indicate that the shallow subduction below the region does not strongly impact the shortening directions in the upper crust and that there is likely a stronger regional influence on deformation related to the interaction of the thrusts in the Precordillera and other active upper crustal structures.

No significant difference exists between the shortening directions for the fault populations in the Precordillera through the three time periods that we analyze (Fig. 4.11). The dominant orientation of the individual and averaged P axes is a gently plunging, WNW-ESE trending axis. This is consistent throughout the time periods, though the P axes from the first period show a wider range of trends.

The shortening directions that we calculate using fault slip data are consistent with the P axis directions from earthquakes throughout the region, especially further

south near Pie de Palo (Siame et al., 2005; 2006). The P axes for the majority of the teleseismic earthquakes around Pie de Palo trend WNW-ESE, and the P axis for the averaged moment tensor sum trends toward ~095° (Siame et al., 2005) (Fig. 4.12). We interpret the agreement between the P axis orientations for both the fault slip data and the earthquake focal mechanisms to indicate that the modern shortening direction is toward 095° – 110° and that our fault slip data are accurately describing the modern shortening direction in the Precordillera.

By comparison, Siame and others (2005) inverted fault slip data to calculate paleostress axes for sites along the road between Jáchal and Huaco as well as one site at the Tranca thrust. The results of the paleostress inversions for the populations in the Cenozoic conglomerates and sandstones show the direction of maximum compression trends ENE. While we prefer our results based on the fault plane calculations over paleostress inversions, which require more assumptions, our data do not reproduce the results from Siame et al. (2005). On average, our fault populations include data from a much broader physical expanse of the fault systems. Additionally, we have chosen to not subdivide our fault slip data for the final calculations on the basis of slip direction, while Siame and others (2005) separate their data based on their interpretation of several phases of deformation preserved in the slip directions.

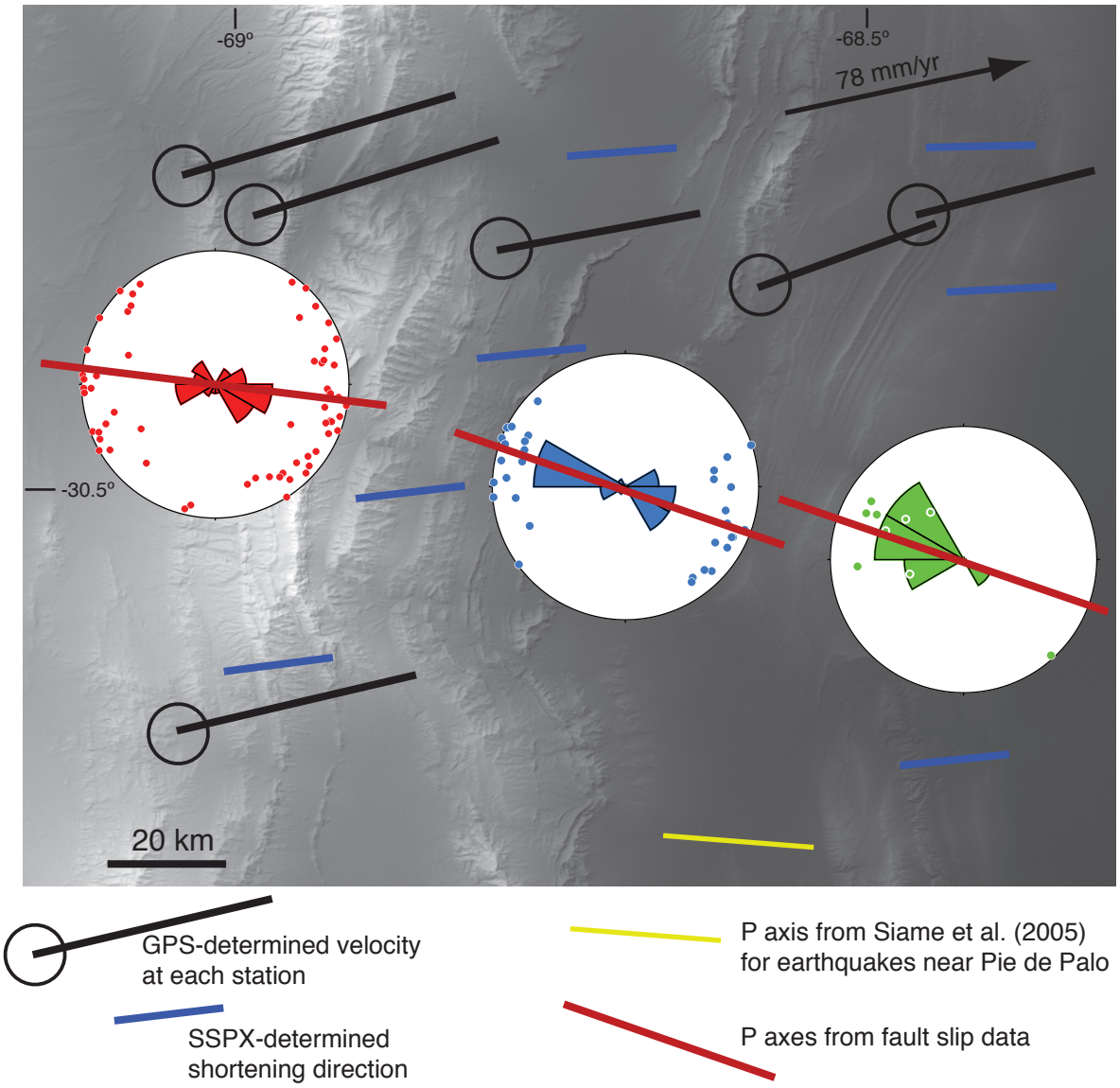

Fig. 4.12: DEM showing the location of the stations from Brooks et al. (2003) used to determine displacements in the Precordillera. The three stereonets are same as from Fig. 4.11, showing the orientation of the individual P axes for the faults active during this time. Compare the shortening directions determine from *SSPX* program to those calculated from fault slip data and earthquakes near Pie de Palo.

The ~20 Ma consistency of shortening directions from our fault slip data is comparable to the relative stability in convergence direction between the Nazca and South American plates since ~25 Ma (Pardo-Casas and Molnar, 1987; Somoza, 1998; Somoza and Ghidella, 2005). The convergence azimuth ranged from 087° to 075° since 25.8 Ma (Somoza, 1998), and the direction have been effectively stable since 20 Ma (Pardo-Casas and Molnar, 1987). The convergence direction determined via magnetic lineations (Pardo-Casas and Molnar 1987; Somoza, 1998) are consistent with the modern convergence directions determined from GPS velocities throughout South America (Brooks et al., 2003; Kendrick et al., 2001).

Additionally, the shortening directions determined from the GPS velocities trend ENE or east-west (Fig. 4.12). We calculate shortening axes for the Precordillera and the Sierras Pampeanas using *SSPX* from Allmendinger and others (2007) and Cardozo and Allmendinger (2008). By calculating the shortening axes over a 20 km grid and including displacements from the surrounding 150 km, we are able to match the spacing of the geologic data relatively well (Fig. 4.12). We see that, as with the results from both Brooks et al. (2003) and Allmendinger and others (2007), the shortening rates calculated from the geodetic displacements are either subparallel to the convergence direction or trend east-west.

The shortening directions we calculate from fault slip data and the P axis orientations from earthquake focal mechanisms are rotated ~20° – 25° clockwise relative

to the convergence direction, and are perpendicular to the main structures in the Precordillera (Fig. 4.11). This clockwise rotation of the shortening axes indicates that the structures in the Precordillera record a different strain pattern than simply the elastic loading due to locking at the plate boundary.

In contrast to our results, geologic shortening directions in the central Andes appear to be consistent with geodetic displacements in the foreland; Hindle and others (2002) show good agreement between shortening orientations from geologic and geodetic data. This agreement is found in other locations, such as the coherence between deformation patterns from GPS and geologic data sets on the north island of New Zealand (Nicol and Wallace, 2007). The agreement between geologic and geodetic shortening directions is found in many orogens, and in locations where the data do not agree, strain partitioning is frequently invoked to explain any discrepancies (e.g. Avé Lallemand and Oldow, 2000; Friedrich et al., 2003; King et al., 1997). The accommodation of strike-perpendicular shortening on the main thrusts in the Precordillera and the rotation of the shortening directions clockwise with respect to the convergence direction suggest that the remainder of the strain due to locking at the plate boundary may be partitioned into other structures in the region. To bring the geologic and geodetic shortening directions into agreement, the simplest means to accommodate the remaining strain would be to look for dextral offsets on steep faults in the region.

To the west of the Precordillera, the El Tigre faults accommodates ~1 mm/yr of dextral offset (Siame et al., 1997) between the towns of Calingasta and Las Flores in the Iglesia basin (Fig. 4.4). North of Las Flores, there are several flower structures, steep faults, and lineaments (Beer et al., 1990; Ruskin and Jordan, 2007) that offset the sediments in the Iglesia basin and may accommodate the right-lateral motion of the El Tigre fault. Combining the shortening directions and rates from the thrusts in the Precordillera with the offset direction and rate on the El Tigre fault yields a resultant vector that nearly parallels the GPS-derived shortening directions (Fig. 4.13).

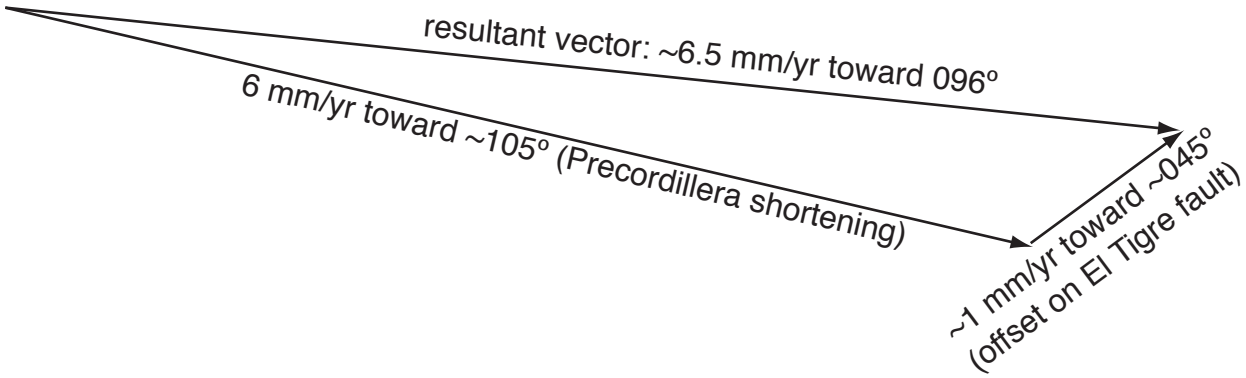

Fig. 4.13: Addition of shortening rate and direction from the major thrusts in the Precordillera and the right-lateral offset direction and rate from the El Tigre fault in the Iglesia basin. The resultant vector is rotated ~10° clockwise from the shortening direction determined from GPS velocities by *SSPX* from Fig. 4.12.

Based on the orientation of paleostress analyses and earthquake focal mechanisms in the Precordillera from Jáchal south to San Juan, Siame et al. (2005) describe strain partitioning throughout the region, extending along the length of the El Tigre fault. However, they do not interpret the deformation partitioning to extend as far north as the majority of our data from the Precordillera, in part due to the termination of the El Tigre fault in the Las Flores - Rodeo region of the Iglesia basin. Because there are steep faults throughout the northern end of the Iglesia basin that have an en echelon geometry with the El Tigre fault and could accommodate the right-lateral displacements that the El Tigre fault no longer can, we extend the zone of strain partitioning farther north to include the Precordillera at the latitude of the Río Jáchal. By allowing the faults in the Iglesia basin to accommodate dextral offset throughout the northern section of the Precordillera, the major thrusts in the region continue to shorten perpendicular to their strike and the overall shortening rate and direction for the region are close to those calculated via GPS data (Allmendinger et al., 2007; Brooks et al., 2003).

Finally, having resolved the discrepancy between the shortening directions, we interpret the relative stability in the shortening and convergence directions over the past ~20 Ma to indicate than any influence that a shallowing slab may have at the Earth's surface is unlikely to impact shortening direction. As the slab shallowed from ~10 – 5 Ma, there appears to be little influence on the shortening directions. While the shallowing slab is likely to change other aspects of the development of the Precordillera

(discussed below), the shortening directions do not show evidence of this changing geometry.

4.6.2 Slab shallowing related to increased interplate coupling

The variation in shortening rates across the Precordillera is temporally correlated to the changing geometry of the subducting Nazca slab. During the earliest period of shortening, the slab subducted at a relatively steep angle, similar to elsewhere along the modern Andean margin. Based on the chemistry of the magmatic rocks from the Precordillera, Kay and Abbruzzi (1996) concluded that the slab was steep and that the South American crust was ~40 km thick. From approximately 26 – 20 Ma, convergence between the Nazca and South American plates was ~150 mm/yr toward 070° – 085° (Kendrick et al., 2001; Pardo-Casas and Molnar, 1987; Somoza, 1998; Somoza and Ghidella, 2005).

Between 12.5 and 10 Ma, the Nazca plate changed in several important ways. At 12.5 Ma, there was a significant reorganization of the plates in the southeast Pacific (Tebbens and Cande, 1997) that preceded a reduction in convergence rate at ~11 Ma from 126 to 109 mm/yr (Somoza, 1998; Somoza and Ghidella, 2005). 10 Ma also marks the stabilization of the subduction location of the Juan Fernández ridge along the South American coast, placing the ridge directly below the Precordillera (Yáñez et al., 2001; 2002). Additionally, Kay and Abbruzzi (1996) indicated that volcanism in the Principal Cordillera ceased by ~10 Ma.

At 9 – 8 Ma, we calculate a significant increase in the shortening rate for the western and central Precordillera from 3 – 5 mm/yr to 11 – 13 mm/yr (Fig. 4.3); even the averaged shortening rate over the 11 – 3 Ma time period is well above the shortening rate for the earlier period (Fig. 4.3b). These increased rates occurred just after the slab began to shallow at 10 Ma, and the convergence rate between the plates decreased, indicating that some tectonic influence other than convergence rate was likely responsible for transferring more motion from the subduction zone to the foreland thrusts. Because the increased shortening rate occurred following the initiation of the shallowing of the Nazca slab, it is possible that the changing geometry led to these changes.

Martinod and others (2010) suggested that the surface area between the Nazca and South American plates increased as the slab geometry changed, which would have decreased the convergence rate as the plate boundary became increasingly more coupled. In addition to decreasing the convergence rate, Martinod and others (2010) and Espurt and others (2008) suggested that locking at the plate boundary could increase shortening above a region of flat slab subduction as less slip was accommodated at the plate boundary.

The shortening rates we calculated for the Precordillera match the theoretical predictions from Martinod and others (2010) as well as the analog models from Espurt and others (2008). In addition, our rates are consistent with other studies showing

increases in shortening rates based on field work (Jordan and Allmendinger, 1986; Jordan et al., 1993; Ramos et al., 2002; Siame et al., 2005). The marked increase in shortening rates after the ridge location stabilized and the slab began to shallow matches the predictions for deformation above a shallow slab, although the uncertainty bounds on the averaged shortening rates do not rule out the possibility that there was no change in rates as the slab shallowed (Fig. 4.3b). Additionally, this increased shortening follows a decrease in convergence rate, which also agrees with the predictions from Martinod and others (2010) and Espurt and others (2008).

The most recent changes in the Nazca slab and the Precordillera occurred between ~5 – 3 Ma. At 4.9 Ma, there was a final decrease in convergence rate to 78 mm/yr another 28% reduction in velocity from the previous 109 mm/yr (Somoza, 1998; Somoza and Ghidella, 2005). Magmatism ceased in the Precordillera by 4.7 Ma (Kay and Abbruzzi, 1996), indicating that there was a significant reduction in the asthenospheric wedge below the Precordillera. After the spike in shortening rates from 8 – 6 Ma, there was a 30% decrease in shortening, followed by a more pronounced decrease at 3 Ma to the current 6 ± 2 mm/yr. Currently, the slab is between 80 and 100 km below the Precordillera and the horizontal segment extends east from the trench (Anderson et al., 2007; Gans et al., 2011; Gilbert et al., 2006). The GPS data from Brooks and others (2003) show shortening rates across the Precordillera of ~4 – 6 mm/yr; while these rates are

slightly lower than the values we calculate for this more recent phase of shortening, it is within the uncertainty band for both profiles (6 ± 2 mm/yr).

We interpret the temporal correlation between the changing shortening rates in the Precordillera and the evolving geometry of the Nazca slab to indicate that the shallowing slab has a strong impact on deformation at the surface. The increased interplate surface area may lead to a stronger coupling between the two plates, transferring more deformation from the locked plate boundary to the thrust belt in the foreland. This increased shortening was not focused on one preexisting structure in the Precordillera: nearly all the faults in the Precordillera were either formed or activated within 2 million years of the slab shallowing. The four largest structures in the central Precordillera, the Blanco, Blanquitos, San Roque, and Niquivil thrusts, all likely formed shortly following the shallowing of the slab, and the faults in the western Precordillera were reactivated.

Examining the percentage of the convergence rate that was accommodated in the Precordillera bolsters the notion that the shallowing slab created a more efficient transfer of elastic loading from the plate boundary to the foreland. From ~20 – 19 Ma, the convergence rate was 126 mm/yr and the shortening rate was 3 – 4 mm/yr, accommodating 2 – 3% of the total plate convergence. By 11 Ma, the convergence rate dropped to 109 mm/yr but the shortening rate increased to 11 – 13 mm/yr, increasing the percentage of shortening accommodated in the foreland to 10 – 12%. After 5 Ma,

both the convergence and the shortening rates dropped again, to 78 mm/yr of convergence and 6 mm/yr of shortening across the central and eastern Precordillera; this represents ~8% of the convergence rate accommodated in the foreland. The correlation between the shallowing slab and the four- to five-fold increase in the percentage of convergence accommodated in the foreland indicates that the changing slab geometry may play a significant role in the coupling between the plates.

4.7 Conclusions

1) The shortening directions in the Precordillera, which we determined through fault slip data and fault plane solutions, do not change significantly as the geometry of the Nazca slab changed from steep to horizontal. The shortening directions are rotated between ~20° – 25° clockwise from the plate convergence direction and this orientation appears to be consistent since 20 Ma.
2) The rotation of the shortening axes combined with the dextral offset of the El Tigre fault are evidence of strain partitioning in the Precordillera. The addition of the 6 mm/yr shortening rates on the thrusts in the western and central Precordillera to the 1 mm/yr offset rate on the El Tigre fault yields a shortening rate and direction that is almost identical to the shortening directions calculated from the GPS velocities.

3) The El Tigre fault has a relatively young documented age of less than one million years, suggesting at least two possible histories for the strain partitioning in the Precordillera:

   A. The El Tigre fault, as well as other steep right-lateral structures, has accommodated a relatively small percentage of the convergence direction in the foreland since ~20 Ma, allowing the thrusts in the Precordillera to shortening perpendicular to their strike for the duration of their shortening history.

   B. The perpendicular motion on the faults in the Precordillera is only as old as the El Tigre fault (< 1 million years) and this youngest phase of motion overprints the older shortening directions on all the faults in the region.

4) We prefer the long-lived strain partitioning history for the Precordillera. While there is evidence for some limited oblique slip on the faults, structures are more consistent with dip-slip motion during their formation.

5) The shortening rates we calculate over the history of the Precordillera show a lagging temporal correlation between the shallowing of the Nazca slab and a sharp increase in shortening and shortening activity. The decrease in the shortening rates at 3 Ma follows a decrease in convergence rate at 4.9 Ma. Whether the decrease in convergence rate at 4.9 Ma was related to a further increase in plate coupling or due to other geomdynamical forces, while an interesting question to pursue, is beyond the scope of this paper.

6) The stability in the convergence direction between the Nazca and South American plates for the past ~25 million years was likely the stronger influence on the shortening directions in the Precordillera as opposed to the geometry of the slab.
7) The shallowing Nazca slab likely does play a role in changing the shortening activity and rates throughout the Precordillera as the interplate surface area increased. A stronger locking at the plate boundary may have slowed the convergence rate but increased shortening in the foreland by transferring motion from the megathrust to the fold and thrust belt in the Precordillera.

4.8 References

Allmendinger, R. W., Cardozo, N. C., Fisher, D., 2012. Structural geology algorithms: vectors & tensors, Cambridge University Press, Cambridge, England, 289 pp.

Allmendinger, R. W., Figueroa, D., Snyder, D., Beer, J., Mpodozos, C., Isacks, B. L., 1990. Foreland shortening and crustal balancing in the Andes at 30ºS latitude. *Tectonics* 9, 789-809.

Allmendinger, R. W., Reilinger, R., Loveless, J., 2007. Strain and rotation rate from GPS in Tibet, Anatolia, and the Altiplano. *Tectonics* 27, TC3013, doi: 10.1029/2006TC002030.

Anderson, M., Alvarado, P., Zandt, G., Beck, S., 2007. Geometry and brittle deformation of the subducting Nazca Plate, Central Chile and Argentina. *Geophysical Journal International* 171, 419-434, doi: 10.1111/j.1365-246X.2007.03483.x.

Avé Lallemand, H. G., Oldow, J. S., 2000. Active displacement partitioning and arc-parallel extension of the Aleutian volcanic arc based on Global Positioning System geodesy and kinematic analysis. *Geology* 28, 739-742, doi: 10.1130/0091-7613(2000)28<739:ADPAAE>2.0.CO;2

Baldis, B. A. J., Chebli, G., 1969. Estructura profunda del área central de la Precordillera sanjuanina. *IV Jornadas Egológicas Argentinas* I, 47-66.

Baldis, B. A. J., Beresi, M. S., Bordonaro, O., Vaca, A., 1982. Sintesis evolutiva de la Precordillera Argentina. *V Congreso Latinoamericana de Geológia Actas* 4, 399-445.

Barazangi, M., Isacks, B. L., 1976. Spatial distribution of earthquakes and subduction of the Nazca Plate beneath South America. *Geology* 4, 686-692.

Beer, J. A., Allmendinger, R. W., Figueroa, D. E., Jordan, T. E., 1990. Seismic stratigraphy of a Neogene piggyback basin, Argentina. *AAPG Bulletin* 74, 1183-1202.

Brooks, B. A., Bevis, M., Smalley Jr., R., Kendrick, E., Manceda, R., Lauría, E., Maturana, R., Araujo, M., 2003. Crustal motion in the Southern Andes (26º – 36ºS): Do the Andes behave like a microplate? *Geochemistry Geophysics Geosystems* 4, doi: 10.1029/2003GC00505.

Cahill, T., Isacks, B. L., 1992. Seismicity and shape of the Nazca plate. *Journal of Geophysical Research* 97, 17503-17529.

Cardozo, N., Allmendinger, R. W., 2008. *SSPX* v. 2.6.

Cembrano, J., González, G., Arancibia, G., Ahumada, I., Olivares, V., Herrera, V., 2005. Fault zone development and strain partitioning in an extensional strike-slip duplex: A case study from the Mesozoic Atacama fault system, Northern Chile. *Tectonophysics* 400, 105-125.

Claypool, A. L., Klepeis, K. A., Dockrill, B., Clarke, G. L., Zwingmann, H., Tulloch, A., 2002. Structure and kinematics of oblique continental convergence in northern Fiordland, New Zealand. *Tectonophysics* 359, 329-358.

Coughlin, T. J., O'Sullivan, P. B., Kohn, B. P., Holcombe, R. J., 1998. Apatite fission-track thermochronology of the Sierras Pampeanas, central western Argentina: Implications for the mechanism of plateau uplift in the Andes. *Geology* 26, 999-1002.

Cristallini, E. O., Ramos, V. A., 2002. Thick-skinned and thin-skinned thrusting in the La Ramada fold and thrust belt: crustal evolution of the High Andes of San Juan, Argentina (32ºSL). *Tectonophysics* 317, 205-235.

Cross, T. A., Pilger, R. H., 1982. Control of subduction geometry, location of magmatic arcs, and tectonics of arc and back-arc regions. *Geological Society of America Bulletin* 93, 545-562.

Dominguez, S., Lallemand, S. E., Malavieille, J., von Huene, R., 1998. Upper plate deformation associated with seamount subduction. *Tectonophysics* 293, 207-224.

Espurt, N., Funiciello, F., Martinod, J., Guillaume, B., Regard, V., Faccenna, C., Brusset, S., 2008. Flat subduction dynamics and deformation of the South American plate: Insights from analog modeling. *Tectonics* 27, TC3011, doi:10.1029/2007TC002175.

Friedrich, A. M., Wernicke, B. P., Niemi, N. A., Bennett, R. A., Davis, J. L., 2003. Comparison of geodetic and geologic data from the Wasatch region, Utah, and implications for the spectral character of Earth deformation at periods of 10 to 10 million years. *Journal of Geophysical Research* 108, doi:10.1029/2001JB000682.

Furque, G., 1979. Descripción geológica de la hoja 18 c, Jáchal, Provincia de San Juan.

Buenos Aires, Argentina, Servicio Geológico Nacional, Boletín 164, 79 pp.

Furque, G., 1983. Descripción geológica de la hoja 19 c, Ciénega de Gualilán, Provincia de San Juan. Buenos Aires, Argentina, Servicio Geológico Nacional, Boletín 193, 111 pp.

Gans, C. R., Beck, S. L., Zandt, G., Gilbert, H., Alvarado, P., Anderson, M., Linkimer, L., 2011. Continental and oceanic crustal structure of the Pampean flat slab region, western Argentina, using receiver function analysis: new high-resolution results. *Geophysical Journal International* 186, 45-58, doi: 10.1111/j.1365-246X. 2011.05023.x.

Gilbert, H., Beck, S., Zandt, G., 2006. Lithospheric and upper mantle structure of central Chile and Argentina. *Geophysical Journal International* 165, 383-398, doi: 10.1111/j.1365-246X.2006.02867.x.

Gutscher, M.-A., Spakman, W., Bijwaard, H., Engdahl, E. R., 2000. Geodynamics of flat subduction: Seismicity and tomographic constraints from the Andean margin. *Tectonics* 19, 814-833.

Hampel, A., Adam, J., Kukowski, N., 2004. Response of the tectonically erosive south Peruvian forearc to subduction of the Nazca Ridge: Analysis of three-dimensional analogue experiments. *Tectonics* 23, TC5003, doi: 10.1029/2003TC001585.

Hindle, D., Kley, J., Klosko, E., Stein, S., Dixon, T., Norabuena, E., 2002. Consistency of geologic and geodetic displacements during Andean orogenesis. *Geophysical Research Letters* 29, doi:10.1029/2001GL013757.

Jordan, T. E., Allmendinger, R. W., 1986. The Sierras Pampeanas of Argentina: A modern analogue of Rocky Mountain foreland deformation. *American Journal of Science* 286, 737-764.

Jordan, T. E., Allmendinger, R. W., Damanti, J. F., Drake, R. E., 1993. Chronology of motion in a complete thrust belt: The Precordiller, 30–31°S, Andes mountains. *Journal of Geology* 101, 135-156.

Jordan, T. E., Isacks, B. L., Allmendinger, R. W., Brewer, J. A., Ramos, V. A., Ando, C. J., 1983. Andean tectonics related to geometry of subducted Nazca plate. *Geological Study of America Bulletin* 94, 341-361.

Jordan, T. E., Schlunegger, F., Cardozo, N., 2001. Unsteady and spatially variable evolution of the Neogene Andean Bermejo foreland basin, Argentina. *Journal of South American Earth Sciences* 14, 775-798.

Judge, P. A., 2012. The spatial and temporal evolution of the Argentine Precordillera at 30ºS: Shortening over a shallow slab. PhD thesis, Cornell University.

Judge, P. A., Allmendinger, R. W., 2011. Assessing uncertainties in balanced cross sections. *Journal of Structural Geology* 33, 458-467, doi:10.1016/j.jsg.2011.01.006.

Kay, S. M., Abbruzzi, J. M., 1996. Magmatic evidence for Neogene lithospheric evolution of the central Andean "flat-slab" between 30ºS and 32ºS. *Tectonophysics* 259, 15-28.

Kay, S. M., Maksaev, V., Mpodozis, C., Moscoso, R., Nasi, C., Gordillo, C. E., 1988. Tertiary Andean magmatism in Argentina and Chile between 28–33ºS: Correlation of magmatic chemistry with a changing Benioff zone: *Journal of South American Earth Sciences* 1, 21-38.

Kendrick, E., Bevis, M., Smalley Jr., R., Brooks, B., 2001. An integrated crustal velocity field for the central Andes. *Geochemistry Geophysics Geosystems* 2, doi: 2001GC000191.

King, R. W., Shen, F., Burchfiel, B. C., Royden, L. H., Wang, E., Chen, Z., Liu, Y., Zhang, X.-Y., Zhao, J.-X., Li, Y., 1997. Geodetic measurement of crustal motion in southwest China. *Geology* 25, 179-182, doi: 10.1130/0091-7613(1997) 025<0179:GMOCMI>2.3.CO;2.

Marrett, R. A., Allmendinger, R. W., 1990. Kinematic analysis of fault-slip data. *Journal of Structural Geology* 12, p. 973-986

Martinod, J., Husson, L., Roperch, P., Guillaume, B., Espurt, N., 2010. Horizontal subduction zones, convergence velocity and the building of the Andes. *Earth and Planetary Science Letters* 299, 299-309, doi:10.1016/j.epsl.2010.09.010.

Nicol, A., Wallace, L. M., 2007. Temporal stability of deformation rates: Comparison of geological and geodetic observations, Hikurangi subduction margin, New Zealand. *Earth and Planetary Science Letters* 258, 397-413, doi:10.1016/j.epsl. 2007.03.039.

Ortíz, A., Zambrano, J. J., 1981. La provincia geológica Precordillera oriental. *VIII Congreso Geológico Argentina Actas* 3, 59-74.

Pardo-Casas, F., Molnar, P., 1987. Relative motion of the Nazca (Farallon) and South American plates since Late Cretaceous time. *Tectonics* 6, 233-248.

Petit, J. P., 1987. Criteria for the sense of movement of fault surfaces in brittle rocks. *Journal of Structural Geology* 9, 597-608.

Pilger, R. H., 1981. Plate reconstructions, aseismic ridges, and low-angle subduction beneath the Andes. *Geological Society of America Bulletin* 92, 448-456.

Ramos, V. A., Cristallini, E. O., Pérez, D. J., 2002. The Pampean flat-slab of the Central Andes. *Journal of South American Earth Sciences* 15, 59-78.

Ruskin, B. G., Jordan, T. E., 2007. Climate change across continental sequence boundaries: Paleopedology and lithofacies of Iglesia basin, northwestern Argentina. *Journal of Sedimentary Research* 77, 661-679.

Siame, L. L., Bellier, O., Sebrier, M., 2006. Active tectonics in the Argentine Precordillera and western Sierras Pampeanas. *Revista de la Asociación Geológica Argentina* 61, 604-619.

Siame, L. L., Bellier, O., Sébrier, M., Araujo, M., 2005. Deformation partitioning in flat subduction setting: Case of the Andean foreland of western Argentina (28ºS–33ºS). *Tectonics* 24, TC5003, doi:10.1029/2005TC001787.

Siame, L. L., Bourlès, D. L., Sébrier, M., Bellier, O., Castano, J. C., Araujo, M., Perez, M., Raisbeck, G. M., Yiou, F., 1997. Cosmogenic dating ranging from 20 to 700 ka of a series of alluvial fan surfaces affected by the El Tigre fault, Argentina. *Geology* 25, 975-978.

Smalley, R. J., Pujol, J., Régnier, M., Chiu, J.-M., Chatelain, J.-L., Isacks, B. L., Araujo, M., Puebla, N., 1993. Basement seismicity beneath the Andean Precordillera thin skinned thrust belt and implications for crustal and lithospheric behavior. *Tectonics* 12, 63-76.

Somoza, R., 1998. Updated Nazca (Farallon)—South America relative motions during the last 40 My: implications for mountain building in the central Andean region.

Journal of South American Earth Sciences 11, 211-215.

Somoza, R., Ghidella, M. E., 2005. Convergencia en el margen occidental de América del Sur durante el Cenozoico: subducción de las placas de Nazca, Farallón y Aluk. *Revista de la Asociación Geológica Argentina* 60, 797-809.

Tebbens, S. F., Cande, S. C., 1997. Southeast Pacific tectonic evolution from early Oligocene to Present. *Journal of Geophysical Research* 102, 12061-12084.

van Hunen, J., van den Berg, A. P., Vlaar, N. J., 2002. On the role of subducting oceanic plateaus in the development of shallow flat subduction. *Tectonophysics* 352, 317-333.

von Gosen, W., 1992. Structural evolution of the Argentine precordillera: the Rio San Juan section. *Journal of Structural Geology* 14, 643-667.

von Gosen, W., 1997. Early Paleozoic and Andean structural evolution in the Río Jáchal section of the Argentine Precordillera. *Journal of South American Earth Sciences* 10, 361-388.

Yáñez, G. A., Ranero, C. R., von Huene, R., Díaz, J., 2001. Magnetic anomaly interpretation across the southern central Andes (32º-34ºS): The role of the Juan Fernández Ridge in the late Tertiary evolution of the margin. *Journal of Geophysical Research* 106, 6325-6345.

Yáñez, G., Cembrano, J., Pardo, M., Ranero, C., Selles, D., 2002. The Challenger–Juan Fernández–Maipo major tectonic transition of the Nazca–Andean subduction system at 33–34ºS: geodynamic evidence and implications. *Journal of South American Earth Sciences* 15, 23-38.

Zapata, T. R., Allmendinger, R. W., 1996. Thrust-front zone of the Precordillera, Argentina: A thick-skinned triangle zone. *AAPG Bulletin* 80, 359-381.

Appendix A:

Help file and MATLAB script for area balancing and error propagation of cross sections, 'Error Propagation'

A.1 Error Propagation help file

Error Propagation help file, February 2011

This program formally propagates error through the area balancing of a cross section.

Below is a brief summary of the code from the .m file (section A.2):

```
% code for uncertainty estimates on polygons
%       1) load polygon data
%       2) calculates the area of the polygon
%       3) calculates the uncertainty of the area of the polygon
%       4) calculates the original width of the thrust best
%       5) calculates the uncertainty of the original width
%       6) calculates shortening in km, percent
%       7) calculates uncertainty in shortening in km, percent
%       8) writes a file that saves the calculated values
```

The program relies on an input file of data that describes the cross section as a polygon with individually determined uncertainties for each vertex and uncertainties on the stratigraphic thicknesses at either end of the cross section. Additionally, an error estimate on the modern width of the region of interest is necessary. These values must be known a priori.

The input file needs to be a comma-delimited .csv file with the following format:

<E1>,<W1>,<dE1>,<dW1>,<dx2>

<Xi>,<Yi>,<dXi>,<dYi>,<Loc(i)>

such that the file (Poly) is an <n + 1, 5> matrix where n is the number of vertices in the polygon and i = 1:n.

The values for E1 and W1 are the stratigraphic thicknesses at either end of the cross section, and dE1 and dW2 are their respective uncertainties. The labels "E" and "W" do not necessitate an east-west trending section but merely serve to distinguish between the two ends of the section. dx2 is the uncertainty on the modern width of the cross section.

Xi and Yi are the cartesian coordinates for each vertex of the polygon that describes the outline of the cross sectional area. The uncertainty associated with each vertex (dXi and dYi) is individually determined by the user. Loc(i) is a numeric tag that identifies the location of each vertex in the cross section: on the decollement (1), at the surface (2), in the subsurface (3), or at an eroded hanging-wall cutoff (4). Of course, any individual vertex may have a specific individual uncertainty (eg, a vertex at the surface may only be constrained by a map and not by a GPS location), and the value may be different from other surface vertices. Remember, though, that by tagging this location as a "surface" vertex, if you chose to change the surface uncertainties, the program will over-write all values tagged "surface."

The first prompt requires the user to upload a .csv file containing the above information.

The second prompt allows the user to manually change individual uncertainty values to explore the influence of specific components of the error calculation. Enter 'n' on the first use to retain the uploaded values. Select 'y' to modify the uploaded values for subsequent calculations. The program will write out an "Output.txt" file that updates after each run and is saved to the current directory so that the results of any modifications to the initial uncertainty values are retained.

The third prompt allows the user to select the type of uncertainty modify. This prompt requires a numeric response. To modify the follow uncertainty value, use the following value:

Stratigraphy = 1 [Both stratigraphic uncertainty values can be changed]
Polygon vertex at the decollement = 2 [Both dX and dY values can be changed]
at the surface = 3
in the subsurface = 4
at the hanging wall cut-offs = 5
To set all uncertainty values to 0 = 6
[This includes the uncertainty on the final width]

If the users selects a value to change, the user must enter a numeric value. If no value is entered and the user selects 'Return' instead, the code will not supply a zero value but instead retain a null entry.

Once all data have been uploaded or modified, the code calculates the area of the cross section and the error associated with the area. The area calculation is based on the

method illustrated by Paul Bourke (among others) at the University of Western Australia:

http://local.wasp.uwa.edu.au/~pbourke/geometry/polyarea/

$A = (1/2) * \text{sum}((X(i)*Y(i+1)) - (X(i+1)*Y(i)))$

The Gaussian uncertainty on the area is calculated using a standard error propagation method where the uncertainty of the Area is the square root of the sum of the squares of the partial derivatives of A with respect to each variable multiplied by the uncertainty in each variable.

Gaussian uncertainty:

$dA = \text{sqrt}(((dA/dx)*dX)^2) + ((dA/dy)*dY)^2))$

The Maximum uncertainty calculation is the sum of the partials multiplied by the associated uncertainty for each term.

Maximum uncertainty:

$dA = (dA/dx)*dX + (dA/dy)*dY$

From the area, the modern width, and the initial stratigraphic thicknesses, the algorithm calculates the initial width and its uncertainty. Knowing the initial width and the final width, the algorithm calculates the shortening in both kilometers and percent, their respective Gaussian uncertainty values, as well the maximum values.

Finally, the code generates a file of data called 'Output.txt' that is saved to the directory in use in MatLab. This .txt file is appended with every run of the code. The Output file is tab-delimited and can be read into Excel or Numbers.

A.2 Error Propagation script

```
% Error Propagation
% February 2011

% code for area balancing and uncertainty estimates on polygons
%
%       1) load polygon data
%       2) calculates the area of the polygon
%       3) calculates the uncertainty of the area of the polygon
%       4) calculates the original width of the thrust best
%       5) calculates the uncertainty of the original width
%       6) calculates shortening in km, %
%       7) calculates uncertainty in shortening in km, %
%       8) writes a file that saves the calculated values

close all
clear all

%  note:  these values in kilometers

%  load polygon data from file:
   %  the polygon file must be in .csv format (comma-delimited)
   %  where the first line contains the stratigraphic thicknesses (E1, W1),
   %  their respective unknowns (dE1, dW1), and the uncertainty on the
   %  modern width (dx2). these values must be known a priori.
   %  the rest of the file consists of one line for each vertex,
   %  with the X,Y points of the vertices of the polygon,
   %  their respective uncertainties, and their location as a numeric tag.
   %  example:
   %  <E1>,<W1>,<dE1>,<dW1>,<dx2>
   %  <Xi>,<Yi>,<dXi>,<dYi>,<Loc(i)>


Poly = input('Whence would you like to import your polygon data? ','s');
```

```
[data] = csvread(Poly,0,0); %  reads in data file

E1 = data(1,1);  %  labels the E stratigraphic thickness
W1 = data(1,2);  %  labels the W stratigraphic thickness

dE1 = data(1,3);  %  labels the uncertainty on E
dW1 = data(1,4);  %  labels the uncertainty on W

%  make two arrays that contain the vertex uncertainty and its location tag
dXL = [data(2:end,3), data(2:end,5)];
dYL = [data(2:end,4), data(2:end,5)];


n = length(data)-1;


%  change the errors included in the uncertainty calculation?

Change = input('Would you like to change the values in the error calculation? (y or n) ','s');

if Change=='y'
   Errors = input('Which values would you like to change? (Strat (1), decol (2), surfc (3), subsf
(4), HWcut (5), all=0 (6)) ','s');          %  this line requires a numeric response.

   if Errors=='1'          %  code uses new dE1, dW1 values
      dE1 = input('Enter new dE1 value (km) ');
      dW1 = input('Enter new dW1 value (km) ');

   elseif Errors=='2'     %  use new values for vertices at decollement
      dXL((dXL(:,2)==1),1) = input('Enter new dX values for the decollement (km) ');
      dYL((dYL(:,2)==1),1) = input('Enter new dY values for the decollement (km) ');

   elseif Errors=='3'     %  use new values for vertices in the surface
      dXL((dXL(:,2)==2),1) = input('Enter new dX values for the surface (km) ');
      dYL((dYL(:,2)==2),1) = input('Enter new dY values for the surface (km) ');

   elseif Errors=='4'     %  use new values for vertices at the subsurface
      dXL((dXL(:,2)==3),1) = input('Enter new dX values for the subsurface (km) ');
      dYL((dYL(:,2)==3),1) = input('Enter new dY values for the subsurface (km) ');


   elseif Errors=='5'     %  use new values for vertices at hangingwall cut-offs
      dXL((dXL(:,2)==4),1) = input('Enter new dX values for the hanging wall cut-offs (km) ');
```

```
      dYL((dYL(:,2)==4),1) = input('Enter new dY values for the hanging wall cut-offs (km) ');

   elseif Errors=='6'     %  changes all input errors to equal 0
            dE1 = 0;
            dW1 = 0;
            data(1,5) = 0;
            dXL(:,1) = 0;
            dYL(:,1) = 0;

   end

else Change==n
end


dx2 = data(1,5);       %  labels the uncertainty on the final width
X = data(2:end,1);     %  labels the x coordinate of the vertex in km
Y = data(2:end,2);     %  labels the y coordinate of the vertex in km
dX = dXL(:,1);         %  labels the uncertainty in X in km
dY = dYL(:,1);         %  labels the uncertainty in Y in km
Loc = dXL(:,2);        %  labels the location of the vertex
                       %  1 = Decollement
                       %  2 = Surface
                       %  3 = Subsurface
                       %  4 = Eroded hanging-wall cutoffs

%  calculate area of deformed state using Paul Bourke's method
   %  http://local.wasp.uwa.edu.au/~pbourke/geometry/polyarea/
   %  A = (1/2) * sum((X(i)*Y(i+1)) - (X(i+1)*Y(i)))

XArea = zeros(1,n);    %  initializes vector

aX = [X; X(1)];
aY = [Y; Y(1)];

XArea = 0.5*(aX(1:end-1).*aY(2:end) - aX(2:end).*aY(1:end-1));

Area1 = (abs(sum(XArea)));

Area = round(Area1)

%  calculate the Gaussian uncertainty of the area of the polygon using standard error propagation
%  method where the uncertainty of the value (Area) is the square root of the sum of the squared
```

```
%  values of the partial derivative of A with respect to each variable in the equation, multiplied
%  by the uncertainty of each variable.
        %  ex: dA = sqrt (((dA/dx)*dX)^2) + ((dA/dy)*dY)^2))

dAx = zeros(1,n);    %  initializes vector
dAy = zeros(1,n);    %  initializes vector

aX = [X(end); aX];
aY = [Y(end); aY];

dAx = 0.5*(aY(3:end) - aY(1:end-2));
dAy = 0.5*(aX(1:end-2) - aX(3:end));


delAx = (dAx.*dX).^2;
delAy = (dAy.*dY).^2;

%  sum the X and Y components
SdelAx = sum(delAx);    %  sums all x components
SdelAy = sum(delAy);    %  sums all y components

%take the square root of the sum of individual components to calculate dA
dA = sqrt(SdelAx+SdelAy);    %  calculates uncertainty in A

dArea = round(dA)


%  calculate the original width of the thrust belt assuming constant Area:
   %  if the initial area   Area = (X1 * E1) + (X1 * (W1-E1)/2)
   %     then the initial width  X1 =  Area/ ((E1)/2 + (W1)/2)


x11 = Area1/(((E1)/2)+((W1)/2));      %  calculates initial width based on area and
                                      %  rounds to an integer value
x1 = round(x11)

x21 = max(X) - min(X);    %  calculates final width from the imported polygon and
                          %  rounds to one decimal place
x2 = round(x21);
```

```
%  calculate the uncertainty of the original width, x1
   %  based on the same method as for the area uncertainty calculation

ddA = 1/(((E1)/2)+((W1)/2));  %partial of x1 wrt Area
ddE1 = -(2*Area1)/((E1)^2+(2*E1*W1)+(W1)^2);    %  partial of x1 wrt E1
ddW1 = -(2*Area1)/((E1)^2+(2*E1*W1)+(W1)^2);   %  partial of x1 wrt W1

dx11 = sqrt(((ddA*dA)^2)+((ddE1*dE1)^2)+((ddW1*dW1)^2));
                %  calculates uncertainty in the original width
dx1 = round(dx11)


%  Maximum error calculation for area
   %  to calculate the non-Gaussian distribution of errors,
   %  we make several for loops that look like this:
   %  sum (1/2 ((Y(i+1) - Y(i-1))*dX(i)) + ((X(i-1) - X(i+1))*dY(i))


dAxM = abs(0.5*(aY(3:end) - aY(1:end-2)));
dAyM = abs(0.5*(aX(3:end) - aX(1:end-2)));

delAxM = dAxM.*dX;
delAyM = dAyM.*dY;

%  sum the X and Y components
SdelAxM = sum(delAxM);    %  sums all x components
SdelAyM = sum(delAyM);    %  sums all y components

%  add everything together to get the maximum uncertainty in A
dAM = SdelAxM+SdelAyM;    %  calculates uncertainty in A

dArea_Max = round(dAM)


%  calculating dX1 Max

ddAM = 1/(((E1)/2)+((W1)/2));      %  partial of x1 wrt Area
ddE1 = -(2*Area1)/((E1)^2+(2*E1*W1)+(W1)^2);      %  partial of x1 wrt E1
ddW1 = -(2*Area1)/((E1)^2+(2*E1*W1)+(W1)^2);     %  partial of x1 wrt W1

dx1Max1 = ((abs(ddA*dAM))+(abs(ddE1*dE1))+(abs(ddW1*dW1)));
          %  calculates uncertainty in the original width
          %  and rounds integer value
```

```
dx1Max = round(dx1Max1)


%  calculating the shortening values in both km, %

Shortening_km1 = x11-x21
      %  calculates the amount of shortening in km

dShortening_km1 = sqrt((1*dx11)^2+(-1*dx2)^2);
      %  calculates the Gaussian uncertainty in km shortening
      %  and rounds to integer value
dShortening_km = round(dShortening_km1)

dShortening_Max_km1 = (dx1Max1+dx2) ;
      %  calculates the maximum uncertainty in km shortening
      %  and rounds to integer value
dShortening_Max_km = round(dShortening_Max_km1)

Shortening_percent1 = (1-(x21/x11))*100;   %calculates the percent shortening
            %  and rounds to an integer value
Shortening_percent = round(Shortening_percent1)


ddx1 = x21/((x11)^2);    %  partial of S wrt x1
ddx2 = -1/x11;     %  partial of S wrt x2

dShortening_percent1 = sqrt(((ddx1*dx11)^2)+((ddx2*dx2)^2))*100;
      %  calculates the Gaussian uncertainty in % shortening
      %  and rounds to integer value
dShortening_percent = round(dShortening_percent1)



dShortening_Max_percent1 = (abs(ddx1*dx1Max1)+(abs(ddx2*dx2)))*100;
      %  calculates the maximum uncertainty in % shortening
      %  and rounds to one integer value
dShortening_Max_percent = round(dShortening_Max_percent1)



% find the error value for dX at the decollement
v4 = dXL(dXL(:,2)==1);
```

```
v4 = v4(1,1);

% find the error value for dY at the decollement
v5 = dYL(dYL(:,2)==1);
v5 = v5(1,1);

% find the error value for dX at the surface
v6 = dXL(dXL(:,2)==2);
v6 = v6(1,1);

% find the error value for dY at the surface
v7 = dYL(dYL(:,2)==2);
v7 = v7(1,1);

% find the error value for dX at the subsurface
v8 = dXL(dXL(:,2)==3);
v8 = v8(1,1);

% find the error value for dY at the subsurface
v9 = dYL(dYL(:,2)==3);
v9 = v9(1,1);

% find the error value for dX at hanging wall cut-offs
v10 = dXL(dXL(:,2)==4);
v10 = v10(1,1);

% find the error value for dY at hanging wall cut-offs
v11 = dYL(dYL(:,2)==4);
v11 = v11(1,1);


% the remainder of the code either creates or appends the 'Output.txt' file

exist 'Output.txt';
fid = fopen('Output.txt', 'a+');
if ans==0;       %  these lines create the header if there is no existing 'Output.txt' file
   %  For header lines, just specify one fprint formatting statement
   fprintf(fid, 'N\tArea\tdArea_G\tdArea_Max\tx1\tdx1\tdx1_Max\tShortening_km
\tdShortening_km\tdShortening_km_Max\tShortening_per\tdShortening_per
\tdShortening_per_Max\tdE1\tdW1\tdx2\tdX_decollement\tdY_decollement\tdX_Surface
\tdY_Surface\tdX_Subsurface\tdY_Subsurface\tdX_HangingWall\tdY_HangingWall\r');
end
```

```
% this line appends the calculated value to the 'Output.txt' file
fprintf(fid, '%.0f\t%.0f\t%.1f\t%.1f\t%.0f\t%.1f\t%.1f\t%.0f\t%.1f\t%.1f\t%.0f\t%.1f\t%.1f\t%.2f
\t%.2f\t%.2f\t%.2f\t%.2f\t%.2f\t%.2f\t%.2f\t%.2f\t%.2f\r', n, Area, dArea, dArea_Max, x1,
dx1, dx1Max, Shortening_km, dShortening_km, dShortening_Max_km, Shortening_percent,
dShortening_percent, dShortening_Max_percent, dE1, dW1, dx2, v4, v5, v6, v7, v8, v9, v10,
v11);

fclose(fid);
```

Appendix B:

B.1: Field data from the Precordillera

Location (Lat., Long.)	*Bedding*	*Faults*	*Slip direction*	*Notes*
Blanco 2008				
1				
30.55373, 68.95393	339 73 W			not great bedding in green sands
	334 58 W			
	335 64 W			
	346 58 W			
	348 61 W			last 2 better
	351 59 W			
	350 56 W			RMG
	341 63 W			
				Fractures:
				025 86 N
				052 74 N
				034 81 N
				069 61 N
				349 62 W
2				
30.55350, 68.95341	296 62 W	249 51 S T?	slicks 34->W [34->216]	red sandstones
	303 60 W	249 56 S T?	slicks 02->W [02->247]	
3				
30.55263, 68.95312	000 44 W			on s-facing river cuts
	004 43 W	049 53 SE T?	slicks 04->219 [04->226]	tops->E?
		029 74 W T	slicks 26->S [26->217] fol: 004 84 W [20->215]	
	340 42 W			bedding sighted towards south
		014 69 E T?	slicks 51->N [51->042]	RMG
4				
30.55263, 68.95312		293 52 S T	slicks 11->306 [11->284]	
		071 78 S T	fol 113 87 N [17->247]	tops -> E ~3m offset
	303 81 N	007 40 W T	slicks 11->N fol: 350 42 N [39->262]	RMG
30.55225, 68.95261		042 57 W T	fol: 025 69 W [39->223] [PAJ]	
		012 55 W T	fol: 295 52 S [22->355] [RMG]	

Blanco 2009				
Transect 1 (DD, D)				
1				
30.43183, 68.92065	284 29			coarse-grained dark red sandstones, thinly bedded
	278 28			folded and eroded, covered in coarse Osj cong.
2				
30.43249, 68.92523	266 18			more coarse-grained sands with white beds as well
	234 23			
3a				
30.43183, 68.92710	283 0			green & dk red coarse ss (eolian?)
	288 57			
	284 56			
	286 55			
	282 0			
	288 58			
	279 37			x-bedding
	265 40			
	269 34			
	~280 60			
3b				
30.43355, 68.93153	236 08			x-bedded
	211 12			
	208 07			
	286 59			
	288 52			
4				
30.43353, 68.94061	290 40	141 20 N	s 19-> 106	in pink-light green SS faults w, 2-5cm sep.
		145 52 N	s 35->085	
		214 20 T	s 08->284	
5				
30.43287, 68.94873				red beds still striking ~N-S but now dipping ~30ºE
6				
30.43337, 68.94973	238 50			big syncline-anticline pair

	031, 52 E			
7				
30.43364, 68.95520	355 10			red sands
8				
30.43291, 68.95670	276 12			
9				
30.43242, 68.95667		284 21 T	s 21->283	the bottom of the fault zone
10				
30.43575, 68.95900	300 19			Osj folded mostly striking NE-SW and dipping 20º
	281 18			faulted as well
	294 12			
	225 20			
	224 08			
	260 30			
	30 20			
	40 19			
	55 20			
	48 20			
11				
30.43051, 68.92241	294 41	304 58 T	s 52 -> 281	faulted red beds. crappy.
Transect 2 (DD, D)				
12				
30.46482, 68.93457	287 22			coarse red SS
	249 18			
	266 18			
	264 20			
	274 39			green SS
				green & red SS are eolian and interlayered
13				
30.46517, 68.93686	256 58			green SS (x-bedded)
	280 40			
14				
30.46900, 68.94723	264 44			red SS w, rounded choiyoi clasts
	302 54			
	265 55			
	281 48			

	286 40			
	264 42			
15				
30.47095, 68.94981	274 50			sandier units but still has choiyoi layers
	258 57			
	258 57			
	257 51			
	253 04			
	268 46			
	278 42			fine-grained sands
	276 45			
16				
30.417112, 68.95135	266 47			red SS cliffs
	276 44			paleocurrent all say from ~300º
	275 47			
	277 39			
17				
30.47103, 68.95170	279 33			(a little shallow)
	268 36			obvious clasts of Osj at this level
18				
30.47189, 68.95420	259 50			still with Choiyoi but also lots of Osj and clasts of mafics
	262 44			
	263 44			
	273 51			
19				
30.47161, 68.95796		300, 43 FP		bottom of gouge zone
		282, 56 T	s 54-> 263	kind of lousy but ok
		278, 47 T	sch: 285, 51 s: 25 -> 343	even worse
Blanquitos				
1				
30.30294, 68.82001	019, 42 W			in Osj
	020, 37 W			
	024, 44 W			
	051, 54 W			
	039, 47 W			
	006, 54 W			Directly above thrust
	007, 52 W			Above thrust
		034, 23 W T	fol: 033, 34 W no slicks.	Osj, T [23->301]
	351, 66 W			in T

	006, 57 W			
	358, 67 W			
	021, 61 NW			Osj
	026, 66 NW			RMG
	032, 65 NW			
	029, 68 NW			
	016, 57 NW			
	034, 66 NW			
	010, 39 W			in T
2				
30.30569, 68.82056		003, 38 W T	fol: 031 56 W slicks 27->312 [18->338] [27->345]*	Osj, T
		358, 54 W T	slicks 44->N; 37->326 [44->314] [37->325]*	
	010, 60 W			bedding in Osj
	004, 62 W			RMG
	356, 61 W			
	357, 54 W			
	019, 56 W			
	021, 55 W			in T
	021, 46 W			
3				
30.30965, 68.81755	301, 32 W			in green eolian sands
	301, 36 W	set 1		w.in T
		348, 28 W T	slicks 24->298	
		004, 25 W T	slicks 22->304	
		351, 29 W T	slicks 21->309	These are mutually cross-cutting and compatible senses of motion
		set 2:		
		281, 20 S T	slicks 06->115	~1m rev.
		056, 24 S T	slicks 19->106	tops->W
	306, 31 W			RMG
	301, 36 W			bedding in green eolian
		324, 49 W		set #1 (no slicks)
		065, 19 SE T	slicks 14->110	
		061, 18 SE		no slicks
4				
30.31372, 68.81884		026, 32 W T	fol 026, 51 W [32->295]	between Osj, T
5				
30.31460, 68.81837	326, 37 W			Notes say all ok, so is likely xbed

	341, 58 W (*)	016, 17 W T	slicks -> 247 [13->247]	
	311, 44 W	001, 14 W T		
		002, 79 W N	slicks 48->341 (fol: 006, 72 W) [48->349]	Large normal faults
		020, 76 W N	slicks 66->339 [66->345]	
		074, 34 S		tops W sep
		281, 31 S T	slicks 25->SE [25->150]	
	356, 41 W	079, 42 S T	slicks: 10->N [10->090]	
	019, 38 W			
	335, 47 W			
		275, 15 S T		no slicks
6				
30.29099, 68.80645	016, 53 W			X-bedded pink and green sands T
	014, 44 W			
7				
30.26311, 68.78419	025, 50 W			
	025, 56 W			
	021, 46 W			
	034, 42 W			
	029, 64 W			
	039, 32 NW			RMG
	036, 30 NW			
	037, 32 NW			
	044, 34 NW			
2009				
1				
30.28065, 68.78696	293 54			x-bedded redbeds
	315 0			Perm
	286 55			
	318 01			
	287 54			
	317 53			
2				
30.27983, 68.79086	277 43			west of qtz-pebble horizon
	291 57			strongly x-bedded
	295 07			Perm
3				
30.27950, 68.79246	287 46			Perm
	291 55			

4				
30.27888, 68.79387	292 47			
	287 55			
	291 45			
San Roque -> Blanquitos transect				
1				
30.36028, 68.75534	291 52			Beds in Osj
	279 54			
	291 51			
	295 54			
2				
30.36228, 68.76002	284 55			Osj
	292 47			
	274 45			
	292 52			
	294 39			sketchy
	293 44			
3				
30.36266, 68.76434	287 50			beneath powerlines
	287 47			
	271 43			
	278 50			
	286 51			
5				
30.36159, 68.76797	280 43			In next unit: "finely" bedded (10-40 cm) as opposed to meter-scale
	267 42			
	272 45			
	279 44			
	272 43			
	278 48			
	279 52			
	275 51			
	288 46			
	276 57			
6				
30.35566, 68.79519	287 46			In Sil./Dev.: sandy & green
	278 46			
	282 41			
	283 50			
	288 45			
7				

30.35507, 68.79703	287 43			Still Sil., Dev.
	307 40			
	286 38			
	292 38			
	288 41			
8				
30.35541, 68.80081	284 46			Sil., Dev.
	286 40			
	293 38			
	292 39			
	290 38			
9				
30.35357, 68.80724	290 47			
	292 50			
	288 50			
	292 52			
	286 58			
10				
30.35387, 68.80926	291 41			Now in Carboniferous
	287 41			
	285 38			
	290 40			
	298 39			
11				
30.35380, 68.80943	304 45			Large rip-up clasts in sandy units
	292 36			
	316 40			
	293 41			
Caracol				
2008				
Day 1				
1				
30.29200, 68.96106	354, 29 E			bedding in red, orange shales
	028, 49 E			
	014, 53 E			
	025, 57 E			
	355, 47 E			RMG
	352, 57 E			
	010, 50 E			
	012, 58 E			

2				
30.29163, 68.96038		016, 59 E T	fol: 035, 76 W [51->148]*	more
			fol: 356, 80 E [36->-42]	less
		347, 58 E T	fol: 354, 66 E [40->1350]	tops->W 3 cm sep
		351, 65 E T	fol: 350, 78 E [65->073]	tops->W 1 cm sep
	041, 79 W			bedding in Miocene
	013, 51 W			bedding in M; RMG
3				
30.29082, 68.96040		351, 63 E T	slicks: 63 down dip [63->070]	
	016, 52 W			RMG
Day 2				
1		004, 52 W T	fol: 044, 62 W [04->001]	
			fol w. slicks 346, 39 W; 39->W [39->326]	
			fol: 039, 56 W [09->001]	
	005, 50 W			sighted
	024, 65 W			bedding in M; RMG
	027, 65 W			
2		011, 49 W T	fol: 034, 58 W 14->358]	good
		009, 49 W T	fol: 328, 64 W [09->197]	
3				
30.28979, 68.97363		015, 41 W T	fol: 048, 58 W [14->358]	Ord, T
4				
30.28900, 68.97385		005, 41 W T	fol: 029, 56 W [20->340]	Ord, T
	006, 34 W			bedding in Ord
5				
30.28864, 68.97384		346, 83 W T	fol: 336, 88 E [42->172]	(not nec. trusty)
6				
30.28837, 68.97306	045, 18 W			bedding in T defined by gravel horizons
7a				
30.28242, 68.97504	301, 40 N			bedding in T
	276, 34 N	011, 80 E T	slicks: 28->N [28->016]	10 cm sep tops S
	276, 28 N			
		018, 67 E		
		031, 70 E		
		034, 77 E		

		276, 34 S		
		075, 31 S		
		088, 34 S		
7b				
30.28211, 68.97415	036, 35 W	010, 34 W T	fol: 005, 45 W [32->258]	fault in T
	045, 34 W			bedding in M
	031, 38 W	046, 36 NW T	fol: 037, 46 W [29->274]	in T
	042, 46 W			
	032, 24 W			
	017, 38 W			bedding in M; RMG
	357, 20 W	017, 74 W	fol: 345, 56 W	(not very confident)
8				
30.28047, 68.97343	028, 42 W	342, 08 E N	fol: 000, 15 W [08->084]	in T; tops->E 1 cm sep
	031, 44 W	279, 38 N N	fol: 048, 41 W [09->087]	1 m tops->E sep
	038, 44 W			bedding in T
	051, 43 W			RMG
	030, 37 W			
	034, 33 W			
9				
30.27728, 68.97179	033, 41 W			pink sands
	036, 47 W			
	008, 36 W			
	014, 51 W			
	018, 50 W			RMG
	009, 60 W			
10				
30.25656, 68.96843	014, 65 W			bedding in Miocene
	332, 68 W	016, 69 W T	fol: 024, 74 W [29->004]	
	040, 55 W	358, 58 W T	fol: 011, 78 W [44->321]	
	019, 79 W			RMG
Caracol 2007				
a				
30.32000, 68.69700		042, 56 NW T	clv: 021, 58 N s: 55->301	O, T
b				
30.32060, 68.96700		182, 40 W T	clv: 220, 42 W	loc. dogy

c				
30.36195, 68.98124		036, 56 E T	fol: 019, 70 E s: 060, 31	O, T
d				
30.36230, 68.98162		034, 52 E T	fol: 350, 65 E s: 038, 04	O, T
e				
30.35195, 68.98121		309, 38 W T	fol: 274, 55 W s: 12->145	O, T
f				
30.34118, 69.97414		320, 24 W T	fol: 321, 52 W s: 24->232	O, T
g				
30.30666, 68.97376		334, 41 w T	fol: 332, 65 W s: 41->239	O, T
h				
30.30625, 68.97373		217, 44 w T	fol: 186, 53 W s: 07->224	O, T
i				
30.30517, 68.97356		240, 71 W T	fol: 025, 67 W s: 12->056	O, T
j				
30.30477, 68.97353		357, 42 W T	fol: 033, 49 W s: 32->314	O, T
k				
30.30412, 68.97359		001, 67 W T	fol: 027 68 W (O) s: 03->182	O, T
			017, 72 W (T) s: 14->355	
l				
30.30267, 68.97292		036, 36 W T	fol: 046, 58 W s: 33->333	O, T
m				
30.30224, 68.97285		351, 74 W T	fol: 339, 76 W s: 09->174	O, T
n				
30.30035, 68.97276		353, 34 W T	fol: 352, 65 W s: 34->259	O, T
o				
30.29964, 68.97277		352, 63 W T	fol: 331, 75 W s: 25->185	O, T
p				
30.29945, 68.97285		007, 61 W T	fol: 359, 69 W s: 40->214	O, T
q				
30.29911, 68.97281		340, 46 W T	fol: 045, 89 W (O) s: 12->328	O, T
			042, 45 W (O) s 17->177	
			336, 62 W (FZ) s 44->231	

r				
30.30118, 68.96568	025, 30 E			bedding in Sil.
				clv 1: 096, 74 N
				clv 2: 340, 38 W
s				
30.29060, 68.95643		017, 15 S T	fol: 285 34 N (#1) s: 06->175	don't use
		301, 53 N	s 01->019	
		297, 37 N	s 03->187	
t				
30.28026, 68.95283		028, 25 E T	fol: 090, 35 S s: 05->038	O, T
Central Tranca				
Day 1				
A				
30.43710, 69.05781				At trace of large thrust fault, verging E, in the Ord
2				
30.44502, 69.03941				Fill at the edge of the valley looks like castano congl. and is folded in a syncline
3				
30.44858, 69.02035	115, 36 (RHR)			WDB
	225, 15 (DD, D)			in folded red beds like Caracol
4				
30.44379, 69.02924	315 21			Gravels w/ some Ch. mostly local
	282 20			
	288 19			
				paleocurrent directions in gravels
				296 48
				257 42
				253 49
				282 37
				276 32
5				
30.44368, 69.02935	262 30			WDB (RHR)
	280 30			
	258 26			
Day 2				
1				
30.43890 69.01977	105 88			vertical green miocene bedding
	091 88			contact between M & congl.
	089 87			323 52
				334 62
				300 68

	261 72			bedding in conglomerate
	230 72			contact between congl & gravels
				298 35
	352 27			bedding in gravels
				paleocurrent in conglomerates
				337 63
				351 77
				327 64
				283 77
				346 67
				001 79
				309 68
				272 83
				339 53
				345 67
2				001 77
30.43639 69.98716	067 65			bedding in dark green shales
	090 66			
	072 70			
	073 72			
	074 76			
	062 70			
	103 79			WDM (DD)
	108 78			
	105 73			Fractures
	100 76			261 54
				263 67
				245 82
				243 69
				246 68
				245 50
				246 79
				245 63
				251 56
3				
30.43621 68.99887	261 79			dark shales w/ coarser sands (+ trace fossils)
	263 85			
	263 89			
	264 85			
	264 85			
	261 88			

	268 88			
	272 88			
	271 84			
	086 86			
	091 84			
4				
30.43654 69.00258	084 88			in sandier beds folded tops -> W?
	085 87			
	085 84			
	084 88			
	080 78			
	077 81			
	078 84			
	079 81			
5				
30.43464 69.00719	063 56			tops -> E ?
	081 57			
	067 62			
	073 63			
	070 60			
	071 63			
	067 59			
	076 61			
Estancia Durazno				
1				
30.55797 68.90525	329 61 W			in silty shales T
	338 47 W			
	344 42 W			
	332 74 W			
	341 56 W			
	335 59 W			
	333 60 W			
	344 59 W			
	343 56 W			
	336 49 W			RMG
	332 54 W			
	330 60 W			
2				

30.55815 68.90591	339 56 W			dark red and white sands
	344 57 W	079 87 N S	slicks: 46->076	6 cm LL offset (tops->W)
	259 87 W	067 83 N D	slicks: 26->063	5 cm RL offset (tops->E)
	247 83 W	081 64 S D	slicks: 38->103	2 cm RL offset (tops->E)
	244 47 W	064 74 N D	slicks: 51->044	0.5m RL offset (tops->E)
		005 65 W		tops->W
	345 51 W	075 85 N D		RMG: RL 35 cm offset
	338 55 W	060 81 N D		RL: 28 cm offset
		067 80 N D	slicks: 40 -> 059	2 m offset RL
3				
30.5584 68.90729	324 66 W			fractures in dark shaley unit
	323 61 W			041 82 N
				049 88 N
				334 55 E
				339 48 S [E?]
				009 59 E
	335 54 W			RMG
	332 57 W			
4				
30.55861 68.90781		009 61 W T	fol: 041 70 W [08->005]	not great, but ok
		086 44 S T	slicks: 34->S [34->219]	minor
		341 57 W T	fol: 008 74 W [325->24]	not great
	358 45 W			bedding in T
	358 48 W			
	355 44 W			bedding in Pal
	356 51 W			RMG
	002 57 W			bedding in M
6				
30.55928 68.90761		299 46 SW T	slicks: 45->191	
7				
30.56088 68.90724	334 71 W			Bedding in T
	336 62 W			
	350 62 W			
		358 88 E T	fol: 011 79 E slicks: 54->S	Not using these fault data
			fol: 014 90 slicks: 49->N	
	354 56 W			RMG
	323 59 W			Bedding in T

8				
30.56018 68.90648		024 84 W RT	slicks: 29->208	(better); 30 RL cm offset; tops->N
		043 84 N N	slicks: 19->225	tops down; LL?
	306 66 W			bedding in M
	304 70 W			
	320 76 W			bedding in T
	322 74 W			RMG
	331 79 W			
9				
30.55730 68.90332	006 54 W			bedding in Pal
	004 56 W			
	002 56 W			
	359 62 W			
	000 51 W			
Roadcut near Huaco				
30.19279 68.49467	286 60			At the new road cut
	284 68			--> Clasts include white & pink granites, limestones, rhyolites,
	270 70			grey ss, brown ss.
	264 71			Granites well rounded
	269 71			
				Paleocurrent indicators
				086 79
				095 75
				103 80
				109 83
				104 87
				106 81
				107 83
				103 83
				106 68
				108 64
				102 70
				110 68
Iglesia				
2007				
30.10376 69.17554		040 26 N T	fol: 001 33 W s: 01->222	
30.1004 69.17738		022 41 W N	fol: 038 23 W s: 39->267	
30.10472 69.17720		042 16 W T		

		048 30 W T		
		241 82 E T	fol: 062 71 N s: 82->162	
30.10889 69.17682	016 32 E			top bed
	028 65 E			bottom bed
		087 44 S T		reidel shear
Iglesia 2008				
1				
30.10073 69.17702	036 25 W			Bedding in 'bottom' unit
	037 30 W			
	046 26 W			
	040 25 W			
	011 35 W			in unit ii
	030 32 W	061 84 W N		20 cm of tops->W sep
	023 22 W			in unit iv
	014 23 W			contact between units iv iii
	020 27 W			
	014 26 W			
	013 29 W			
2				
30.09953 29.17226	022 80 W			bedding in paleozoic devonian
	024 82 W			049 58 E
	023 77 W			039 51 E
	026 86 W			034 58 E
				020 52 E
				039 44 E
				034 64 E
	015 79 W			RMG
	027 73 W			
	029 73 W			
	029 72 W			
	029 58 W			
	026 60 W			
	033 57 W			
	022 67 W			
	028 65 W			
	028 61 W			
30.10032 69.17123	021 59 W			Fractures:
	021 61 W			274 43 S
	018 52 W			304 68 N
	022 64 W			276 52 S

				272 41 S
				282 42 S
				296 67 N
				322 74 N
				289 80 N
3				
30.09811 69.16880	048 79 W			Bedding in paleozoic
	045 81 W			
	046 79 W			
4				
30.09719 69.16776	011 30 E			Bedding in Seq. II
	028 20 E			
5				
30.10084 69.16900	021 64 E			Bedding in Seq. III+
	023 64 E			
	028 75 E			
	019 51 E			RMG
	017 64 E			
Day 2				
1				
at seq1 seq2 F				
30.096133 69.176164		044 24 NW T	slicks: 19->290	(slicks good)
			fol 084 43 N	less good
		038 34 W T	slicks: 32->288	
		358 34 W T	fol: 016 46 W [21->324]	
	062 70 N			gypsum veins
	071 62 N			
	071 61 N			
	005 54 W			
	003 59 W			
2				
-30.09551 -69.17088	018 22 W	003 26 W T	fol: 014 61 W [25->292]	bedding in HW
	008 32 W			bedding in FW
		346 34 W T	fol: 011 41 W [08->334]	in FW of previous F
	156 40 W			bedding in FW
				Fractures:
				289 60 S
				281 63 S
				275 56 S
				031 42 E
				034 35 E

				032 48 E
Iglesia 2009				
Day 1				
2				
30.06360 69.28893	260 09			Bedding in lower Iglesia units
	234 21			
	248 08			
	253 07			
	231 07			
	285 16			(WDB)
	281 14			It looks like from the GE imagery,
	282 10			that the dd towards ~260-280 are correct
3				
30.06361 69.28789	206 15			
	215 16			
	210 10			
	246 15			
	288 09			WDB
	295 14			
	298 14			
	289 08			
	300 30			
4				
30.06452 69.28616	[215 06]			
	236 10			
	223 07			
	234 11			
	320 12 (?)			
	287 06			WDB
	284 04			
	286 04			
5				
30 06504 69.28345	300 08			
	291 06			WDB
	275 09			
	296 06			
	285 05			
	280 09			

6				
30.06520 69.28181	284 08			WDB
	318 11			
Day 2				
1				
30.07511 69.19820	266 70			
	261 71			
	253 67			
	256 60			
	257 67			
	251 73			
2				
30.07543 69.19756	326 15	080 46 S N	s: 46->170	
		031 36 E N	s: 33->148	
3				
30.07588 69.19670	210 54			collected ash "IG ASH STOP #3"
	198 56			
4				
30.07638 69.19630	301 49			
	293 59			
	296 52			
	276 54			
5				
30.07669 69.19462	285 50	269 46 T	s: 237 42	not great
	271 36			
	241 43	251 62 T?	s: 316 39	not good
	264 49			
Two independent transects				
6				
30.09151 69.18963				spring at this location
7				
30.09473 69.19035	298 24			in sequence II? in white beds
	290 23			
8				
30.09463 69.19091	310 18			

9					
30.09419	69.19163	294 16			
		278 13			
10					
30.09410	69.19243	314 08			
11					
30.09395	69.19273	036 09			
		051 09			
12					
30.09421	69.19292	098 15			
		092 14			
13					
30.09396	69.19298	120 17			
14					
30.09385	69.19309	082 19			
15					
30.09353	69.19302	077 18			
16					
30.09365	69.19450	076 10			
17					
30.09342	69.19521	037 05			
18					
30.09381	69.19793	350 08			
19					
30.09446	69.19944	287 16			
22					
30.08277	69.19073	056 21			WDB - RHR
		049 27			
		060 20			
23					
30.08218	69.18983	065 14			
		055 15			
		056 13			
24					

30.08180 69.18884	060 30			
	051 37			
	054 28			
25				
30.08197 69.18757	050 45			
	053 46			
	052 38			
26				
30.08213 69.18736	055 22			
	061 28			
27				
30.08214 69.18709	059 09			
	055 07			
28				
30.08312 69.18643	050 35			
	058 32			
	052 40			
29				
30.08320 69.18613	110 24			
	110 12			
30				
30.08349 69.18575	173 27			
	140 30			
	164 30			
31				
30.08385 69.18533	166 30			
	165 31			
	156 24			
32				
30.08297 69.18438	176 30			
	170 30			
	178 32			
20				
30.08209 69.18746		141 21 T	s: 131 21	these are basicall out-of-the-syncline faults
		141 35 T	s: 135 35	

21				
30.16604 69.12421	265 35	171 57 N	s: 151 55	
Médano surfaces				
1				
29.83755 69.18360	040 06 W			in gravels at level 1
	061 11 N			Paleocurrent indicators
	084 12 N			290 50
				305 36
				305 45
				300 32
				295 45
				295 35
				300 32
				281 27
				280 23
				272 38
				290 32
				290 27
				255 25
				235 40
				283 23
				273 33
				320 16
				275 37
				274 35
				280 20
				276 44
2				
29.83693 69.18807	340 05 W			gravels at 2
	348 11 W			sourced from N with red SS clasts
				Paleocurrent indicators
				310 30
				000 30
				280 26
				315 38
				310 26
				310 32
				352 32
				310 30
				315 38
North of Huaco				
1				
29.96978 68.48831	066 52			this looks like Mogna, but the

	112 30			clasts are very different
	116 53			-->mostly Osj & mafics
	088 36			
	102 50			
	114 63			
Niquivil anticline 2008				
A				
30.25677 68.47218	038 76 E			Western limb of Salinas anticline
	042 81 E			
	038 84 E			sighted
1				
30.32088 68.52065	032 88 E	279 34 N D		bedding in Jarillal(?) - N side
	026 64 W	276 22 N D		
		089 68 N		large fault
		089 66 N D	slicks: 19->W [19->278]	parallel to or main
	011 75 W			beds on S side of stream (RMG)
	011 81 W			Fractures:
	016 80 W			085 47 S
				076 38 S
				128 39 SE (better)
				136 40 SE
2	018 67 W			bedding at #2 N side
	013 72 NW			S side
4				
30.32871 68.54861	013 57 E			north
	014 71 E			south
		071 80 S D	Fol: 056 85 S D slicks: 18->W [18->248]	good
5				
30.32877 68.55067		291 58 S D	slicks: 38->W [38->262]	~1 m hor. offset
6				
30.32481 68.55078	~010 60 E	077 67 S D	slicks: 15->W [15->251]	20 cm gouge; [not great]
	038 66 E			
7				
30.31905 68.54840	007 61 E			"transition zone"
	034 59 E			

	036 67 E			
	341 64 E	076 39 S		no consistent slicks
				white beds on the farthest E
	036 60 E			
	007 61 E			
8				
30.31922 68.54823		087 63 S D	slicks: 34->W [not great]	
Niquivil Anticline 2007				
0543196 6644658		255 88 SE D	s: 25->254	UTM loc.
0543220 6644648		236 46 SE D	s: 28->205	
0544903 6645433		019 72 W D	s: 55->227	
Niquivil terraces				
Terrace #1				
Contact between upper and lower units 064 09 S				
Likely the Quebrada del Cura fm?				
Terrace #2				
Contact 031 25 W				
a bedding in T 044 39 NW				As move toward the north, the gravel has more and more
				sandstone and volcanic clasts, and the lower unit is more coarse
b bedding in T 327 34 NE				with larger clasts
c bedding in T 334 34 NE				
d bedding in T 115 14 N				
e bedding in T 171 32 E				
Terrace #4				
Bedding in T 211 25 E		056 42 SE		Small thrust with 30 cm sep.
Rio Francia 2007				
Q T fault				
1				
30.62440 68.73624		303 13 SW		This is the Q/T fault sans kin. ind.
		326 26 SW		

		336 24 SW		
		305 23 SW		
		342 45 W		
		356 50 W		
		282 19 SW	fol: 282 50 SW s: 19->194	
2				
30.62983 68.73488		300 22 W T	s: 22->216	Q T
Main thrust				
1				
30.62050 68.78002		118 82 S		T slicks down-dip but sketchy
2				
30.61987 68.78146		161 31 S T	fol: 161 39 W s: 31->253	
3				
W side of large T outcrop		124 42 S T	fol: 001 52 S s: 05->130	O/T
		001 68 W		
		017 79 W T	fol: 009 78 W s: 09->015	(upper)
			fol: 355 66 W s: 33->010	(lower)
4				
30.61813 68.78288		140 41 W T	fol: 146 44 W s: 21->294	
		011 32 W	clv: 172 17 W	not good
		164 44 S T	fol: 166 80 W s: 44->260	
5				
30.61696 68.78323		095 41 S T	fol: 118 47 S s: 08->266 s: 09->265	
6				
30.61706 68.78365		120 35 S T	mullions: 35->210	
Day 2				
30.58842 68.82897		117 67 S T??	slicks: 67->216	better
Up at Osj thrust	165 31 W			bedding in T
	166 59 W			bedding in Osj
	170 55 W			
	161 67 W			
30.58984 68.83510	081 08 S			bedding in conglomerate

	326 59 W			bedding in T
	330 34 W			
	346 36 W			
	348 51 W			
30.58867 68.82500		144 50 W T	fol: 130 69 W s: 38->186	
Near camp				
30.61943 68.77882	014 84 W			bedding in gravels near camp
		096 70 S T	fol: 091 73 S s: 108 30	fault T Cong
		076 76 S T	fol: 094 87 W s: 29->248	
30.62067 68.77858	281 63 E	078 54 S T	fol: 084 64 S s: 45->212	bedding in T near camp; (Dev/T)
	122 66 S			bedding in Dev
Rio Francia, etc 2008				
1				
30.57071 68.75562	030 52 W			bedding in Osj at the Niq. thrust
	011 48 W			
	026 35 W			
	021 36 W			
	006 51 W			
	040 42 W			
	014 39 W			
	018 42 W			RMG
	035 31 W			
	044 41 W			
2				
30.57449 68.73833	331 10 E			alluvial gravels
	016 31 E			
	306 11 S			
	034 57 NW			lower gravels
	032 59 NW			
	049 41 NW			
	029 60 NW			RMG
	031 53 NW			
	019 57 NW			
	027 62 NW			
3				
30.57719 68.73976	031 69 W			lower gravels

Day 1					
	4				
30.61428	68.78264	274 64 S			Carb? beds
		082 74 S			
		091 80 S			
	5				
30.61565	68.78519	294 75 S			Tertiary beds
		293 86 S			
		306 63 S			
	6				
30.61633	68.78510		296 46 S T	fol: 304 60 S [40->242]	(in black)
				fol: 272 41 S [18->278]	(in yellow)
			274 36 S T		too folded to get foliation
		119 47 S			bedding in Carb
		097 53 S			RMG
		095 55 S			
	7				
30.61645	68.78470		312 29 S T	slicks: 31->237 [28->237]	
				fol: 323 38 S [17->278]	
				FZ fol: 284 50 S	
			355 35 EN T	fol variable	
		302 44 S			white layer
	8				
30.61660	68.78442		289 45 S T	fol: 283 51 S [33->151]	in black gouge
			291 54 S T	fol: 296 69 S [51->230]	
			316 52 SW N	fol: 308 64 SW [42->180]	
	9				
30.61674	68.78386		344 27 S T	fol: 351 30 W [16->309]	
			343 48 SW T	fol: 323 57 W [17->179]	
	10				
30.61708	68.78358		132 28 S T	slicks: 25->W [25->253]	
				fol: 150 34 S [12->289]	
			140 57 S, T		
			304 71 S, T		
Day 2					
	11				
30.60145	68.81185	012 71 W			Bedding in Perm
		019 73 W			

	003 63 W			
	349 29 W			
	013 42 W			
	026 46 W			
	004 34 W			
	003 32 W			
	351 48 W			RMG
	011 69 W			
12				
30.60057 68.81337	324 64 W			Fractures:
				064 16 W
				061 20 W
	352 55 W			068 18 W
	354 54 W			bedding in 'undeformed' ss
	349 55 W			RMG
	355 54 W			
	319 58 S			not great
				Fractures:
				051 71 NW
				056 69 NW
				326 45 N
				319 48 N
				324 57 N
13				
30.60495 68.79441	014 47 W			Bedding in Osj
	015 53 W			
	016 51 W			
	027 51 W			
	009 54 W			RMG
	016 60 W			
	022 46 W			
14				
30.60667 68.78939	322 54 S			Fractures:
	321 53 W			024 70 E
	326 55 S			034 55 E
	321 53 S			045 77 E
	322 52 S			019 71 E
	326 55 S			043 61 E
	321 56 W			039 81 E
	321 53 W			034 76 E
	319 58 W			021 70 E
	317 51 W			

	319 53 SW			RMG
	319 52 SW			Fractures:
	324 50 SW			061 77 N
	314 54 SW			076 56 N
	312 56 SW			075 65 N
				066 66 N
				074 71 N
				071 63 N
15				
30.61588 68.78781		026 50 E T	fol: 026 78 E [50->118]	
		026 74 E		Carb T
16				
30.61945 68.77870	064 84 SE			Gravels
	069 88 E			
	339 84 SW	061 28 E T	slicks: 14->213	Tertiary; tops N 15 cm sep.
	340 85 SW	001 00		Tops to N ~10 cm offset no slicks
	342 76 SW			
	024 80 W			gravels in river bed
	023 88 W			RMG
	032 75 W			
	017 71 W			
		090 74 S T?	slicks: 41->W [41->256]	
Day 3				
1				
30.62362 68.73696		033 28 N T	fol: 032 41 N [28->308]	T T fault
2				
30.62386 68.73697		019 37 N T	fol: 018 56 N [37->289] slicks: 31->S [31->250]	T T faults
				[s-shear 339 56 N]
				[p-shear: 088 24 S L-lateral offset]
3				
30.62445 68.73618		301 14 S T	slicks: 14->216	[perfect] T Q fault
		297 11 S T]	slicks: 10->W [10->220]	(not as perfect)
		289 16 S T	slicks: 15->216	T Q fault
4				
30.62891 68.73516		345 26 W T	fol: 341 64 W [26->248]	T T fault
5				
30.62990 68.73491		340 11 W		General trend of T/Q f. (sighted)

6				
30.63147 68.73397		294 59 SW T	slicks: 58->187	Minor T T faults
		089 56 N T	slicks: 50->035 (tops S)	
		086 34 S T	fol: 345 48 W [11->102]	
	291 35 SW			tertiary bedding
7				
30.63394 68.73437		310 21 W T	fol: 294 72 W [20->199]	T T fault
8				
30.63368 68.73376	319 36 SW	306 27 W T	fol: 291 59 W [25->190]	T T
9				
30.63597 68.73096	309 52 W			Bedding in Huachipampa (?)
	315 55 W			
	311 46 W			
	305 27 W			
10				
30.63636 68.73132		045 73 S T	slicks: 36->W [36->213]	tops E LL offset T T
				Fractures:
				057 57 S
				346 46 W
				337 43 W
11				
30.63667 68.73204		302 50W T	fol: 312 68 W slicks roughly 50º DD [43->251]	
All T T faults		065 54 S		~30 cm L offset
		310 51 N T?	fol: 339 52 W [46->073]	
2009				
Day 1				
1				
30.60977 68.77872	304 57			bedding in Carb
	307 60			
	299 70			
	282 67			
2				
30.60901 68.77847	308 58			Carb
	304 57			
3				
30.60820 68.77847	221 81			Osj
	223 81			
	224 79			

	221 80			
	236 75			
9				
30.60815 68.77841	230 65			Osj (WDB)
	228 72			
	237 77			
4				
30.60539 68.77657	284 41			Osj
	268 30			better
		284 35		
		298 34 T	sch: 200 49; [s 17->001]	
		286 28		Fault zone gouge
		(293 41)		This is not great: Osj/Carb fault
5				
30.60528 68.77571	252 85			Steeply dipping T gravel beds
	254 80			similar to those near the camp.
	252 87			The Osj/Carb fault is exposed,
	259 77			below the [covered] Carb/T fault
	261 88			
	262 84			
6				
30.61481 68.79597	198 84			dodgy bedding in the Perm
		300 76 NS(?)	sch: 304 57 [slip 262 72]	
7				
30.61555 68.79650	193 71	330 87 TS(?)	clvg: 317 78 [slip: 058 37]	Perm bedding
8				
30.61599 68.79699		317 88 NS	clv: 315 70 [slip: 241 83]	
	239 55			bedding in Carb (WDB)
	239 58			
	234 53			
	249 59			
Day 2				
1				
30.57965 68.81581	256 54			bedding in Carb tops->W
	258 51			
	266 49			
	266 49			
	269 44			
	257 43			

	275 51			WDB
	268 39			
	277 48			
	274 54			
	169 38			
2				
30.57451 68.81693	232 20			destroyed outcrop of Carb
	244 35			really shallow dips are too low
	238 51			better to trust the 40-50º dips
	232 46			
	244 38			
	211 33			
	241 48			
	246 50			
	239 55			WDB
	239 58			
	234 53			
	249 59			
3				
30.57661 68.81799	251 26			in Perm
	290 28			some bedding-parallel shear, but
	242 43*			there are ~parallel to the beds above the shear zone
	252 51*			
	247 57*			
	256 43			
Rio Huaco road transect				
a				
30.14879 68.60445	008 68 W	002 76 W T	slicks: 55->N [55->342]	
b	007 69 W			
C1				
30.16190 68.62943	030 52 W			C1 in c. conglomerates (mogna)
	016 48 W			
	022 49 W			
	026 46 W			
	031 46 W			
	024 49 W			
	319 06 S			in second unit
C2				
30.16116 68.62999	007 42 W			Mogna

	287 09 S			second unit
C3				
30.15945 68.63095	281 11 N			second unit
	109 16 N			
C4				
30.15964 68.63277	040 08 NW			unit 2
	042 06 SE			not great
	105 12 N			not great
	027 19 SE			not great
C5				
30.15891 68.63322	342 19 NE			weird - unit 2
	346 20 NE			but seems right
	015 20 SE			
C6				
30.15223 68.62528	026 64 NW			Mogna
C7				
30.15268 68.62101	015 44 NW			Mogna
	014 64 NW			
	015 56 NW			
	006 45 W			lower unit
	009 48 W			lower
	089 07 S			upper
	061 04 S			Contact
C8	191 46 W			Mogna
	183 38 W			
Ls1				
30.14928 68.61716	356 57 W			Osj - Ls1 & Ls2
	354 61 W			Fractures in Osj
	008 58 W			048 47 SE
	354 62 W			036 61 SE
	358 45 W			042 51 SE
	356 54 W			056 44 SE
				074 88 S
	179 57 W			072 90
	180 58 W			079 90
	175 56 W			064 59 S
				073 46 S
				081 53 S
				071 51 S
				081 51 S
				088 47 S

		348 56 W T?	slicks: 51->NW [51->293]	086 58 S
				106 77 N
				076 79 N
				091 84 N
				091 86 N
				101 84 N
				106 76 S
Ls3				
30.15036 68.61144		151 87 E	fol: 089 14 S slicks: 09->W [230 09]	[A]
		326 34 E D	slicks: 26->N [012 26]	[B] 2 m offset
		336 56 W T	slicks: 54->S [240 54]	[A] ~2 m offset
		346 86 W T	slicks: -> (86) [270 86]	minor
		354 45 W		
		346 44 W D	fol: 012 23 E N? slicks: 03->N [017 03]	[A]
		324 45 E N	slicks: 33->S [A] [103 33]	
			fol: 031 11 E [033 43]	
		068 40 SE T	slicks: 13->N [083 13]	sep. 25 cm
	336 64 W			[RMG's notes not great]
	324 74 W			
1				
30.13841 68.53139	019 81 W			(west side of road)
	021 76 W			
	014 74 W			
	351 74 W			
	010 76 W			
	011 74 W			RMG - E side
	011 77 W			
	019 80 W			
	007 85 W			
	010 86 W			
2				
30 14211 68.53289	027 66 W			(west side) w. tops to E
	041 62 W			
	011 70 W			
	024 78 W			
	010 82 W			
	173 86 E			RMG - E side
	005 84 E			
	007 86 E			
	001 84 W			
	350 79 W			

	351 74 W			
3				
30.14451 68.53422	001 71 E			[sighted] - probably truly to W
	004 84 E			
	002 87 E			
4				
30.14376 68.53757	349 88 W			
	351 88 E			
	001 86 E			
	359 71 W			
	000 74 W			
	356 86 W			RMG - S side
	000 80 W			
	003 80 E			
5				
30.14271 68.54049	359 77 E	344 60 W T	fol: 340 57 W	these x-cut everything; sep tops E
	341 67 E	344 56 W T		tops to E sep ~1m
	352 72 E			
	359 86 E			
	356 64 E			
	356 88 W			RMG - near bridge
	002 88 E			
	359 86 E			
	356 90			
	359 87 E			
6				
30.14491 68.54136	357 77 E			
	[320 34 E]			
	354 82 E			
	355 52 E			
	354 78 E			
	355 66 E			RMG - E side
	355 75 E			lots of minor folding
	353 80 E			
7				
30.14562 68.54293	001 87 E			
	009 87 E			
	356 85 E			
	354 85 E			

	351 47 E			
	352 41 E			
	331 46 E			
	347 15 E			RMG - carb on E
	352 35 E			
	356 41 E			
	352 39 E			
	354 42 E			
8				
30.14575 68.54372	004 52 W	012 50 W T	slicks: 50 down-dip [282 50]	
	002 84 W			
	346 36 E			RMG - Osj
	345 41 E			
	005 41 E			
	001 45 E			
	348 36 W			
	014 40 W			
9				
30.14179 68.54523	046 26 SE			
	039 17 SE			
	312 18 NW			
	282 07 S			
	337 05 W			RMG - Osj
	072 04 S			
	026 11 E			
	009 10 SE			
10				
30.14375 68.54722	323 28 W			(majority of bedding orientation)
	317 28 W			
	021 12 W			small fold
	110 38 S			RMG - Carb?
	165 32 SW			
11				
30.14176 68.55033		086 06 S		
12				
30.14443 68.56158	001 33 W			
	016 28 W			
	355 32 W			
	002 32 W			

		002 29 W			
		357 37 W			RMG
		006 41 W			
		344 40 W			
		002 28 W			
		005 30 W			
13					
30.14684	68.56565	003 28 W			
		012 33 W			
		002 39 W			
		359 38 W			RMG - E side Carb
		358 41 W			
		002 37 W			
14					
30.15155	68.57160	005 50 W			(south side of road)
		003 51 W			
		011 44 W			RMG
		009 43 W			north side
15					
30.15154	68.57700	005 46 W			
16					
30.15318	68.58752	357 46 W			
17					
30.15394	68.58907	022 45 W			large cross beds in the Vallecito
		022 48 W			Fractures:
		004 88 E			356 68 E
		020 88 W			349 36 W
					351 58 E
					356 64 E
					002 34 W
		344 80 W			356 32 W
		345 83 W			RMG
		348 82 W			
		349 83 W			
18					
30.15413	68.59000	015 78 W	391 42 NW T	slicks: 35->346	
		017 88 E	000 41		
		011 67 W	015 40 W T	slicks: 35->071	conjugate with F 1?
		000 67 W			

	001 56 W			
	005 63 W			RMG
	001 62 W			
	005 64 W			
	003 61 W			
	000 61 W			
19				
30.15639 68.59125	015 70 E			grey-red unit sighted S
20				
30.15350 68.59458	010 82 W			everything at this stop is faulted
	005 89 E			
21				
30.15318 68.59686	011 87 W			
	014 77 W			
	007 75 W			RMG
	004 85 W			
	011 75 W			
22				
30.14883 68.60634	357 87 W	155 29 W T	slicks: 24->S [209 24]	In coarse conglomerates
	357 83 W	007 60 W		Tops->E diplacement; no slicks
	350 89 E			RMG
	357 88 W			
	355 87 W *			
23				
30.14939 68.60848	329 89 W	315 74 E N	slicks: 74 down-dip [035 74]	still in conglomerates
	336 76 W	339 71 E N	slicks: down-dip [079 71]	~8cm down E sep.
	356 67 W			
	357 69 W	355 83 W S		RMG; 22 cm offset
		191 79 W N	slicks: 69->341	
24				
30.14872 68.61447	340 51 W	031 20 E N	slicks: -> 105 [105 19]	
	356 58 W	082 41 E T	slicks: -> 254 [254 07]	tops to E (maybe?)
	345 55 W	039 35 E		
		334 31 W		
		024 30 E		

		074 14 N T	slicks: 13->036 [036 09]	
San Roque - north end				
1				
30.16370 68.61051	359 69 E	061 71 N T	slicks: 56->N [029 56]	
		052 76 N T	slicks 72->N [003 72]	not great
2				
30.16343 68.61147		028 35 W T		clast offset by 1.5 cm
		019 77 E N		not great
30				
30.16330 68.61192	358 56 e			
4				
30.16329 68.61264		017 34 W T	slicks: 32->N [310 32]	Ord T thrust
5				
30.16324 68.60396	027 64 E			
6				
30.17212 68.60926	024 79 E	306 28 S	no slicks. 2 cm LL sep	
	021 83 E	039 76 E N	slicks: 73->S [167 73]	[A-] based on sep
	030 82 E	086 28 S		
		072 41 N T	slicks: 28->W [290 28]	[A]
		042 54 N T	slicks: 48->W [276 48]	[A] 20 cm sep.
		309 42 NE T?	slicks: 06->W [316 06]	
		027 28 NW		
		042 60 NW T	slicks: 57->W [284 57]	
		036 44 W T	slicks: 28->W [249 28]	via offset
		281 59 N T	slicks: 24->W [296 24]	"conjugate" w. prev?
				Fractures:
				304 64 S
				309 58 S
				310 45 S
				018 21 W
				162 13 W
				009 76 W
				034 63 W
				Fracture set 1
				286 88 N
				287 88 N
				289 89 N
				281 80 S
				276 88 N
				Set 2

				354 31 W
				001 26 W
				341 50 W
				347 44 W
				Gypsum in fractures
				028 31 W
				065 25 N
				068 36 N
				067 44 N
	020 87 E	136 36 W		w. normal sep.
	027 79 E	079 72 N T?	slicks: 71->NE [012 71]	RMG
	019 79 E	104 71 S D	slicks: 24->W [275 24]	22 cm sep
		110 59 S S		12 cm sep
		118 65 S S		18 cm sep
		061 46 N ?	slicks: 67->NW	
		002 72 W N?		
		120 46 N N	slicks: 09->E [111 09]	direction good, slicks not great
		140 86 NE N	slicks: 57->SE [133 57]	
		071 38 N N	slicks: 26->E [067 26]	[PAJ measurement]
		279 29 N S	slicks: 24->E [045 24]	[PAJ measurement]
7				
30.17267 68.60998	025 70 E			Fractures:
	012 79 W			280 65 S
				278 77 S
				294 72 S
				286 86 S
				281 74 S
				286 70 S
				282 77 S
				283 59 S
				001 38 W
				012 35 W
				021 48 W
				006 38 W
				354 42 W
				020 24 W
				048 34 W
				[040 36 W]
				[058 41 W]
				RMG - fractures
				109 30 NE
				108 31 NE
				114 24 NE
				104 25 NE
				090 22 N

8				Fractures:
30.17253 68.60967				046 21 NW
				075 56 S
				274 21 N
				288 29 N
				304 34 N
				286 34 N
				296 26 N
				082 57 S
				278 56 S
				088 59 S
				272 60 S slicks 13->E (no sense)
				308 38 N
				279 40 N
				046 36 N
				281 74 S
				067 39 S
				076 46 S
				274 69 S
				RMG - fractures
				065 30 N
				071 30 N
				071 33 N
				062 33 N
				053 32 N
				159 22 N
				050 22 N
				Veins
				086 24 N
				077 34 N
				085 44 N
				094 33 N
9				Fractures:
30.17553 68.61016	024 84 E			312 48 N
	027 85 E			323 44 N
				007 26 W
				006 34 W
	023 80 E			RMG
	026 79 E			
	022 81 E			
	027 83 E			
10				Everything in this valley shows oblique slip to NW (~285°)
30.17605 68.60860	024 73 E	132 18 N T	slicks: 01->E tops [129 01]	W sep 60 cm
	030 64 E	052 19 E T	slicks: 03->N dex. [060 03]	offset 14 cm sep

				Fractures:
				270 41 N
				064 19 N
				048 61 W
				041 62 W w. slicks 55->W
				050 68 W
				001 26 E
				051 74 N
				006 30 E
				006 24 E
	021 77 E	040 24 E	slicks: 10->N	045 67 N
		031 44 W	slicks: 38->S	032 66 N
				RMG
				047 27 S
2009				053 33 SE
Day 1				
1				
30.17482 68.60733	292 83	331 32 T N?	s 28->300	Fnit at the base of Cerro morado
				Beds generally dips steeply to W
				Maybe progressively less steep to
				W until the bottom of the thrust (Osj/T) on W side of the valley
2				
30.17509 68.60705	283 87	353 41 N	s: 05 -> 269	still in conglomerate
	136 85			Did the SR thrust extend to here?
	124 89			lots of mafics (and Cu)
	110 89			
		331 57 N	s: 50->291	Notes not great on this
		292 85 N	s: 85->291	in cerro morado. Def. N
Day 2				
1				
30.17463 68.61020	114 89			in T on transect up to Osj T fault
	106 83			
	110 81			
2				
30.17442 68.61111		283 40 N T	s: 306 18	tops are to W, meaning things are overturned at this spot
		278 24 N T	s: 309 13	
3				
30.17408 68.61172	289 89	103 40 T	sch: 351 52	(~5cm separation)
	112 88	008 24 T	sch: 346 34	
	100 80			

	290 87			
	102 88			
4				
30.17430 68.61261	104 82	324 50 T	s: 292 47	bedding just below FZ, in Osj
	101 84			
	107 89			
	103 84			
5				
30.17350 68.61437	283 78			bedding in T from below thrust
	294 69			
On backside of San Roque				
1				
30.17704 68.64466	299 74			bedding in Mogna (Lower Unit)
	292 68			
	294 71			
	235 16			bedding in Upper Unit
	220 10			
	263 13			
2				
30.18183 68.63895	311 45			Osj-rich beds--unconsolidated w.
	320 61			largely pebble-sized clasts
	321 60			some choiyoi clasts, permian SS
	334 70			NOT mogna
3				
30.18423 68.63737	353 70			Osj bedding
	352 58			
	328 54			
	339 63			
	336 70			
	283 73			contact between Ls-Cong
				this contact is folded, though

			"The contact between the Osj and conglomerate is faulted, but the conglomerates look congruent with the contact. The cong. w/ permian ss area at the base, not the top. So, the unit with the ss-Osj clasts maybe represents the first phase of deposition from the river to the NW, which was then covered by the Mogna? FZ is ~3-4 m. thick w/ relatively competent Osj to the east thick package of gouge, then pretty congl. to west. How does this happen? The bottom of the SR fault zone dips ~50º to W and, if i'm not mistaken, the top is ~30º. How do you get 70º dips on the west side and 30-50º on the east? There must be several phases of faulting that affects this area.	
4				
30.18521 68.63790	292 70			beds in Osj
	303 70			Remember that there is a big, steep fault zone in internal part
				of the SR Osj near the dique
S. Tranca 2007				
30.55054 69.03307	010 16 N			bedding in grey conglomerates
	350 10 W			
At base of Osj	024 63 W			bedding in red beds
30.52460 69.045515	066 23 S	248 40 E T	slicks: 34->193	bedding in Osj cong
	010 78 W			
30.52137 69.01672	352 81 W			T bedding near Osj
	004 85 W			
	353 45 W			T beds 85m W from prev. meas.
30.51970 69.01887	040 19 W			bedding in T
30.51795 69.02032	008 70 W			bedding in T
30.51468 69.02048	154 27 W	349 71 W T	fol: 001 77 W s: 24-> 340	Q T contact
		161 52 W	s: 64-> 304	
		018 83 E		reidel shear
30.54873 69.04683	026 47 W	348 40 E T	fol: 015 72 E s: 28->129	
Southern Tranca				
2008				
Day 1				

1				
30.55028 69.05637	354 61 W			bedding in Dev? highly cleaved P
	344 74 W			
	346 56 W			
	349 63 W			RMG
	347 64 W			
	342 60 W			
2				
30.54531 69.05375	344 70 W	332 84 E w	slicks: 72->146 T [132 72]	red bedding in Sil?
	352 82 W	346 86 W		
	359 80 W	347 86 W		Fol 346 89 E
	026 70 E	357 64 W	slicks: 49->211 T	pebble horizon in T
		358 59 W		
		021 26 E T	fol: 344 40 E [036 07]	
		021 56 E T	fol: 344 88 W [044 30]	RMG
3				
30.54503 69.05296	331 64 SW	045 63 S		D offset of 5 cm
		000 65 W	fol: 034 58 SE	tops->W 40 cm
		038 34 SE		5 cm tops->W(conjugates?), T
		321 64 E		offsets prev by 5 cm tops down
		009 81 W		RMG
		012 79 W		292 85 N (frac)
		002 81 W		285 75 S (frac)
4				
30.54287 69.04942	356 83 W			green sands
	359 88 W			
	351 84 W			
	341 74 W			
	356 85 W			
	346 80 W			tops->E
	345 76 W			RMG
5				
30.54202 69.04726	291 44 N	304 63 SW T	fol: 297 74 W [161 49]	T redbeds; tops->NE up 2 m
	069 25 N			
	301 59 E			
	287 44 E			
	302 49 E			
	298 58 E			
6				

30.53991 69.05095	347 41 W	308 44 SW		
		354 52 W T	fol: 008 64 W [327 30]	
	000 70 W			RMG - moderate confidence
7				
30.54178 69.05162	076 25 S			green sands
	082 24 S			
	071 18 S			
	061 21 S			
	078 20 S			RMG
	064 19 S			
	058 23 S			
Day 2				
1				
30.51554 69.01902	023 84 W			red brown sands below congl.
	019 86 W			
	022 82 W			
	021 83 W			RMG
	022 85 W			
2				
30.51558 69.01935	023 67 W			more sands muds
	005 69 W			
	009 78 W			
	007 76 W			
	009 68 W			
	012 80 W			RMG
	013 76 W			
	004 71 W			
3				
30.51567 69.01954	015 78 W			red&whites sands shales
	020 66 W			
	002 64 W			
	350 54 W			
	002 69 W			
	346 49 W			tops->W
	008 65 W			RMG
	008 61 W			
	356 49 W			
	014 63 W			

4				
30.51602 69.02000	020 58 W			coarse sands
	015 54 W			
	018 63 W			
	014 57 W			
	010 65 W			RMG
	008 68 W			
5				
30.51639 69.02010	015 65 W			sandy unit
	015 80 W			
	014 71 W			
	021 68 W			RMG
	020 65 W			
6				
30.51665 69.02061	014 61 W			bedding in T
	013 56 W			Contact between cong and T
				004 24 W
				359 33 W
	354 27 W			RMG
	019 28 W			
7				
30.52145 69.01669	008 75 W			bedding in dark red congl
	004 65 W			
8				
30.52173 69.01694	349 46 W	330 63 W T	fol: 330 77 W slicks: 44->N [300 44]	brown sands sans Osj
	336 46 W			
	349 53 W			RMG
	352 51 W			
9				
30.52508 69.01678	358 67 W			brown sands
	009 72 W			
	000 56 W			
	000 68 W			RMG
10				
30.52559 69.01695	008 55 W			brown sands
	015 58 W			
	009 63 W			

	010 59 W			
	007 54 W			RMG
	008 59 W			
	008 59 W			
11				
30.52636 69.01710	010 51 E			Osj bedding
	001 44 E			
12				
30.52722 69.01717	350 56 W			dark red congl
	355 70 W			poorly sighted measurements
Tranca 2007				
Near 2008 #28		010 45 W T	s: 41->250	
1				
30.30745 69.01629	159 14 W			bedding in cong
	167 26 W			
2				
30.30910 69.02184		064 57 W T	fol: 056 75 s: 50->296	W (O)
	030 59 W		fol: 024 73 W (T) s: 12->252	
3				
30.30642 69.01951	062 36 W			
4				
30.30624 69.01958	015 22 W	031 32 W T	fol: 034 46 W s: 31->312	good exposure (T)
			fol: 036 59 W s same	(O)
		045 10 N T	fol: 132 12 W s: 07->005	T/C slicks, not great. toward NW
5				
30.30540 69.01944		166 12 W T	fol: 204 40 W s: 08->306	O T
5b		204 44 W T	fol: 046 51 W s: 10->014	O T
6				
30.30461 69.01813		185 23 W T	fol: 218 45 W s: 13->333	T C
			182 39 W s 33->271	better?
7				
30.30329 69.01872		182 37 W T	fol: 194 64 W s: 34->299	O T

8				
30.30219 69.01787		033 46 W T	fol: 030 63 W s: 45->290	T C
9				
30.30209 69.01817		024 39 W T	fol: 011 66 W s: 35->262 [slicks: 29->246]	O T
10				
30.30153 69.01781		052 41 W T	fol: 019 64 W (T) s: 19->255	O T
			fol: 031 65 W (O) s: 29->272	
a				
30.30061 69.01714		032 66 W T	fol: 032 73 W (O) s: 44->238	O T
b				
30.30040 69.01633		046 36 W T	slicks: 31->281	T C
c				
30.28493 69.01395		162 32 W T	fol: 136 69 W (O) s: 25->209	T O
			fol: 172 45 W (T) s: 27->286	folded
		161 80 W	fol: 151 62 W	not a typical outcrop
d				
30.28413 69.01411		121 39 N T	fol: 061 52 N (O) s: 116 04	O T
			fol: 117 44 N (T) s: 357 34	
e				
30.28675 69.01861		029 58 N T	fol: 029 60 N (O) s: 58->299	O T
			fol: 040 74 N (T) s: 44->352 slicks 57->313	
e3		016 48 W T	fol: 038 52 W (T) s: 04->012	O T
f				
30.28306 69.01569		027 31 W T	fol: 045 54 W (O) s: 31->286	O T
			fol: 021 64 W (T) s: 25->337	
g				
30.28214 69.01506		031 60 W T	fol: 021 75 W (O) s: 45->247	O T
h				
30.27973 69.01408		006 31 W T	fol: 015 67 W (O) s: 30->292 slicks: 28->305	O T
i				
30.27916 69.01281		004 70 W T	slicks: 52->336	T C
j				
30.27817 69.01283		204 63 W T	slicks: 63->295	T C

k				
30.27042 69.01223		326 46 W T	fol: 325 68 W s: 46->232	T/C S
l				
30.27060 69.01213		179 63 W T	slicks: 63->255	T C
m				
30.26992 69.01388		038 74 W T	fol: 198 82 W s: 19->224	O T
n				
30.26793 69.01179		340 44 W T	fol: 161 76 W s: 44->253	T C
o				
30.26791 69.01357		187 67 W T	fol: 133 44 W (T) s: 47->213	
			fol: 194 59 W (O) s: 38->348	
p				
30.25743 69.01225		011 66 W T	slicks: 66->290	T C
		358 51 W		bottom of fault zone
q				
30.23856 69.01424		335 52 W T	fol: 322 57 W (O) s: 18->169	O T
			fol: 346 67 W (T) s: 41->293	
r				
30.23896 69.01427		347 54 W T	fol: 004 71 W (O) s: 34->318	O T
			fol: 352 70 W (T) s: 51->283	
s				
30.23604 69.01449		359 56 W T	fol: 348 67 W (O) s: 37->209	O T
			fol: 350 68 W (T) s: 43->217	
t				
30.23591 69.01453		332 67 W T	fol: 317 74 W (O) s: 37->171	O T
			fol: 312 66 W (T) s: 07->329	
u				
30.23349 69.01372		212 46 W T	fol: 206 67 W s: 44->282	GC T
v				
30.23172 69.01273		354 71 W T	fol: 151 67 W s: 13->350	T CC
			fol: 170 81 W s: 62->214	
w				
30.23182 69.01280		010 44 W T	fol: 017 51 W s: 32->329	GC T

x				
30.23003 69.01191		055 30 W T	fol: 215 49 W s: 22->279	GC T
Tranca 2008				
1				
30.31622 69.02332		226 61 W T	fol: 039 68 S [229 60]	between Ord & pink
1b		014 77 W T	fol: 015 82 E	(green foliation)
			fol: 015 84 W [321 74]	(red foliation)
			fol 005 89 W [211 51]	
2				
30.31488 69.02297		006 70 W T	fol: 357 72 W [190 12]	(fol a little rough)
		009 67 W T	fol: 013 81 W Ord [318 61]	Ord fault react.
		004 55 W T	fol: 346 62 W [196 61]	10 cm sep
			fol: 016 63 W (#2) [343 27]	
4				
30.31320 69.01911	344 18 W	018 14 W T	fol: 018 55 W [288 14]	pink cross-bedded sandstones
	323 08 W	018 13 W T	fol: 018 25 W [288 13]	
		004 75 W N		10 cm sep
		341 90		RMG; sep 3 cm
		335 89 W		sep.: 9 cm (tops down to SW)
		345 88 W		sep.: 2 cm (tops down to SW)
		315 42 N		sep.: 9 cm (tops down to NE)
5				
30.30881 69.01923	350 15 W			bedding in Unit I
	349 12 W			
	285 11 S			RMG
	306 10 S			
	080 19 S			
	280 12 S			
6				
30.30898 69.02174		056 61 W T	fol: 054 67 W [296 57]	(in black)
			fol: 049 67 W [260 36]	(in black)
		071 86 N		RMG
				fault plane of Ord Ord
7				

30.30621 69.01958		048 52 W T	fol: 031 57 W [237 11]	fault Ord T
7b		045 48 W T	fol: 036 59 W [268 37]	
7c		[034 50 W T	slicks: 39->351]	[not the greatest]
8				
30.30595 69.01849		356 12 W T	fol: 350 41 W [258 12]	T CC; not great.
		026 21 NW T		RMG
8b		038 16 NW T	fol; 356 55 W [254 10]	T CC; not great
8c		053 15 NW T		
		050 24 NW T		
		052 23 NW T	fol: 013 57 W [266 13]	
9				
Ord T scarp W from 8		019 42 W T	fol: 358 56 W [226 22]	(in black)
9b		012 46 W T	fol: 008 66 W [266 45]	(in black)
10				
30.30457 69.01944		065 42 W T	fol: 048 68 W gouge [292 33]	Ord T
10b		051 60 W T	fol: 028 65 W in red [235 08]	Ord T
11				
30.30463 69.01817		354 24 W T	fol: 348 41 W [249 23]	
11b		356 29 W T	fol: 337 31 W [181 03]	RMG; T C
12				
30.30324 69.01882		049 59 W T	fol: 036 69 W gouge [251 32]	Ord T
13				
30.30260 69.01803		278 50 N T	fol: 081 56 N	
14				
50 m from 15 at fault		015 63 W T	fol: 002 72 W [212 30]	Ord T
				gypsum veins
				182 29 W
15				
30.30220 69.01790		034 49 W T	fol: 032 62 W [291 48]	T CC
15b		040 48 W T	fol: 032 62 W [273 42]	RMG

16				
30.30149 69.01736		015 25 W T	fol: 019 55 W [292 25]	T CC; not great
17				
30.30072 69.01720		014 55 W T	fol: 031 73 W [345 35]	Ord T
18				
30.30072 69.01720		028 42 W T		don't use
19				
30.30031 69.01633		005 39 W T	fol: 019 69 W [307 35]	T CC
20				
30.29991 69.01678		016 57 W T	fol: 005 64 W [215 27]	Ord T
21				
30.29967 69.01614		031 25 E T	fol: 010 35 E slicks downd [f: 062 13] [s: 105 25]	T CC
21b		063 57 W T	fol: 058 66 W slicks: 50->W [290 49]	
22				
30.29742 69.01589		005 44 W T	fol: 006 53 W [283 44]	Ord T
23				
30.29552 69.01452		359 46 W T	fol: 001 69 W [275 46]	T CC
24				
30.29511 69.01456		002 46 W T	fol: 359 63 W [259 45]	T CC
25				
30.26666 69.00352	352 22 W			Bedding in CC
	356 22 W			
	015 25 W			
	337 12 W			
	004 17 W			
	021 19 W			RMG
	043 20 W			these not great
	025 17 W			
	359 21 W			ok
26				
30.25581 69.01051	338 19 W			Bedding in CC
	356 17 W			
	359 16 W			
	351 23 W			RMG
	010 17 W			

	000 14 W			
27				
30.23640 69.01478	005 45 W			Bedding in grey conglomerate
	011 46 W	006 46 W T	slicks: 44->250	within GC
	007 45 W			
	001 49 W			
		359 57 W T	slicks: 56->249	
		324 48 E		L-l offset
		329 36 E T	fol: 001 46 E	(tops -> NW)
				contact between GC and Ord
				331 37 W
	036 48 W			338 36 W
	014 47 W			
	356 45 W			RMG
	002 51 W			
	005 46 W			
	003 47 W			
	344 45 W			more reliable
28				
30.23604 69.01454		001 66 W T	fol: 357 69 W [200 37]	Ord/T, below GC
29				
30.23539 69.01452		008 39 W T	fol: 022 53W slicks: 33->329 [327 28]	GC T
		009 42 W T	fol: 009 46 W slicks: 29->234	much better exposure
30				
30.23532 69.01454		040 26 W T #1		GC T
		035 26 W T		
		336 43 W T		
		350 49 W T		
		011 83 E N #3		
		022 72 W N		
		334 50 W foliation #4		
		342 48 W		
		022 72 E T	fol: 001 83 E [030 24]	
		003 65 W T	slicks: 33->188 [201 33]	
		004 53 W T	fol: 340 34 [320 43]	tops W

		336 43 W #2		RMG
Villa Mercedes 2009				
1				
30.11108 68.85081	072 52			"So" but actually prob. a later clvg
	097 51			"S1" but prob. actually bedding
	106 49			In sed. cover, the clasts from 330
	098 60			consistent with topography
	100 60			
	305 83			
	298 85			
	314 76			
	311 84			
	306 73			
2				
30.11118 68.84895	276 59			Sil. Dev. bedding
	277 56			
	274 58			
	283 56			
	278 54			
3				
30.11197 68.84565	089 61			Sil. Dev. bedding
	091 63			
	093 53			
4				
30.10806 68.84086	137 34			Sil. Dev. bedding
	146 31			V. folded but is dominant fabric
	189 23			
	171 31			
	166 32			
6				
30.07655 68.83256	117 65			Sil.Dev. bedding
	121 64			
	120 66			
	112 65			
	109 75			
7				
30.10807 68.80319	090 74			Sil. Dev. bedding
	085 70			
	084 68			
	082 73			

	089 76			
				contact between intrusive and Sil.
				351 78 E
8				
30.10754 68.80271	074 65			Carb bedding: laminated w/ dropstones
	079 66			
	083 65			
	077 71			
9				
30.10748 68.80240	082 60			Coarse white rounded pebbles in Carb/Perm
	088 62			
	078 78			
	079 64			
	081 68			
10				
30.10720 68.80209	066 79			white x-bedded Perm sands
	068 68			
	077 63			
	082 58			
	073 73			
11				
30.10630 68.80089	066 47			in waterfall--top of sequence
	062 52			
	079 40			
	082 61			
12				
30.10597 68.79908	081 46	078 65 T	s: 124 55	Carb bedding; (tops->E)
	083 54			fault is roughly to contact with
	099 54			dike/sill
	100 53			
	070 50			

Appendix C:

C.1: Fault slip populations for the Precordillera

Fault number	*Fault strike*	*dip*	*Striae trend*	*plunge*	*Slip*	*T trend*	*plunge*	*P trend*	*plunge*
21.6 – 19.5 Ma									
Tranca 1									
1	155	52	293	41	TL	2	64	268	2
2	167	54	283	51	TL	28	75	268	8
3	179	56	217	43	TR	146	61	245	5
4	152	67	329	7	TL	13	21	108	11
5	181	66	200	37	TR	140	45	238	8
Tranca 2									
1	218	74	224	19	TR	175	25	266	2
2	187	67	213	47	TR	142	52	250	14
Tranca 3									
1	162	32	286	27	TL	319	67	93	16
2	301	39	357	34	TR	308	71	192	9
3	209	58	352	44	TL	65	60	323	7
4	207	31	337	25	TL	10	65	143	18
5	196	48	12	4	TL	50	32	157	25
Tranca 4a									
1	211	32	312	31	TL	329	76	128	14
2	166	12	306	8	TL	317	52	118	36

Fault number	*Fault strike*	*dip*	*Striae trend*	*plunge*	*Slip*	*T trend*	*plunge*	*P trend*	*plunge*
3	204	44	14	10	TL	52	39	162	23
4	182	37	299	34	TL	342	74	108	10
5	204	39	262	35	TR	213	72	96	8
6	212	66	238	44	TR	169	51	274	12
7	194	77	308	76	TL	97	58	289	32
8	186	70	190	12	TR	144	23	52	5
9	214	50	351	39	TL	57	64	148	1
10	199	42	226	22	TR	182	52	72	15
11	192	46	266	45	TR	181	82	274	1
12	195	63	212	30	TR	157	42	249	2
13	194	55	345	35	TL	44	54	315	0
14	196	57	215	27	TR	163	45	69	4
15	185	44	283	44	TL	355	86	99	1
Tranca 4b									
1	244	57	296	50	TR	204	68	318	9
2	244	57	252	12	TR	208	32	109	14
3	232	41	255	19	TR	214	50	102	18
4	226	61	299	60	TR	156	73	310	16
5	236	61	292	57	TR	182	69	313	15
6	228	52	237	11	TR	195	35	92	17
7	225	48	268	37	TR	206	64	111	3
8	245	42	292	33	TR	239	66	131	8
9	231	60	235	8	TR	192	27	94	15
10	229	59	251	32	TR	195	48	285	1

Fault number	*Fault strike*	*dip*	*Striae trend*	*plunge*	*Slip*	*T trend*	*plunge*	*P trend*	*plunge*
Caracol 6									
1	28	25	38	5	TR	14	44	239	36
2	16	59	148	51	TL	239	66	124	11
3	347	58	135	40	TL	201	56	104	5
4	351	65	73	65	TR	268	70	78	20
5	351	63	70	63	TR	272	71	77	18
Caracol 7									
1	184	52	326	38	TL	30	61	300	0
2	191	49	358	14	TL	41	40	145	17
3	195	41	358	14	TL	37	45	150	21
4	185	41	340	20	TL	22	51	134	17
5	240	71	56	12	TL	102	22	194	5
6	177	42	314	32	TL	5	64	113	9
7	181	67	355	14	TL	41	27	134	6
8	216	36	333	33	TL	13	73	142	11
Caracol 8									
1	189	49	197	9	TR	157	35	51	21
2	166	83	172	42	TR	115	34	221	23
3	154	41	239	41	TR	210	85	61	4
4	217	44	224	7	TR	187	36	77	25
5	171	74	174	9	TR	128	18	37	5
6	173	34	259	34	TR	251	79	81	11
7	172	63	185	25	TR	134	38	43	1
8	187	61	214	40	TR	149	53	248	6

Fault number	*Fault strike*	*dip*	*Striae trend*	*plunge*	*Slip*	*T trend*	*plunge*	*P trend*	*plunge*
9	160	46	231	44	TR	150	80	241	0
Caracol 9									
1	36	56	60	31	TR	4	49	272	2
2	34	52	38	4	TR	358	29	255	23
11 – 3 Ma									
Tranca 1a									
1	212	46	282	44	TR	202	80	292	0
2	190	44	329	32	TL	22	62	127	8
3	235	30	279	22	TR	247	61	115	20
4	186	46	250	44	TR	173	77	263	0
5	179	57	249	56	TR	120	75	261	12
6	329	36	139	7	TL	172	41	291	29
7	188	39	327	28	TL	12	62	127	13
8	22	72	30	24	TR	340	30	72	4
9	183	65	201	33	TR	144	43	239	5
10	184	53	320	43	TL	33	65	296	3
Tranca 1b									
1	174	71	214	62	TR	113	59	248	23
Tranca 2									
1	146	46	232	46	TR	117	88	234	1
2	179	63	255	63	TR	103	71	264	18
3	160	44	253	44	TL	308	88	72	1

Fault number	*Fault strike*	*dip*	*Striae trend*	*plunge*	*Slip*	*T trend*	*plunge*	*P trend*	*plunge*
4	191	66	290	66	TL	94	69	284	21
Tranca 3									
1	184	70	336	52	TL	54	53	298	18
2	204	63	295	63	TL	113	72	294	18
Tranca 4									
1	185	23	268	23	TR	263	68	90	22
2	213	46	290	45	TR	202	83	297	1
3	226	36	281	31	TR	239	69	115	12
4	176	12	258	12	TR	256	57	79	33
5	218	16	254	10	TR	239	53	85	34
6	174	24	249	23	TR	238	68	74	22
7	278	50	290	14	TR	247	39	144	16
8	214	49	291	48	TR	180	83	298	4
9	220	48	273	42	TR	201	71	292	0
10	195	25	292	25	TL	298	70	110	20
11	31	25	105	25	TR	92	69	290	20
12	243	57	290	49	TR	204	66	314	9
13	179	46	275	46	TL	20	87	272	1
14	182	46	259	45	TR	171	83	266	1
Caracol 5									
1	11	80	16	28	TR	325	27	61	12
2	190	34	258	32	TR	226	74	87	12
3	226	36	274	29	TR	232	66	111	13

Fault number	*Fault strike*	*dip*	*Striae trend*	*plunge*	*Slip*	*T trend*	*plunge*	*P trend*	*plunge*
4	342	8	84	8	NR	263	37	86	53
5	279	38	87	9	NR	239	26	122	42
Blanco 10									
1	51	20	106	17	NL	295	27	90	60
2	55	52	85	33	NL	294	3	28	55
3	124	20	284	8	TL	304	49	88	35
Blanco 11									
1	194	21	283	21	TR	282	66	103	24
Blanco 12									
1	192	56	263	56	TR	133	76	274	11
2	188	47	343	25	TL	31	51	134	11
Blanco 13									
1	69	51	216	34	TL	274	57	9	3
2	69	56	247	2	TL	287	25	28	22
3	49	53	226	4	TL	266	28	8	22
4	209	74	217	26	TR	166	30	260	7
5	14	69	42	51	TR	325	53	80	17
6	113	52	284	11	TL	326	35	69	17
7	71	78	247	17	TL	295	21	203	3
8	187	40	262	39	TR	215	81	89	6
9	192	55	355	22	TL	44	42	141	8
10	222	57	223	39	TR	175	46	270	4

Fault number	*Fault strike*	*dip*	*Striae trend*	*plunge*	*Slip*	*T trend*	*plunge*	*P trend*	*plunge*
Blanquitos 14									
1	214	23	301	23	TR	299	68	122	22
2	183	38	345	27	TL	25	54	137	15
3	178	54	314	44	TL	29	65	290	4
4	206	32	295	32	TR	293	77	115	13
Blanquitos 15									
1	168	28	298	22	TL	326	63	105	21
2	184	25	304	22	TL	325	65	115	22
3	171	29	309	21	TL	340	60	113	22
4	101	20	115	6	TR	95	47	312	37
5	56	24	106	19	TR	84	61	298	25
6	65	19	110	14	TR	93	57	301	30
7	196	17	247	13	TR	233	57	76	31
8	101	31	150	25	TR	117	64	345	18
9	79	42	90	10	TR	53	40	301	24
Blanquitos 16									
1	182	79	349	48	NR	302	23	54	41
2	200	76	345	66	NR	305	28	86	55
Estancia Durazno 17									
1	189	61	5	8	TL	48	26	145	14
2	161	57	325	24	TL	15	42	110	6

Fault number	*Fault strike*	*dip*	*Striae trend*	*plunge*	*Slip*	*T trend*	*plunge*	*P trend*	*plunge*
Estancia Durazno 18									
1	247	83	63	26	NR	17	13	113	23
2	81	64	103	38	TR	41	48	140	7
3	244	74	44	51	NR	1	21	116	48
4	247	80	59	40	NR	12	19	116	35
5	204	84	208	29	TR	157	25	254	16
6	223	84	225	19	NL	270	9	178	18
San Roque 19									
1	197	34	310	32	TL	343	74	121	12
San Roque 20									
1	241	71	29	56	TL	115	55	352	21
2	232	76	3	72	TL	127	57	332	30
San Roque 21									
1	252	41	290	28	TR	243	60	132	12
2	222	54	276	48	TR	188	70	296	6
3	309	42	316	6	TR	280	37	168	27
4	222	60	284	57	TR	166	71	301	14
5	216	44	249	28	TR	200	57	94	10
6	281	59	296	24	TR	246	41	152	4
7	259	72	12	71	TL	158	62	355	27
8	312	18	129	1	TL	146	43	292	41
9	52	19	60	3	TR	41	45	257	39

Fault number	*Fault strike*	*dip*	*Striae trend*	*plunge*	*Slip*	*T trend*	*plunge*	*P trend*	*plunge*
10	283	40	306	18	TR	266	50	152	19
11	278	24	309	13	TR	284	54	145	29
12	234	50	292	45	TR	210	73	309	3
Niquivil 22									
1	192	50	282	50	TR	102	85	282	5
Río Francia 23									
1	210	76	262	72	NL	291	30	135	58
2	240	87	58	37	TL	111	27	8	23
3	227	88	241	83	NL	310	43	144	46
Río Francia 24									
1	161	31	253	31	TL	256	76	72	14
2	124	42	130	5	TR	94	36	342	28
3	140	41	294	21	TL	336	52	88	16
4	164	44	260	44	TL	329	87	77	1
5	95	41	266	8	TL	302	39	55	26
6	120	35	210	35	TR	210	80	30	10
7	116	46	278	18	TL	321	45	68	16
8	132	29	237	28	TL	254	72	52	17
9	109	45	151	33	TR	96	63	353	7
10	111	54	230	51	TL	331	74	214	8
11	136	52	180	42	TR	109	65	204	2
12	164	27	309	16	TL	337	56	112	26
13	163	48	179	17	TR	135	43	31	15

Fault number	*Fault strike*	*dip*	*Striae trend*	*plunge*	*Slip*	*T trend*	*plunge*	*P trend*	*plunge*
14	132	28	253	25	TL	279	67	63	19
Río Francia 25									
1	96	70	108	30	TR	54	37	149	6
2	76	76	248	29	TL	300	31	204	10
3	78	54	212	45	TL	289	66	188	5
4	61	28	213	14	TL	242	53	14	27
5	90	74	256	41	TL	317	41	213	16
Río Francia 26									
1	213	28	308	28	TL	314	73	126	17
2	199	37	250	31	TR	206	68	86	12
3	165	26	248	26	TR	241	71	70	19
4	114	59	187	58	TR	48	74	198	14
5	269	56	35	50	TL	128	70	15	8
6	86	34	102	11	TR	69	46	307	27
7	130	21	199	20	TR	187	64	25	25
8	126	27	190	25	TR	168	68	19	19
9	45	73	213	36	TL	270	38	170	12
10	122	50	251	43	TL	325	69	231	2
11	310	51	73	46	TL	157	72	56	4
Río Francia 27									
1	208	34	356	12	TL	31	51	156	25

Fault number	*Fault strike*	*dip*	*Striae trend*	*plunge*	*Slip*	*T trend*	*plunge*	*P trend*	*plunge*
3 – 0 Ma									
Río Francia 28									
1	102	19	194	19	TL	195	64	13	26
2	120	22	216	22	TL	220	67	34	23
3	121	14	216	14	TL	218	59	35	31
4	117	11	220	10	TL	223	55	38	35
5	109	16	216	15	TL	223	60	32	30
Niquivil 29									
1	269	66	278	19	TR	230	31	138	3
2	71	80	248	18	NR	204	6	296	20
3	111	58	262	38	NR	230	3	325	54
4	77	67	251	15	NR	30	5	297	27
5	87	63	247	34	NR	211	4	305	46
6	68	71	235	32	NR	194	8	290	37
7	75	88	254	25	NR	207	16	302	19
8	56	46	205	28	NR	359	9	255	55
9	199	72	227	55	TR	146	53	266	21

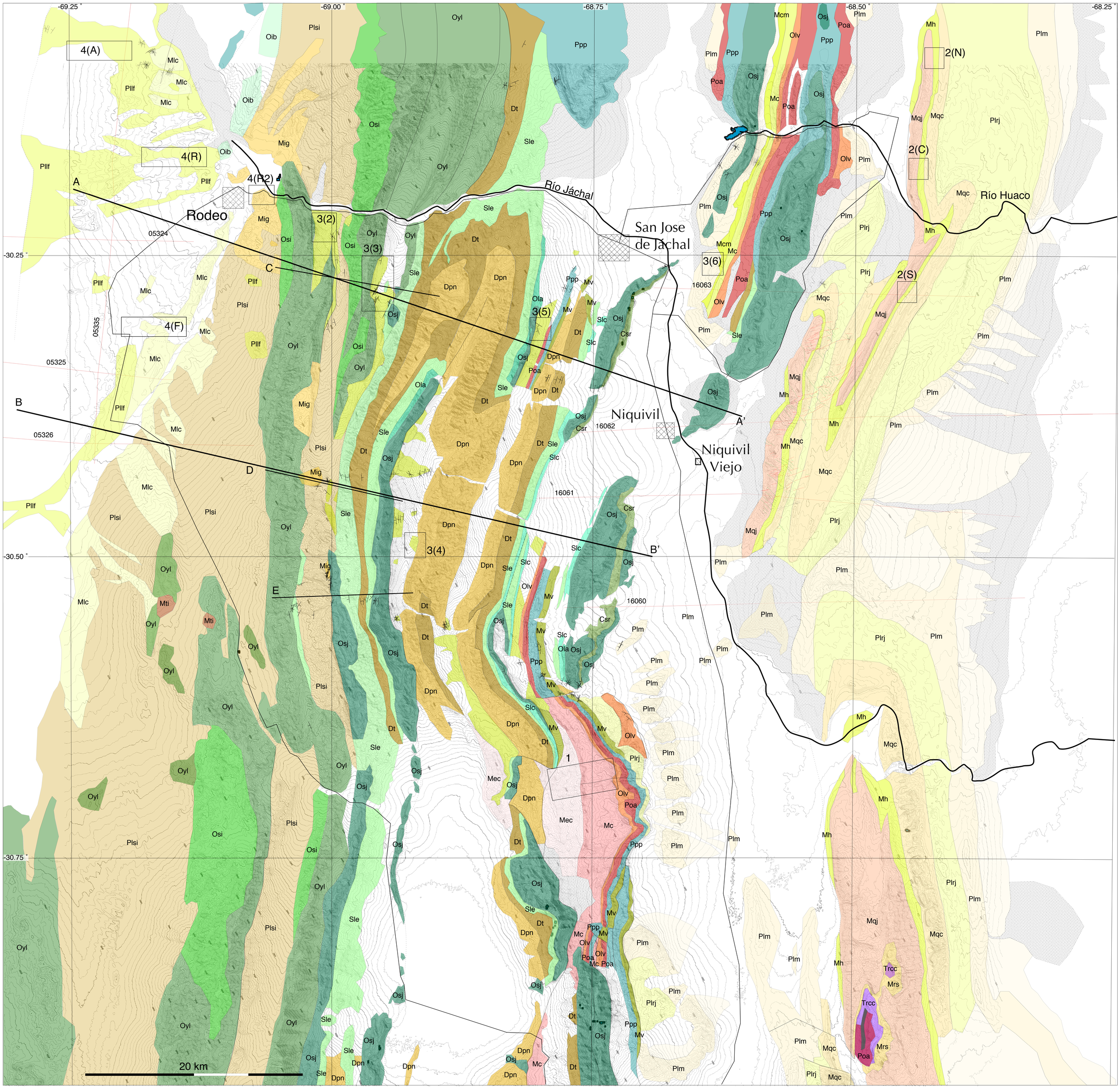

- (s) Los Espejos
- (s-o) La Chilca
- (o) Igneous bodies (basic)
- (o) Yerba Loca
- (o) Sierra de la Invernada
- (o) Los Azules
- (o) San Juan
- (c) San Roque
- (m) Cerro Morado
- (ol) Vallecito
- (Tr) Cañon Colorado
- (p) Ojo de Agua
- (Pp) Panacan
- (M) Volcan
- (d) Punta Negra
- (d) Talacasto
- (pl) Mogna
- (pl) Rio Jáchal
- (m) Quebrada del Cura
- (m) Huachipampa
- (m) Quebrada del Jarillal
- (m) Rio Salado
- (m) Cauquenes
- (pls) Iglesia
- (pl) Las Flores
- (m) Tertiary intrusives
- (m) Lomas del Campanario
- (m) Iglesia group
- (m) El Corral
- (m) Cuculi

1: Jordan et al 1990
2: Beer and Jordan 1989
3: Jordan et al 1993
4: Ruskin and Jordan 2007

- (q) alluvial deposits
- (hl) active fan deposits
- (pls) relict fan deposits